Supporting Information for:

Ligand Assisted Volatilization and Thermal Stability of Bisimidodichloromolybdenum(VI) ([(*t*-BuN=)$_2$MoCl$_2$]$_2$) and Its Adducts

Michael A. Land,*,† Katherine N. Robertson,‡ and Seán T. Barry†

† Department of Chemistry, Carleton University, 1125 Colonel By Drive, Ottawa, Ontario K1S 5B6, Canada

‡ The Atlantic Centre for Green Chemistry, Department of Chemistry, Saint Mary's University, Halifax, Nova Scotia B3H 3C3, Canada

*Corresponding Author. E-mail: Michael.land@carleton.ca

Table of Contents

Summary of Compounds

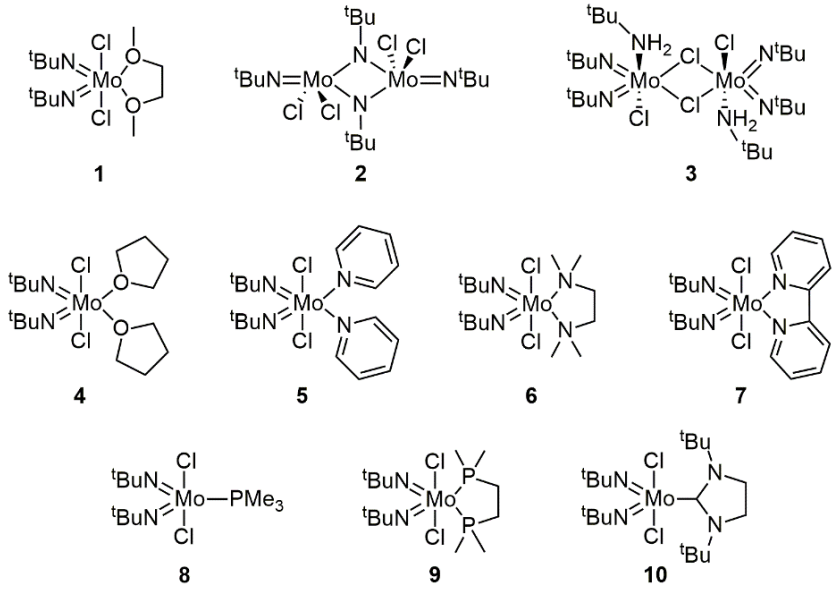

Thermogravimetric Analysis (TGA) Curves

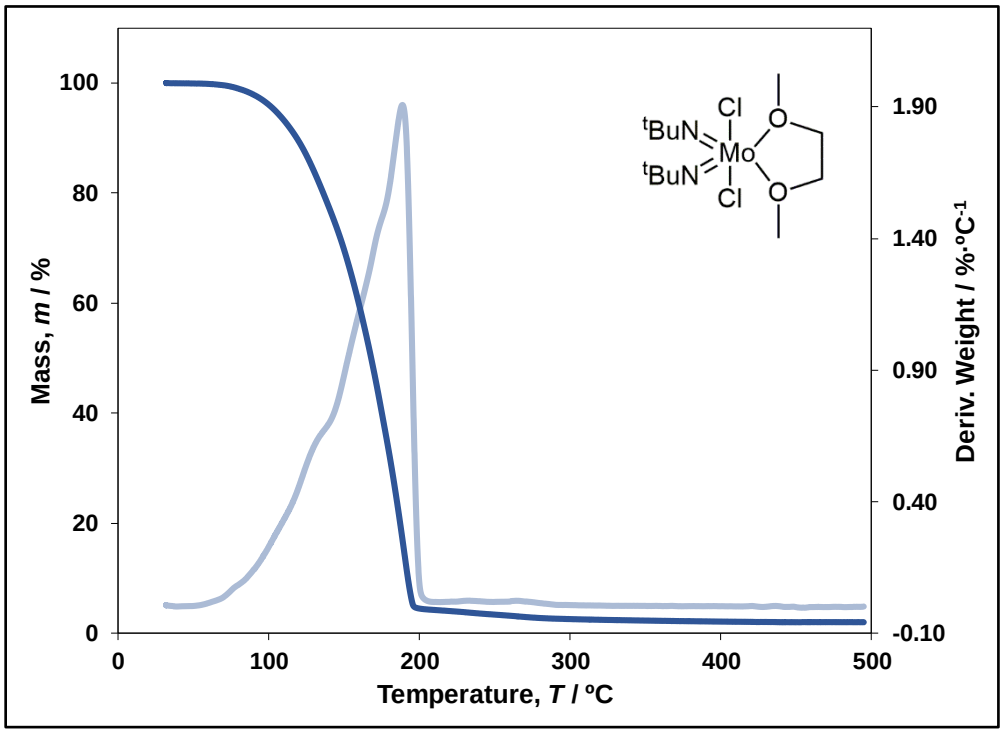

Figure S1: Thermogravimetric analysis of (*t*-BuN=)$_2$MoCl$_2$·dme **1** with a heating rate of 10 ºC/min. The mass loading was 9.9 mg and the residual mass was 2.0%.

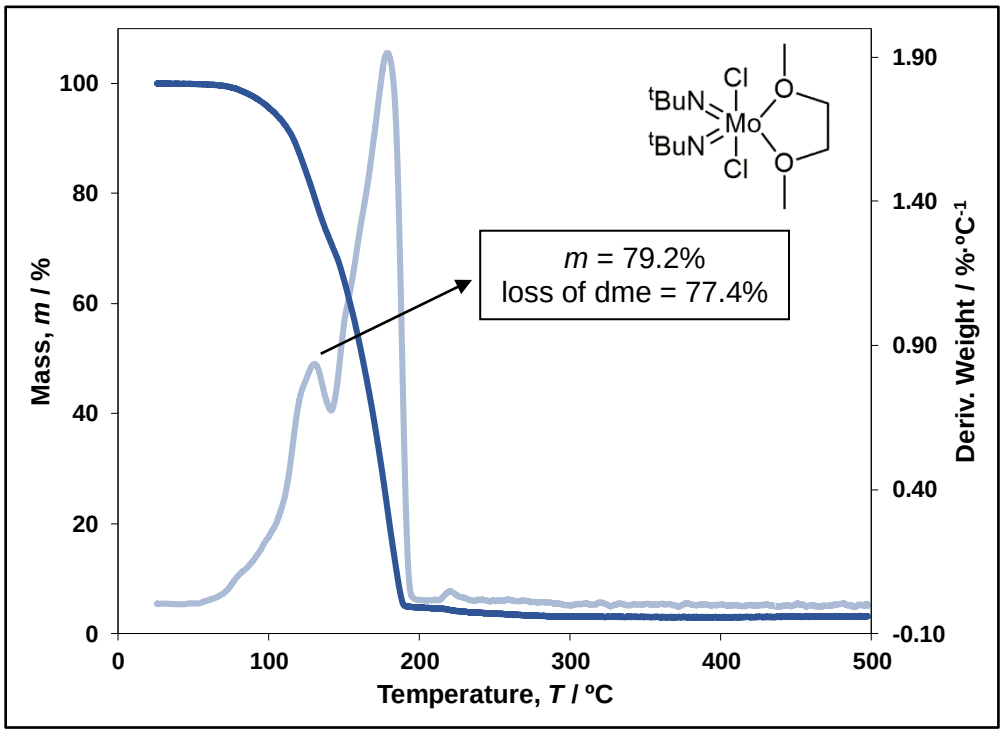

Figure S2: Thermogravimetric analysis of (*t*-BuN=)$_2$MoCl$_2$·dme **1** with a heating rate of 5 ºC/min. The mass loading was 15.2 mg and the residual mass was 3.2%.

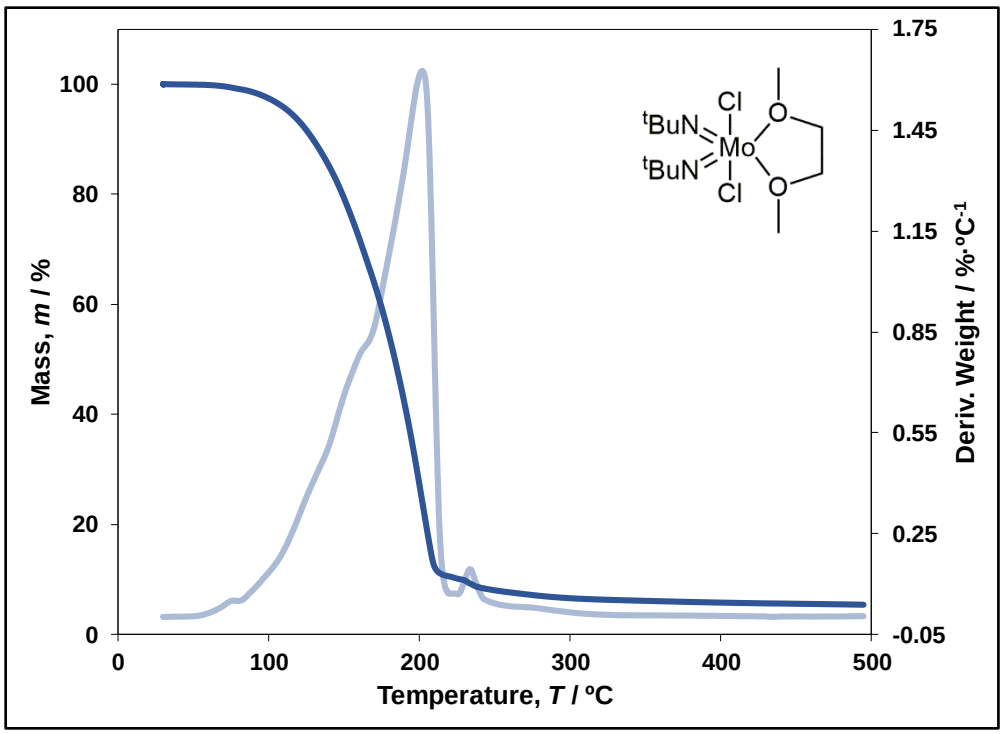

Figure S3: Thermogravimetric analysis of (*t*-BuN=)$_2$MoCl$_2$·dme **1** with a heating rate of 10 ºC/min. The mass loading was 20.4 mg and the residual mass was 5.4%.

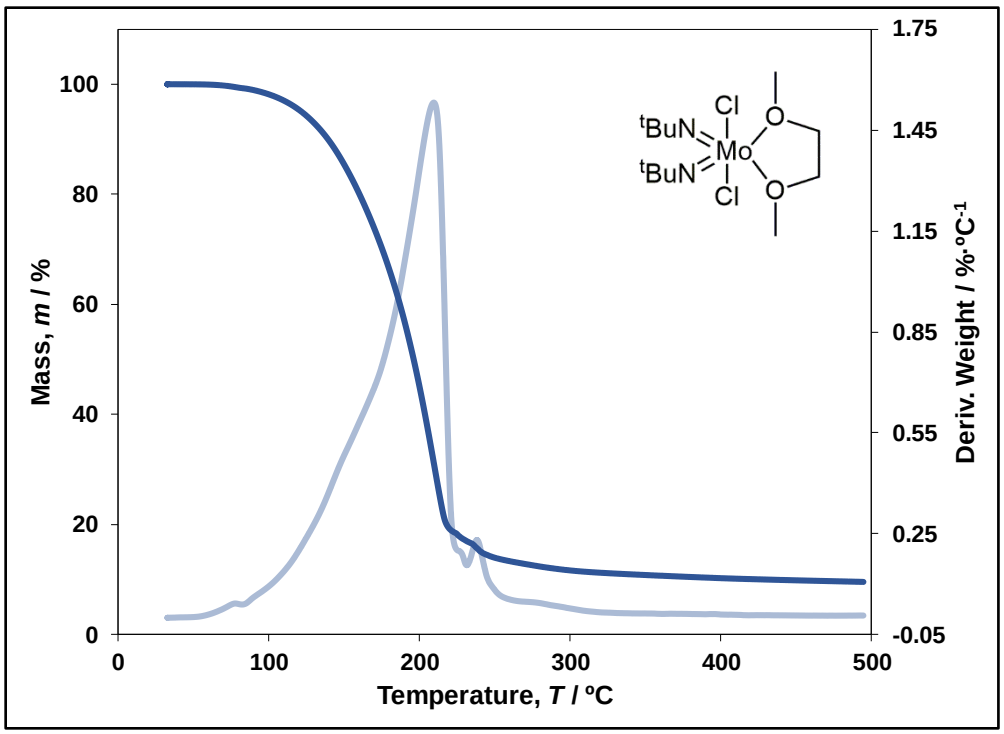

Figure S4: Thermogravimetric analysis of (*t*-BuN=)$_2$MoCl$_2$·dme **1** with a heating rate of 10 ºC/min. The mass loading was 30.4 mg and the residual mass was 9.6%.

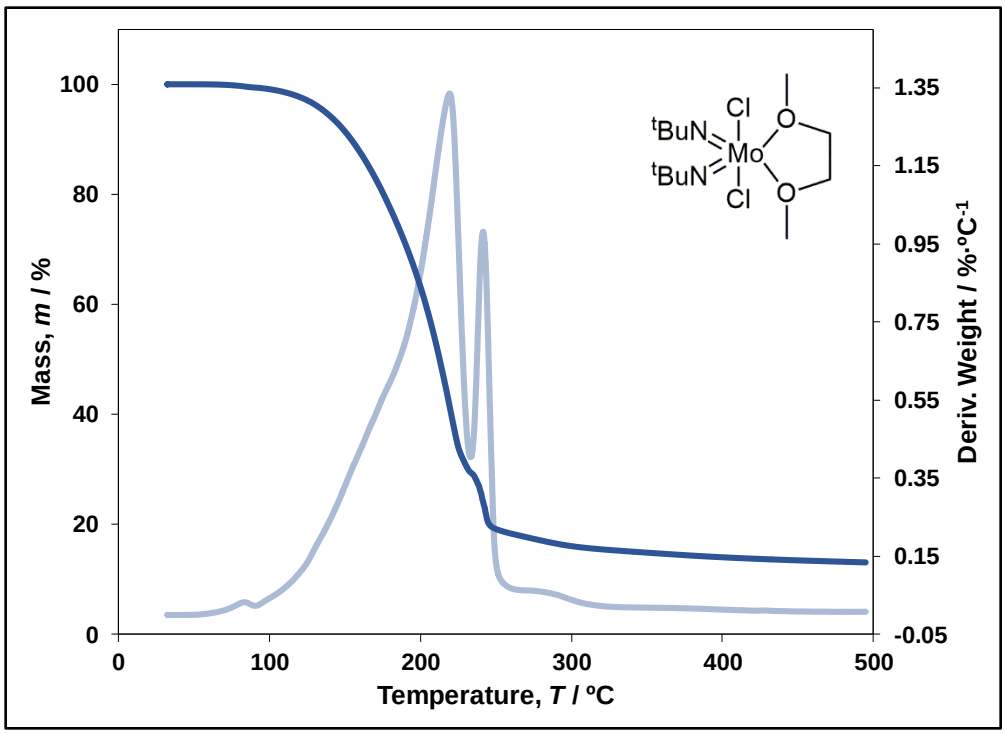

Figure S5: Thermogravimetric analysis of (*t*-BuN=)$_2$MoCl$_2$·dme **1** with a heating rate of 10 ºC/min. The mass loading was 55.1 mg and the residual mass was 13.1%.

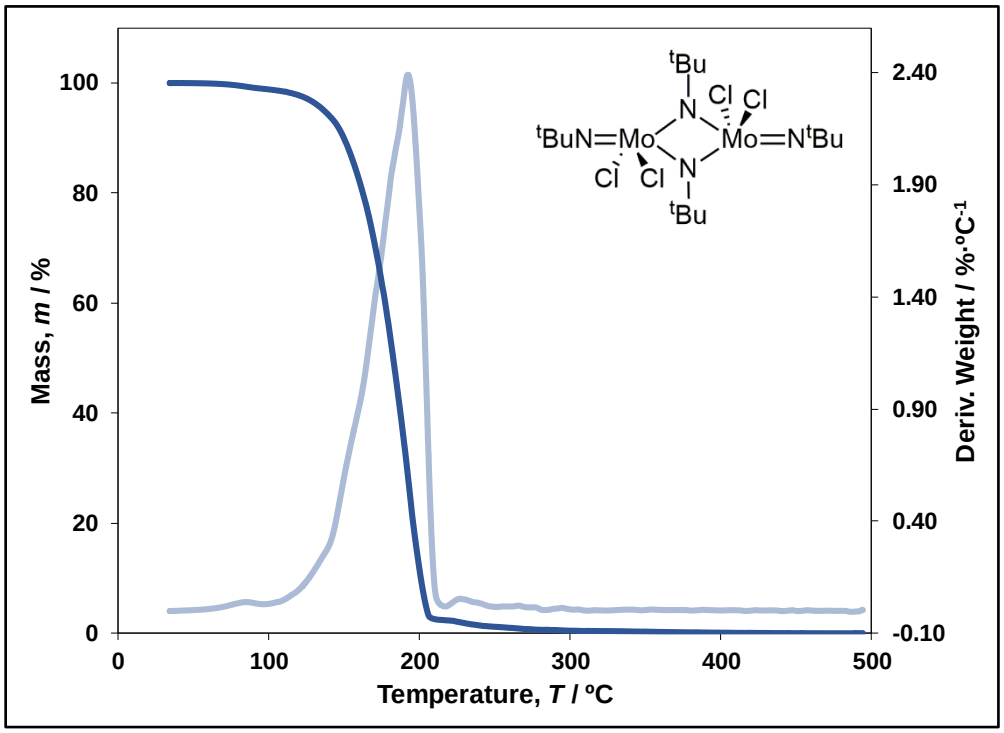

Figure S6: Thermogravimetric analysis of [(*t*-BuN=)$_2$MoCl$_2$]$_2$ **2** with a heating rate of 10 ºC/min. The mass loading was 10.0 mg and the residual mass was 0.0%.

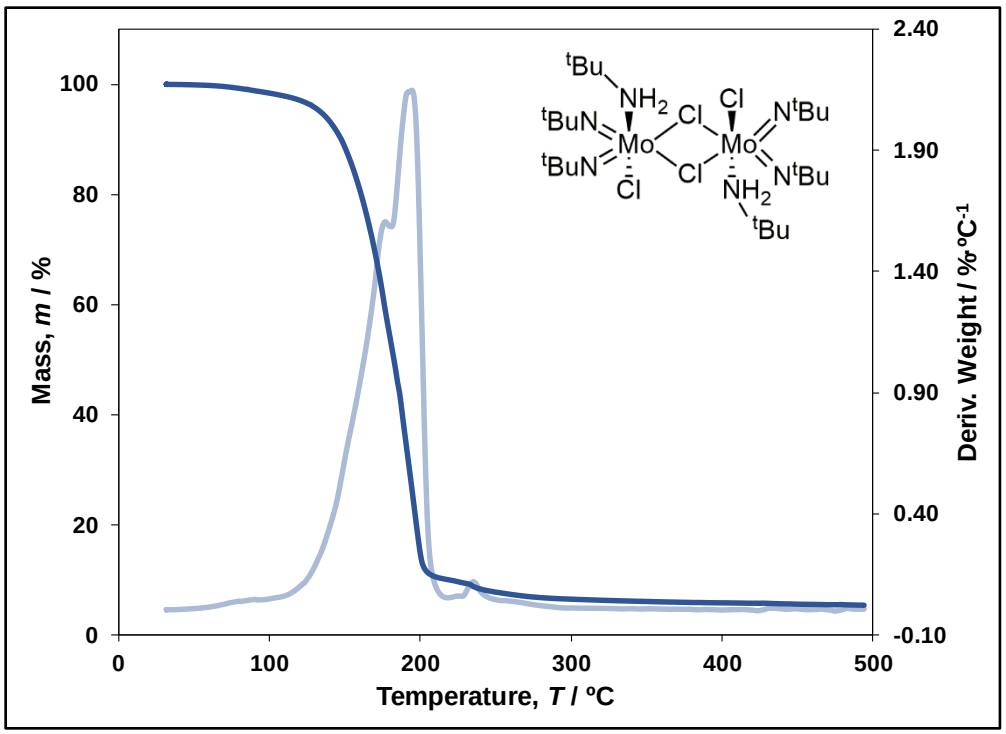

Figure S7: Thermogravimetric analysis of $[(t\text{-BuN=})_2MoCl_2\cdot(t\text{-BuNH}_2)]_2$ **3** with a heating rate of 10 ºC/min. The mass loading was 10.1 mg and the residual mass was 5.4%.

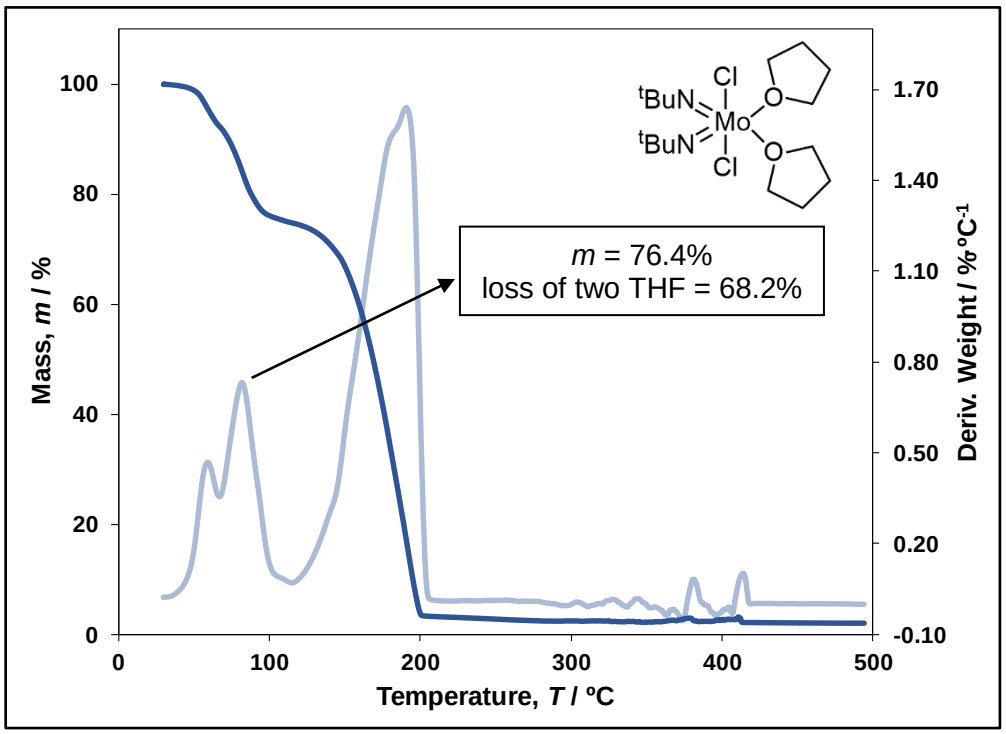

Figure S8: Thermogravimetric analysis of $(t\text{-BuN=})_2MoCl_2\cdot(THF)_2$ **4** with a heating rate of 10 ºC/min. The mass loading was 10.0 mg and the residual mass was 2.1%.

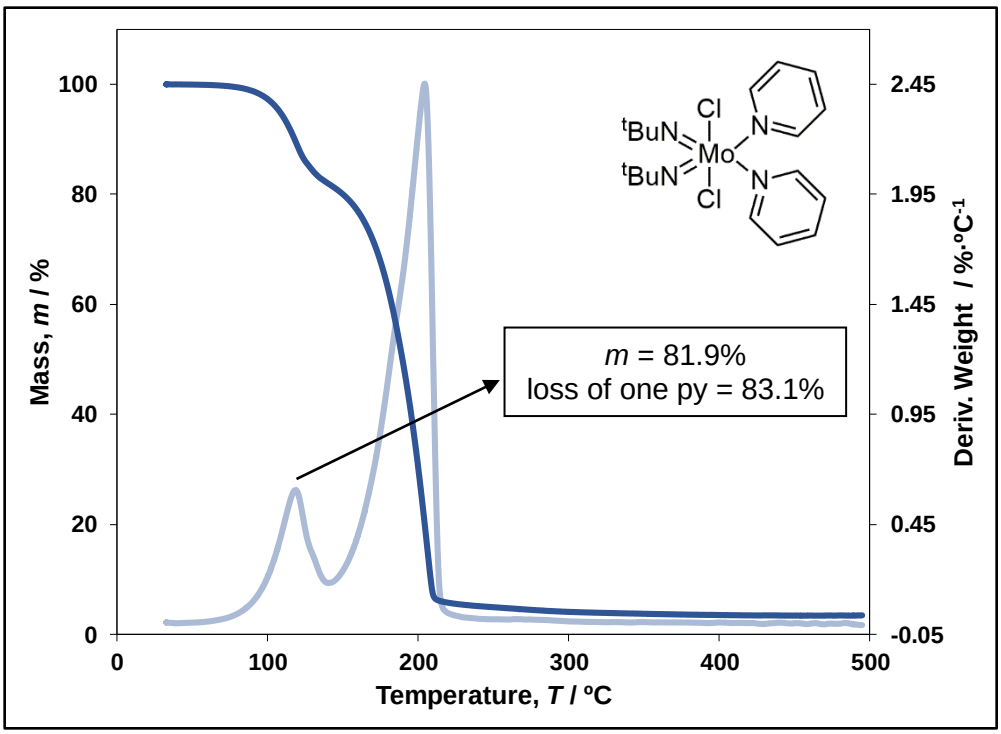

Figure S9: Thermogravimetric analysis of (*t*-BuN=)$_2$MoCl$_2$·(py)$_2$ **5** with a heating rate of 10 ºC/min. The mass loading was 9.9 mg and the residual mass was 3.5%.

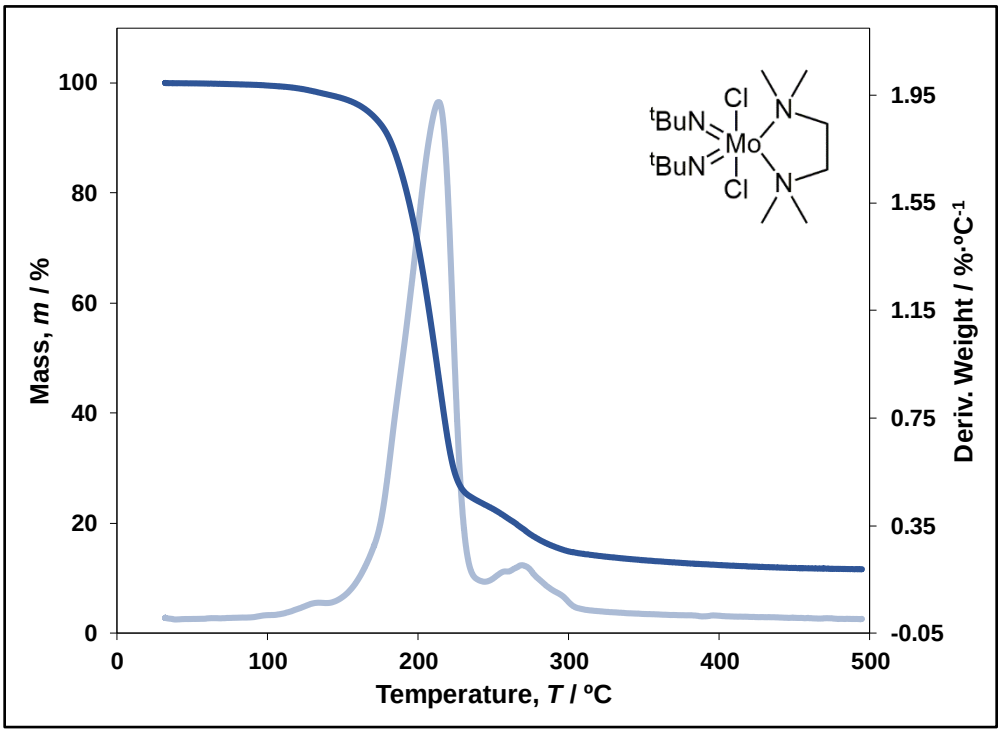

Figure S10: Thermogravimetric analysis of (*t*-BuN=)$_2$MoCl$_2$·TMEDA **6** with a heating rate of 10 ºC/min. The mass loading was 10.0 mg and the residual mass was 11.6%.

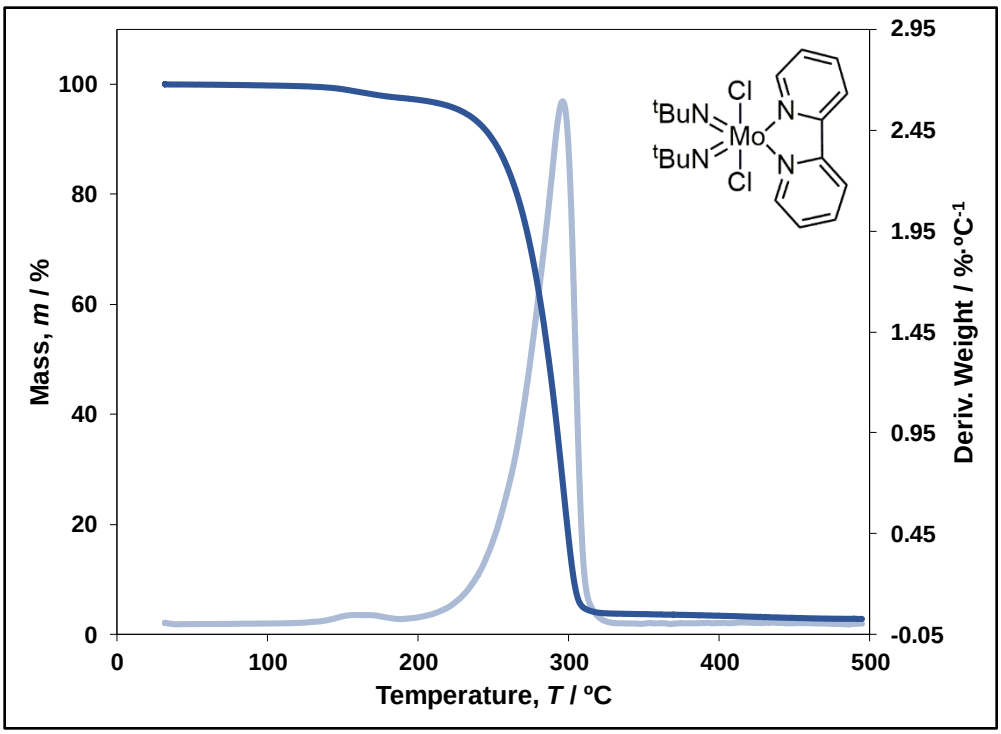

Figure S11: Thermogravimetric analysis of (*t*-BuN=)$_2$MoCl$_2$·bpy **7** with a heating rate of 10 ºC/min. The mass loading was 10.0 mg and the residual mass was 2.8%.

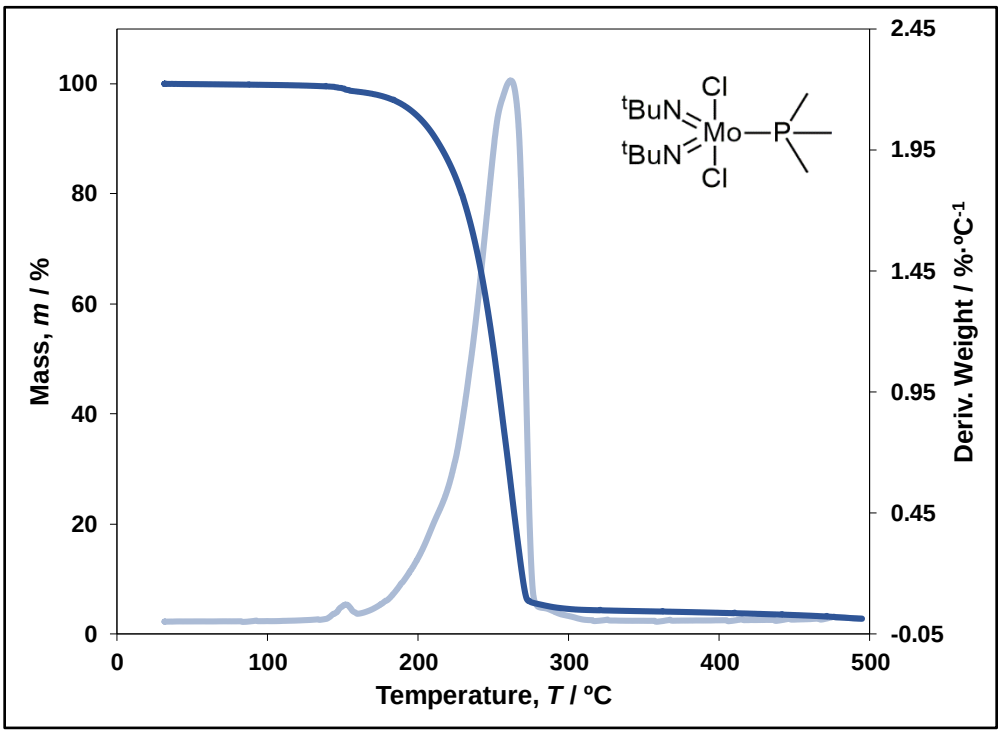

Figure S12: Thermogravimetric analysis of (*t*-BuN=)$_2$MoCl$_2$·PMe$_3$ **8** with a heating rate of 10 ºC/min. The mass loading was 10.0 mg and the residual mass was 2.8%.

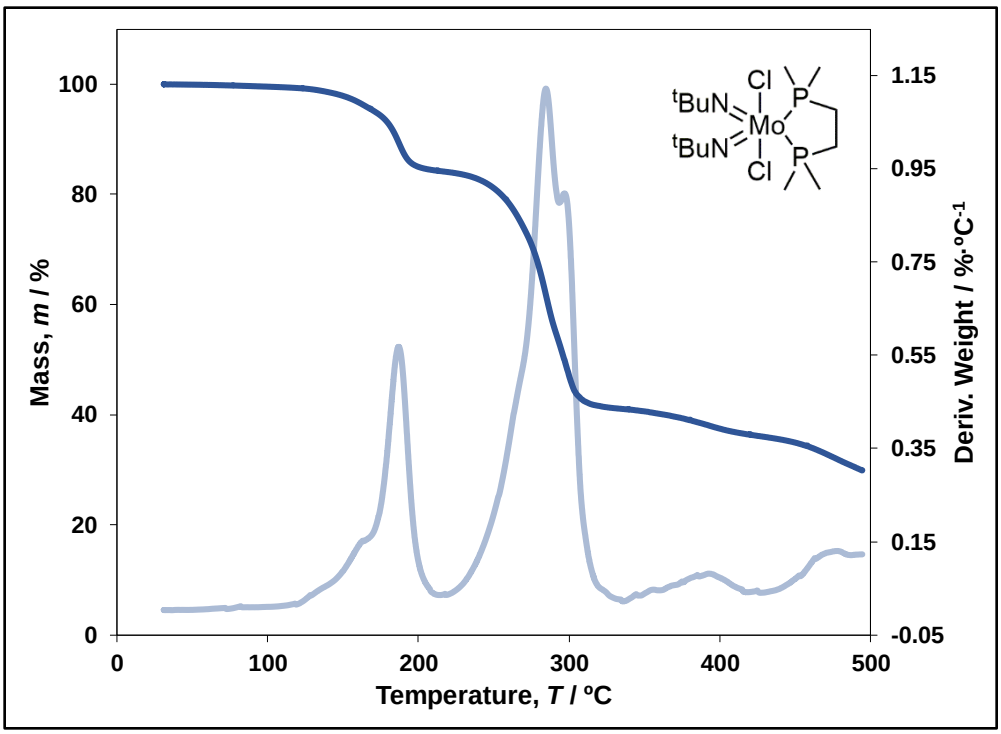

Figure S13: Thermogravimetric analysis of (*t*-BuN=)$_2$MoCl$_2$·dmpe **9** with a heating rate of 10 ºC/min. The mass loading was 10.1 mg and the residual mass was 29.9%. Molybdenum is 20.9 wt% of **9**.

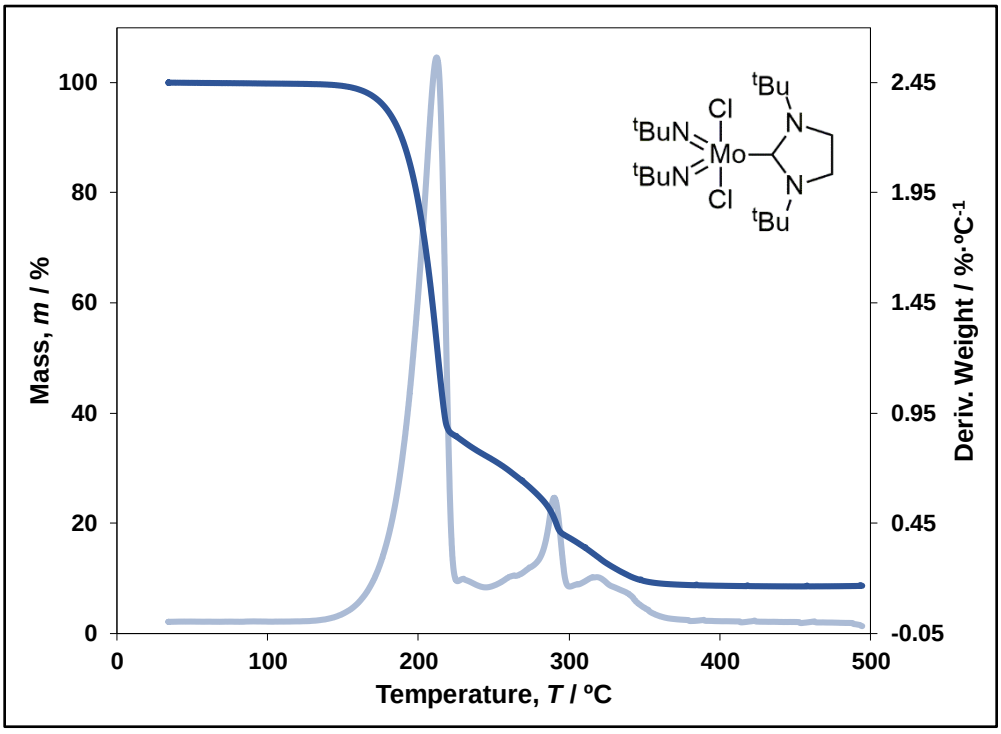

Figure S14: Thermogravimetric analysis of (*t*-BuN=)$_2$MoCl$_2$·(SI*t*-Bu) **10** with a heating rate of 10 ºC/min. The mass loading was 9.8 mg and the residual mass was 8.6%.

Differential Scanning Calorimetry (DSC) Plots

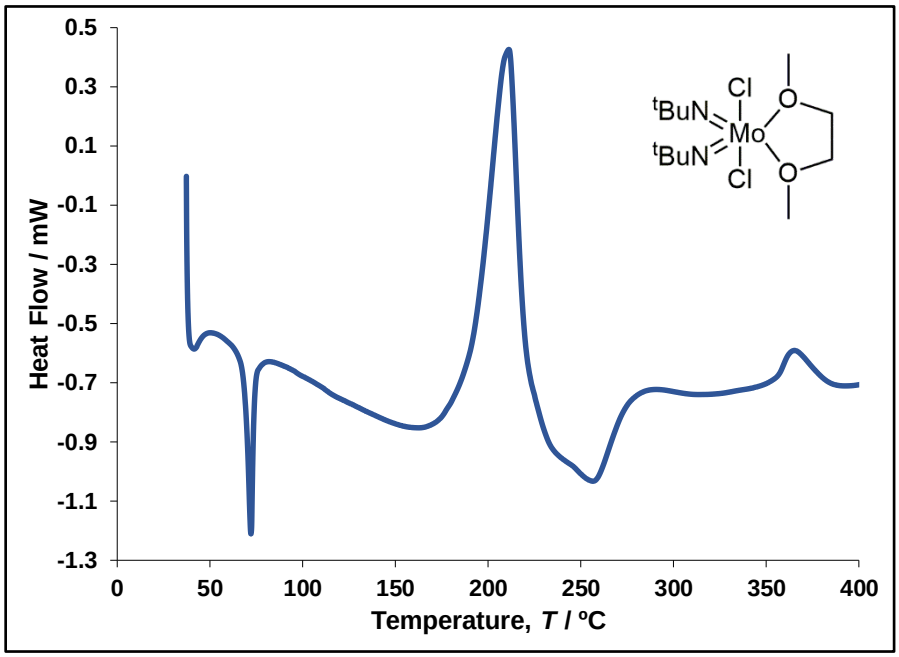

Figure S15: Differential scanning calorimetry plot of (*t*-BuN=)$_2$MoCl$_2$·dme **1** with a heating rate of 10 ºC/min and a mass loading of 0.354 mg. Melting temperature, T_m = 72 ºC, T_D = 178 ºC.

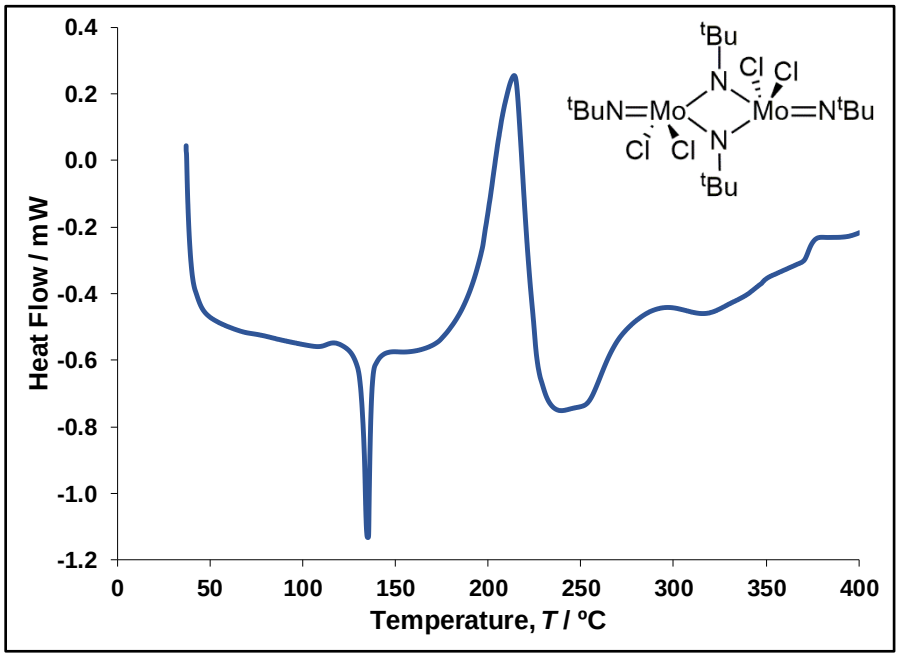

Figure S16: Differential scanning calorimetry plot of [(*t*-BuN=)$_2$MoCl$_2$]$_2$ **2** with a heating rate of 10 ºC/min and a mass loading of 0.289 mg. T_m = 135 ºC, T_D = 175 ºC.

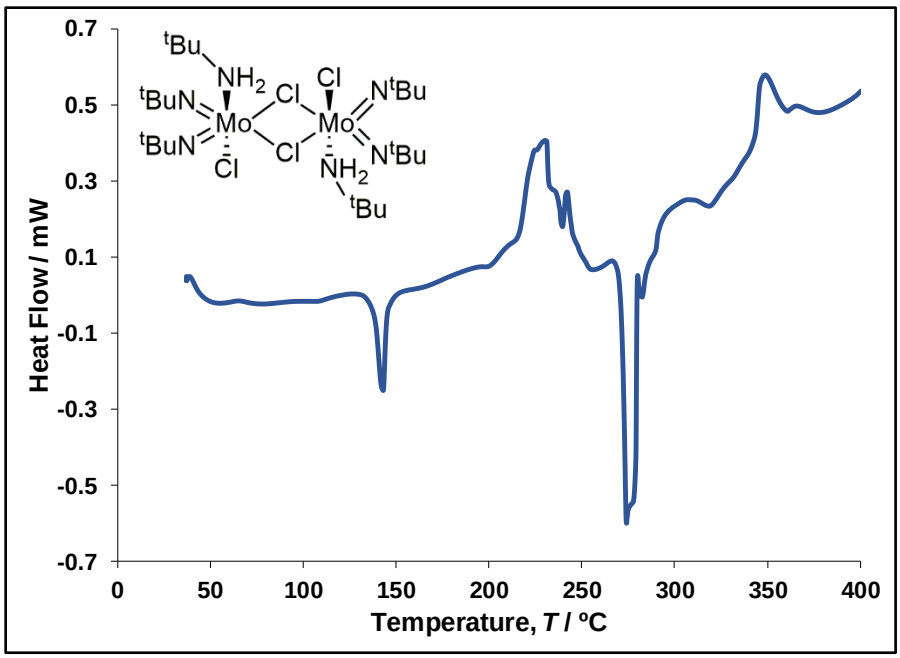

Figure S17: Differential scanning calorimetry plot of $[(t\text{-BuN=})_2MoCl_2\cdot(t\text{-BuNH}_2)]_2$ **3** with a heating rate of 10 ºC/min and a mass loading of 0.373 mg. T_m = 143 ºC, T_D = 203 ºC.

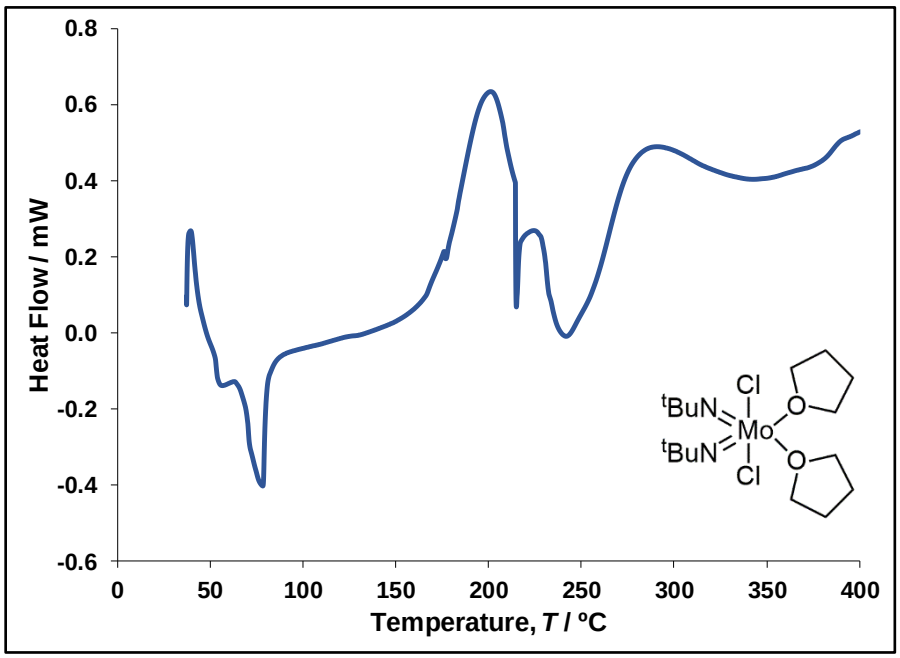

Figure S18: Differential scanning calorimetry plot of $(t\text{-BuN=})_2MoCl_2\cdot(THF)_2$ **4** with a heating rate of 10 ºC/min and a mass loading of 0.538 mg. T_m = 78 ºC, T_D = 152 ºC.

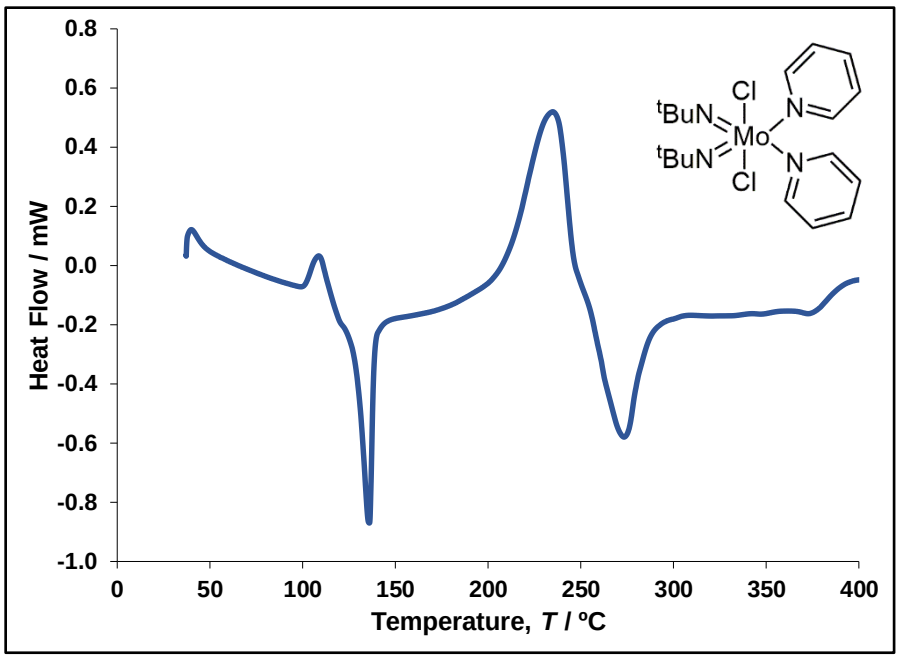

Figure S19: Differential scanning calorimetry plot of (*t*-BuN=)$_2$MoCl$_2$·(py)$_2$ **5** with a heating rate of 10 ºC/min and a mass loading of 0.416 mg. T_m = 136 ºC, T_D = 183 ºC. The second exotherm was chosen as the onset of decomposition. The first exotherm (at 109 ºC) overlaps with the loss of pyridine (by TGA, Figure S9), however, this does not arise from the irreversible decomposition of **5**.

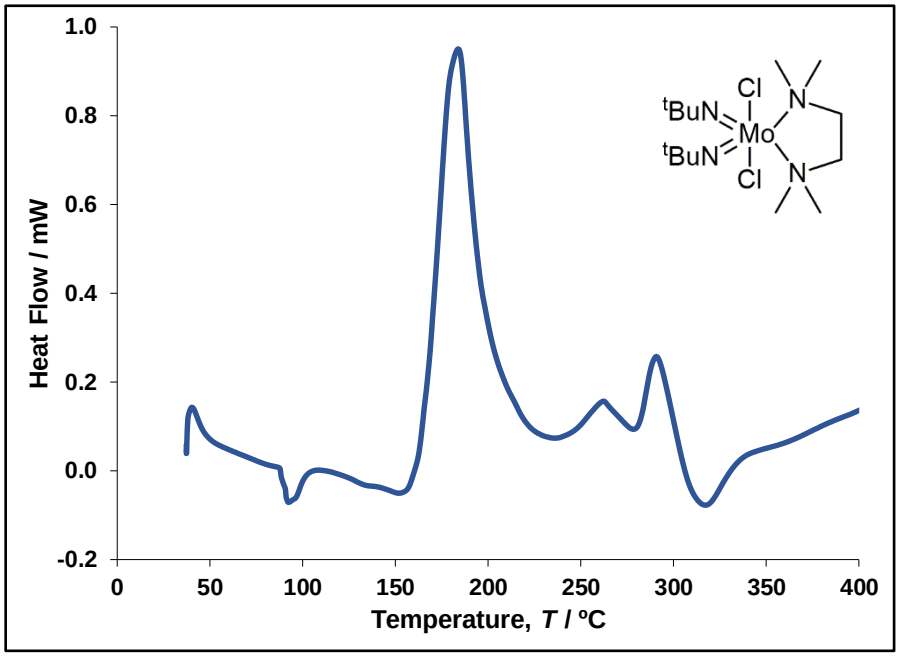

Figure S20: Differential scanning calorimetry plot of (*t*-BuN=)$_2$MoCl$_2$·TMEDA **6** with a heating rate of 10 ºC/min and a mass loading of 0.342 mg. T_m = 92 ºC, T_D = 160 ºC.

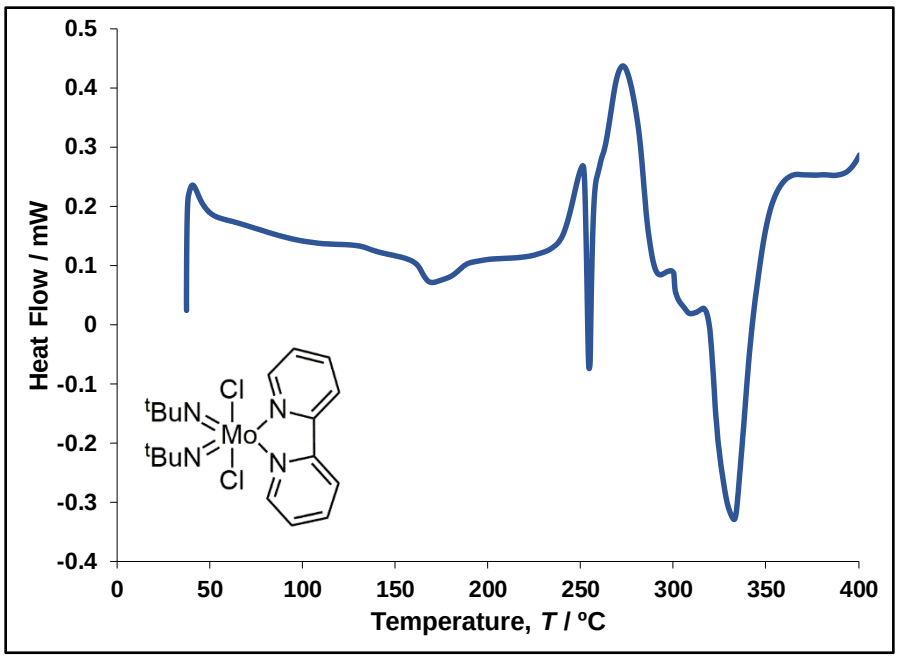

Figure S21: Differential scanning calorimetry plot of (*t*-BuN=)$_2$MoCl$_2$·bpy **7** with a heating rate of 10 ºC/min and a mass loading of 0.375 mg. The sample did not appear to melt prior to decomposition, which was confirmed *via* visual inspection using a melting point apparatus. The endotherm at 170 ºC is likely a solid-solid phase change. T_D = 236 ºC.

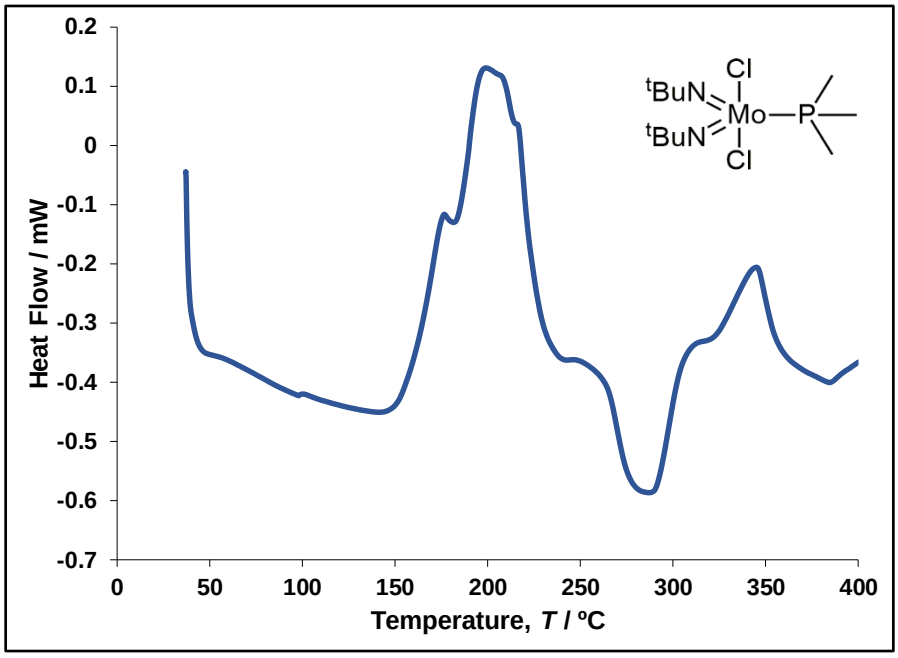

Figure S22: Differential scanning calorimetry plot of (*t*-BuN=)$_2$MoCl$_2$·PMe$_3$ **8** with a heating rate of 10 ºC/min and a mass loading of 0.223 mg. The sample did not appear to melt prior to decomposition, which was confirmed *via* visual inspection using a melting point apparatus. T_D = 151 ºC.

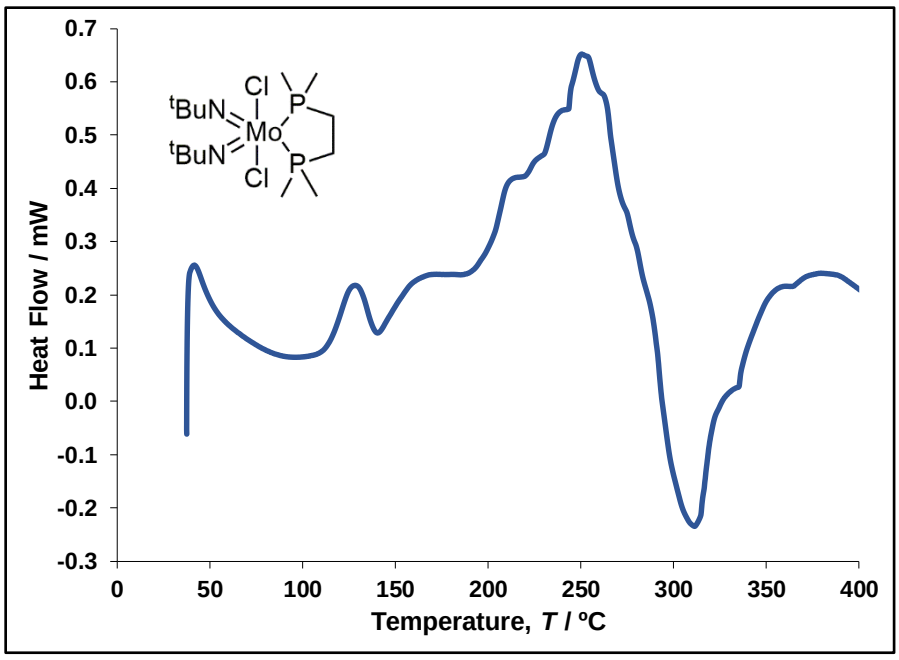

Figure S23: Differential scanning calorimetry plot of (*t*-BuN=)$_2$MoCl$_2$·dmpe **9** with a heating rate of 10 ºC/min and a mass loading of 0.475 mg. The sample did not appear to melt prior to decomposition, which was confirmed *via* visual inspection using a melting point apparatus. T_D = 108 ºC.

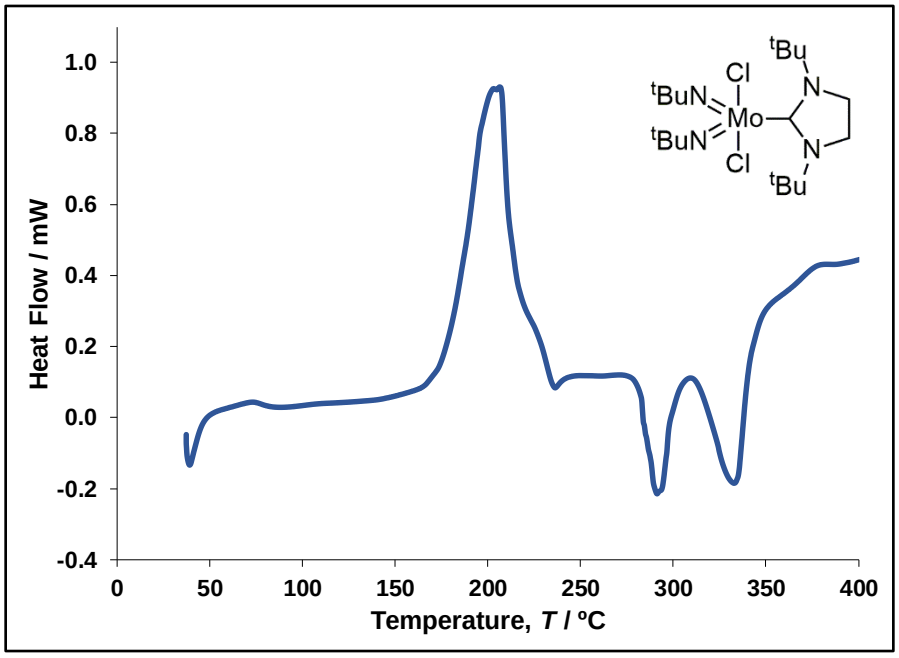

Figure S24: Differential scanning calorimetry plot of (*t*-BuN=)$_2$MoCl$_2$·(SI*t*-Bu) **10** with a heating rate of 10 ºC/min and a mass loading of 0.349 mg. The sample did not appear to melt prior to decomposition, which was confirmed *via* visual inspection using a melting point apparatus. T_D = 167 ºC.

Langmuir Vapor Pressure Curves

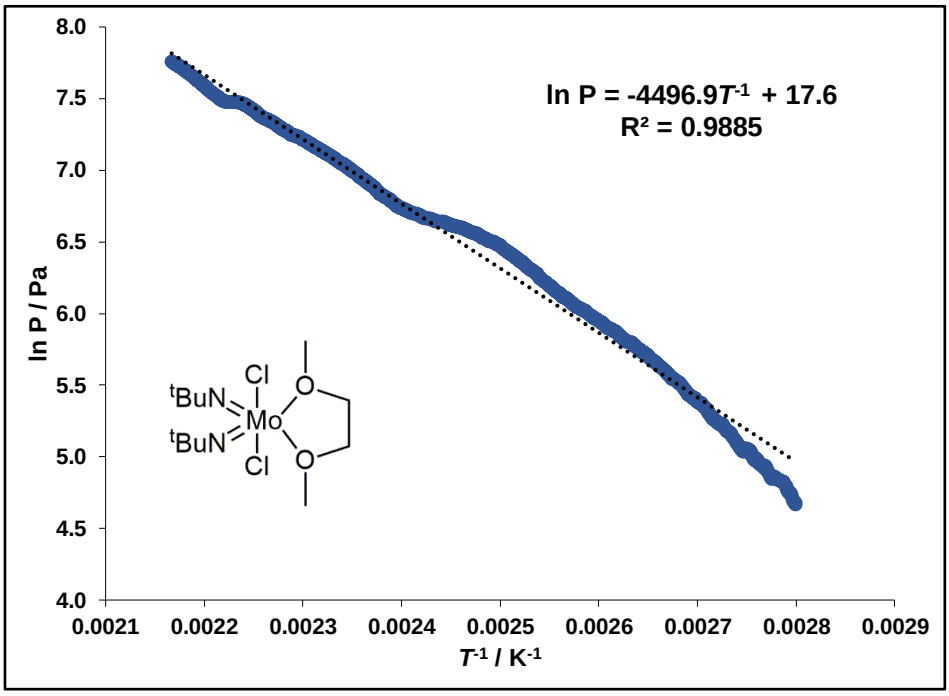

Figure S25: Vapor pressure of (*t*-BuN=)$_2$MoCl$_2$·dme **1** modeled according to the Langmuir equation estimated from TGA (Figure S1). T_V = 82 ºC.

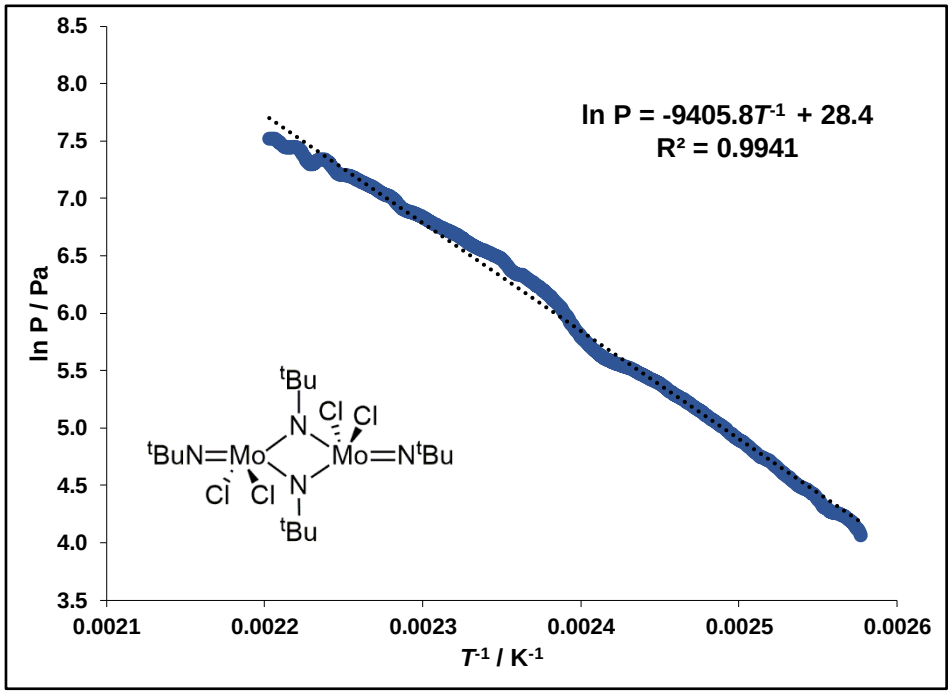

Figure S26: Vapor pressure of [(*t*-BuN=)$_2$MoCl$_2$]$_2$ **2** modeled according to the Langmuir equation estimated from TGA (Figure S6). T_V = 127 ºC.

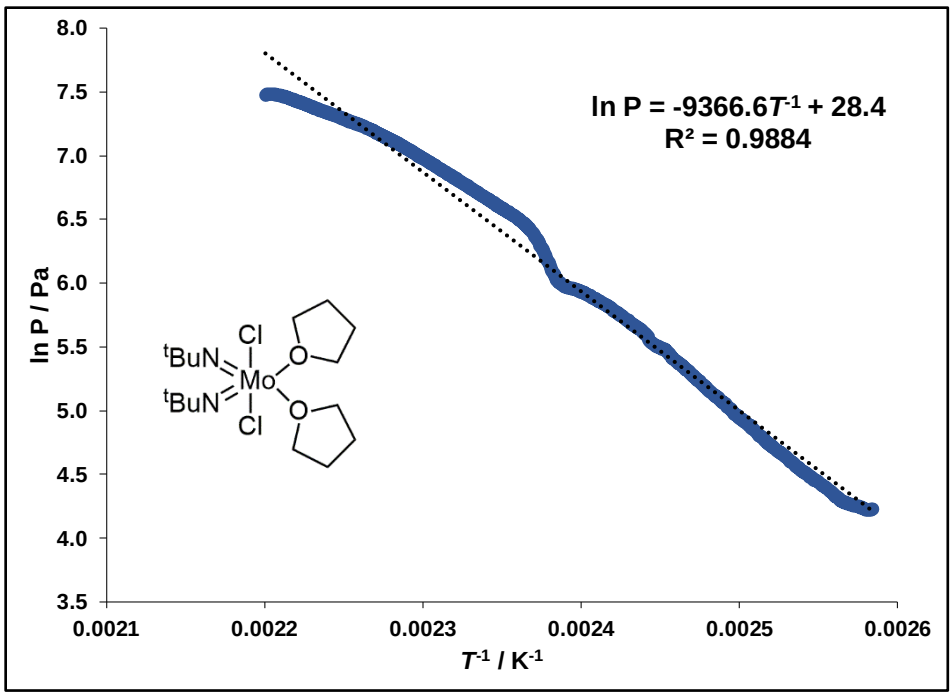

Figure S27: Vapor pressure of (t-BuN=)$_2$MoCl$_2$·(THF)$_2$ **4** modeled according to the Langmuir equation estimated from TGA (Figure S8). T_V = 125 ºC.

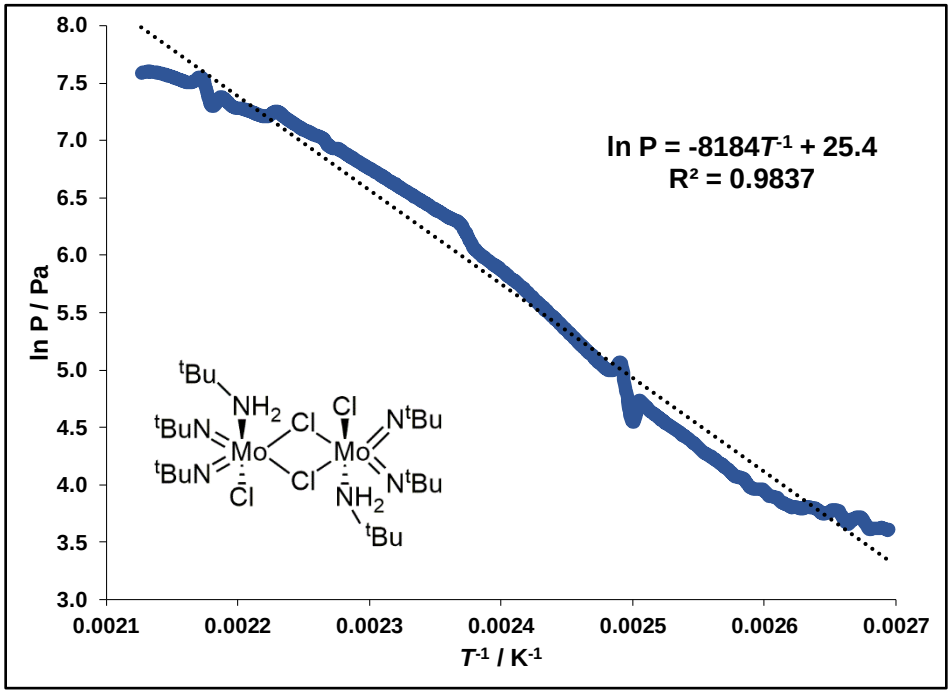

Figure S28: Vapor pressure of [(t-BuN=)$_2$MoCl$_2$·(t-BuNH$_2$)]$_2$ **3** modeled according to the Langmuir equation estimated from TGA (Figure S7). T_V = 126 ºC.

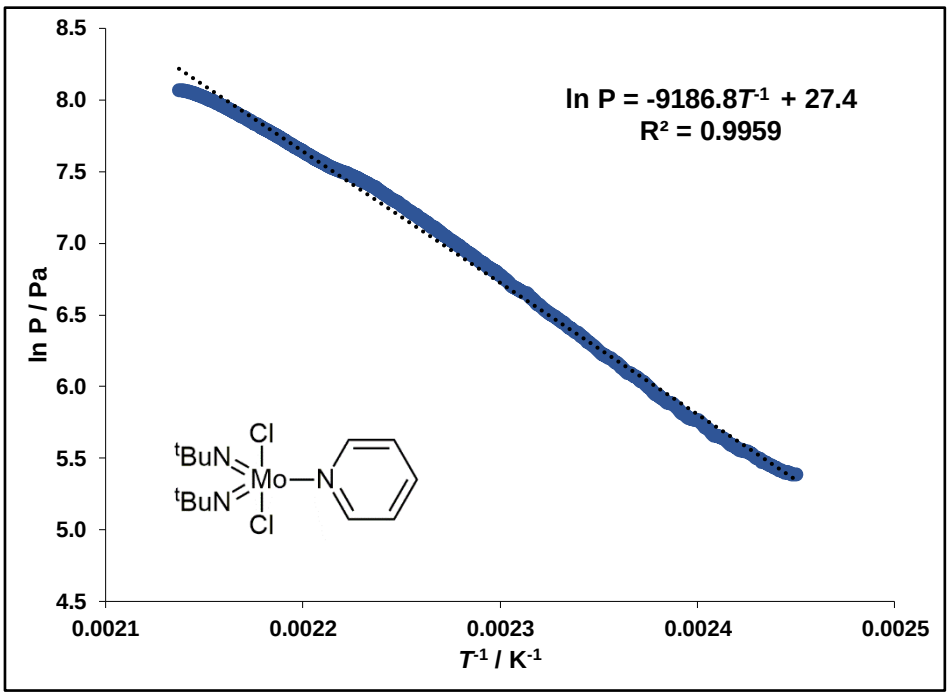

Figure S29: Vapor pressure of (t-BuN=)$_2$MoCl$_2$·(py)$_2$ **5** modeled according to the Langmuir equation estimated from TGA (Figure S9). The TGA has two mass-loss events. The first was attributed to the dissociation of one equivalent of pyridine, resulting in a stable volatile species (the speculated product is shown in the inset). The second mass-loss event was used for this model. T_V = 135 ºC.

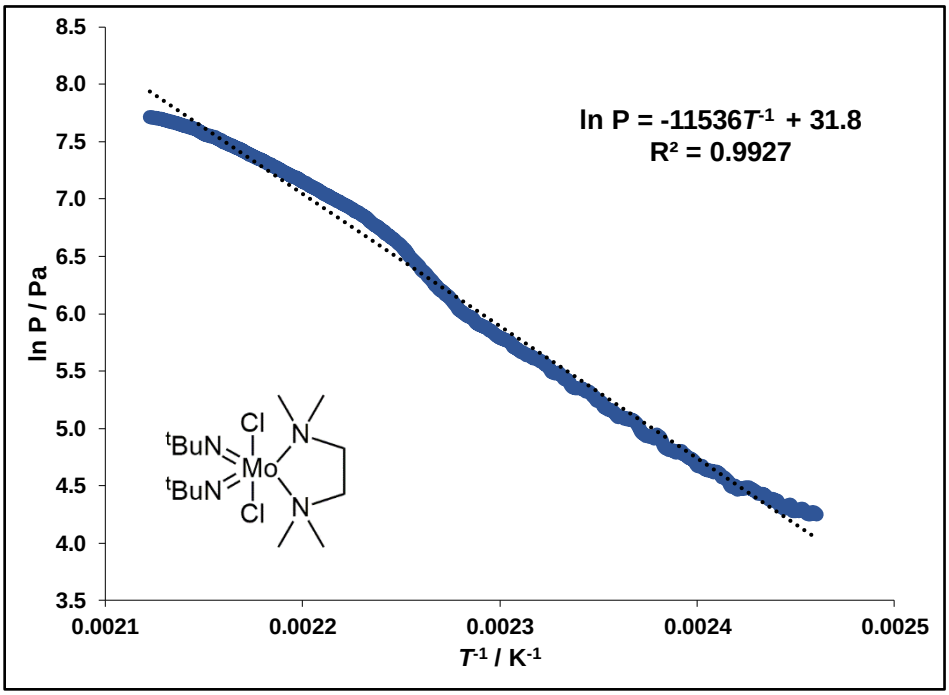

Figure S30: Vapor pressure of (t-BuN=)$_2$MoCl$_2$·TMEDA **6** modeled according to the Langmuir equation estimated from TGA (Figure S10). T_V = 155 ºC.

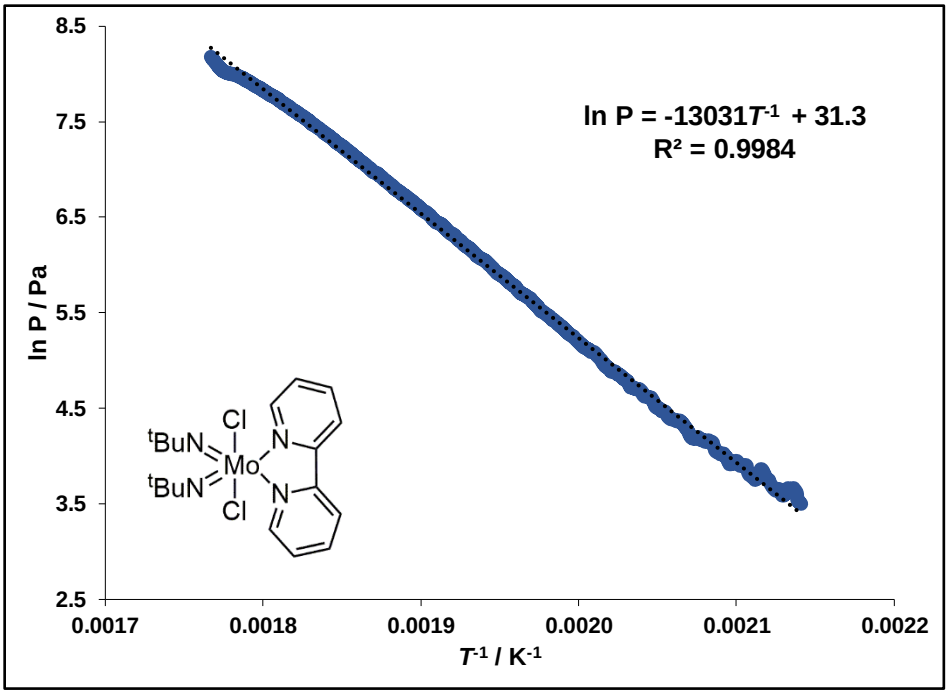

Figure S31: Vapor pressure of (*t*-BuN=)$_2$MoCl$_2$·bpy **7** modeled according to the Langmuir equation estimated from TGA (Figure S11). T_V = 220 ºC.

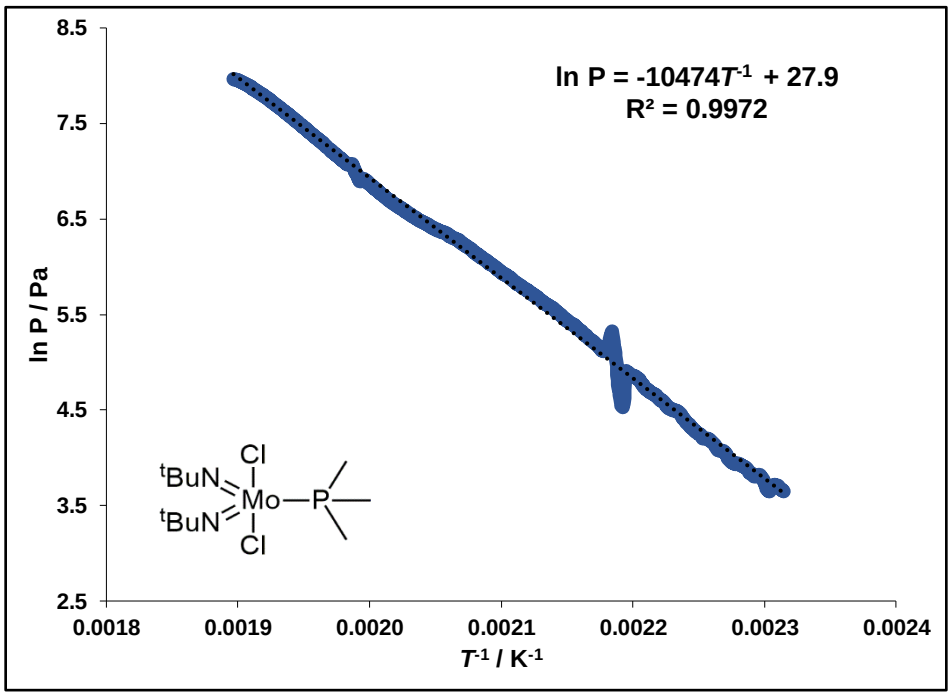

Figure S32: Vapor pressure of (*t*-BuN=)$_2$MoCl$_2$·PMe$_3$ **8** modeled according to the Langmuir equation estimated from TGA (Figure S12). T_V = 183 ºC.

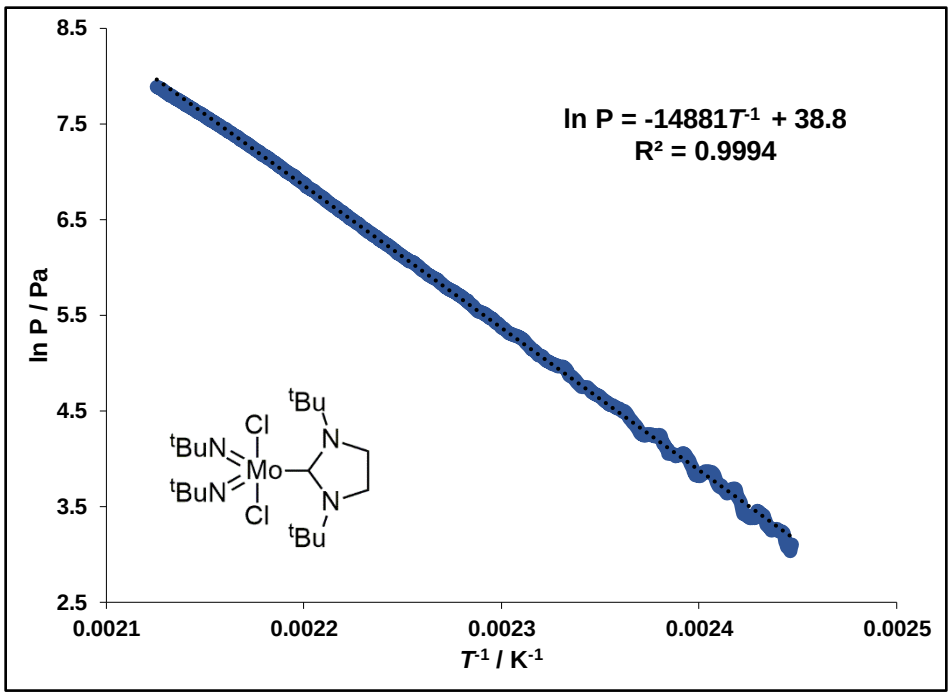

Figure S33: Vapor pressure of (*t*-BuN=)$_2$MoCl$_2$·(SI*t*-Bu) **10** modeled according to the Langmuir equation estimated from TGA (Figure S14). T_V = 165 ºC.

***In Situ* Thermolysis Reactions**

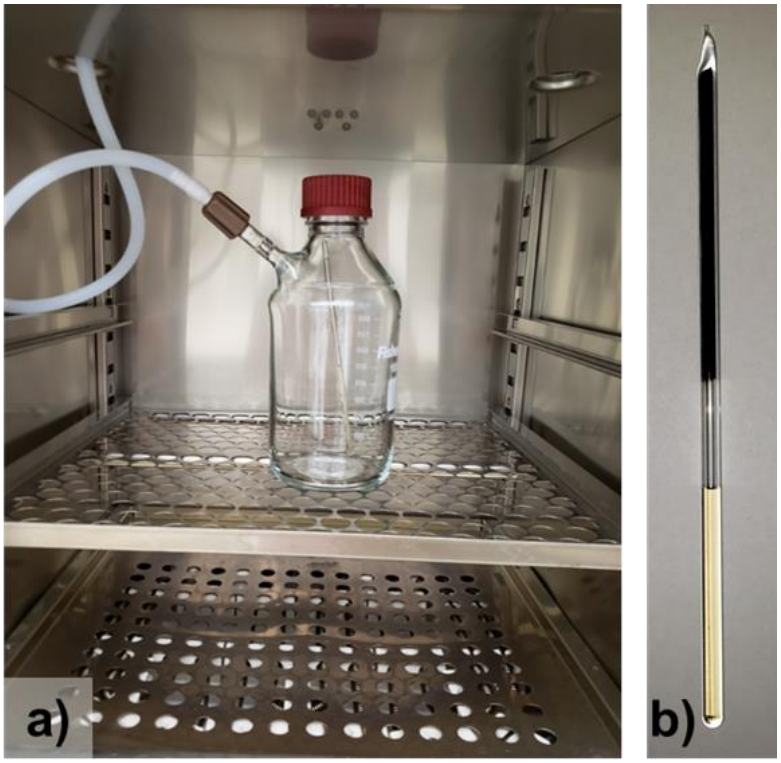

Figure S34: *a)* Photograph showing the experimental setup used for *in situ* thermolysis. The flame-sealed NMR tube was kept inside a glass solvent bottle equipped with a Schlenk tap. The bottle was also kept under a continuous flow of nitrogen and the entire bottle was stored in an oven at 170 °C; *b)* Photograph of the flame-sealed NMR tube containing the thermolysis products of **2** in C_6D_6, after 72 hours. The NMR tube was stored upside-down in the oven because black solids deposited on the inside walls of the NMR tube which affected the shimming.

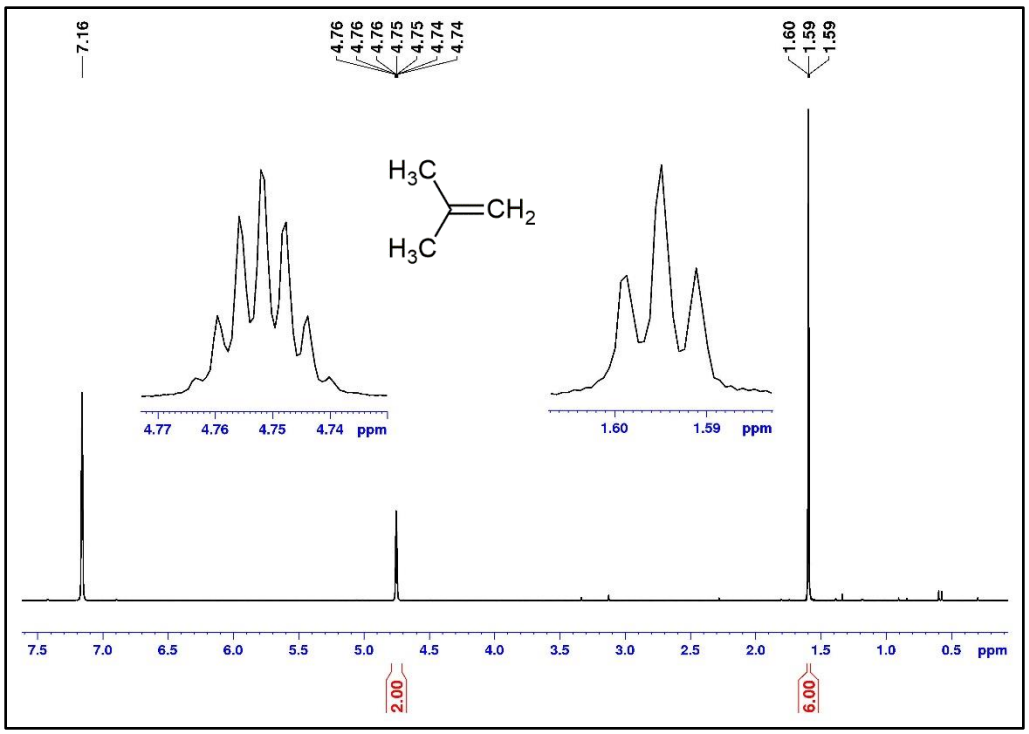

Figure S35: ^{1}H NMR spectrum after the thermolysis of [(*t*-BuN=)$_2$MoCl$_2$]$_2$ **2** in C_6D_6. The flame-sealed NMR tube was stored at 170 ºC for 72 hours; isobutylene was the only product observed.

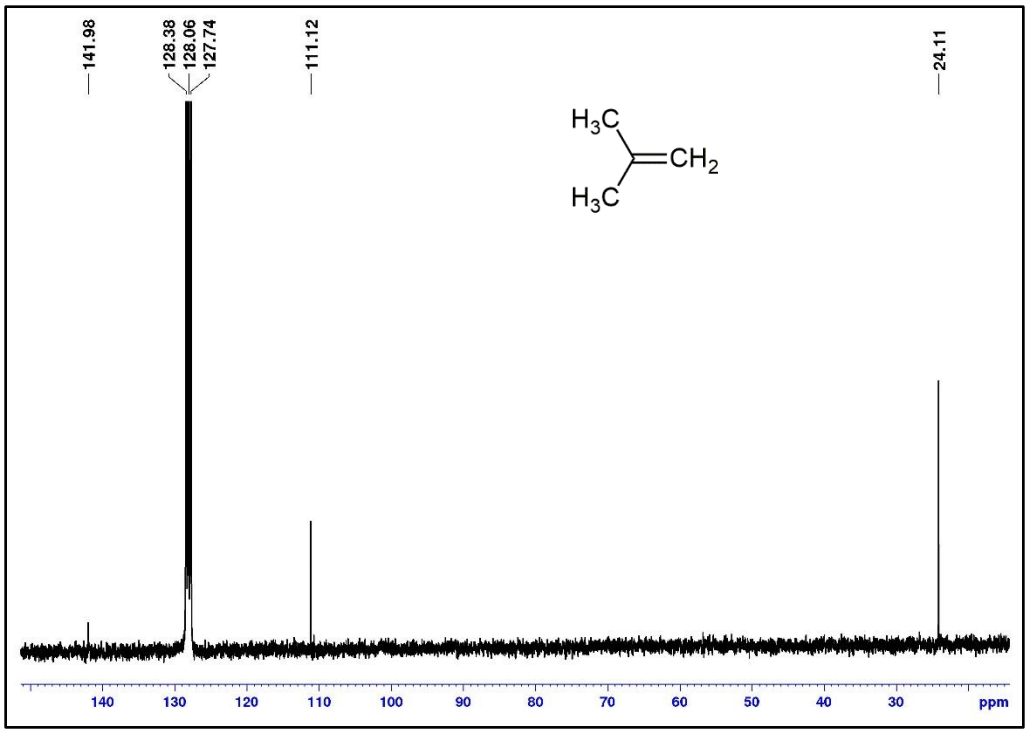

Figure S36: ^{13}C{^{1}H} NMR spectrum after the thermolysis of [(*t*-BuN=)$_2$MoCl$_2$]$_2$ **2** in C_6D_6. The flame-sealed NMR tube was stored at 170 ºC for 72 hours; isobutylene was the only product observed.

Table S1: Kinetic data for the thermolysis of [(*t*-BuN=)$_2$MoCl$_2$]$_2$ **2** in C_6D_6 at 170 ºC, obtained from the relative integration of the ^{1}H NMR spectra. The initial integration (*t* = 0) has been omitted because the integration of **2** drastically decreased almost immediately. This was likely not due to decomposition because the same result was observed after 10 minutes (0.17 h) at 170 ºC. The starting material had completely disappeared, and the formation of isobutylene ceased, somewhere between 26 and 42 hours.

Time, *t* / h	$(CH_3)_2C{=}C\boldsymbol{H}_2$		$(C\boldsymbol{H}_3)_2C{=}CH_2$		[((C***H***$_3$)$_3$CN=)$_2$MoCl$_2$]$_2$	
	Integration	normalized	integration	normalized	integration	normalized
0	--	--	--	--	3.1849	--
0.17	--	--	--	--	1.8964	--
1	0.0056	0.0577	0.0280	0.08270	1.8457	1.0000
3	0.0089	0.0918	0.0372	0.10989	1.7772	0.9629
4	0.0112	0.1155	0.0545	0.1610	1.7078	0.9253
5	0.0143	0.1474	0.0587	0.1734	1.6849	0.9129
20	0.0654	0.6742	0.2375	0.7014	1.1636	0.6304
22	0.0757	0.7804	0.2714	0.8015	1.0809	0.5856
24	0.0890	0.9175	0.3127	0.9235	0.9565	0.5182
26	0.0970	1.0000	0.3386	1.0000	0.8459	0.4583

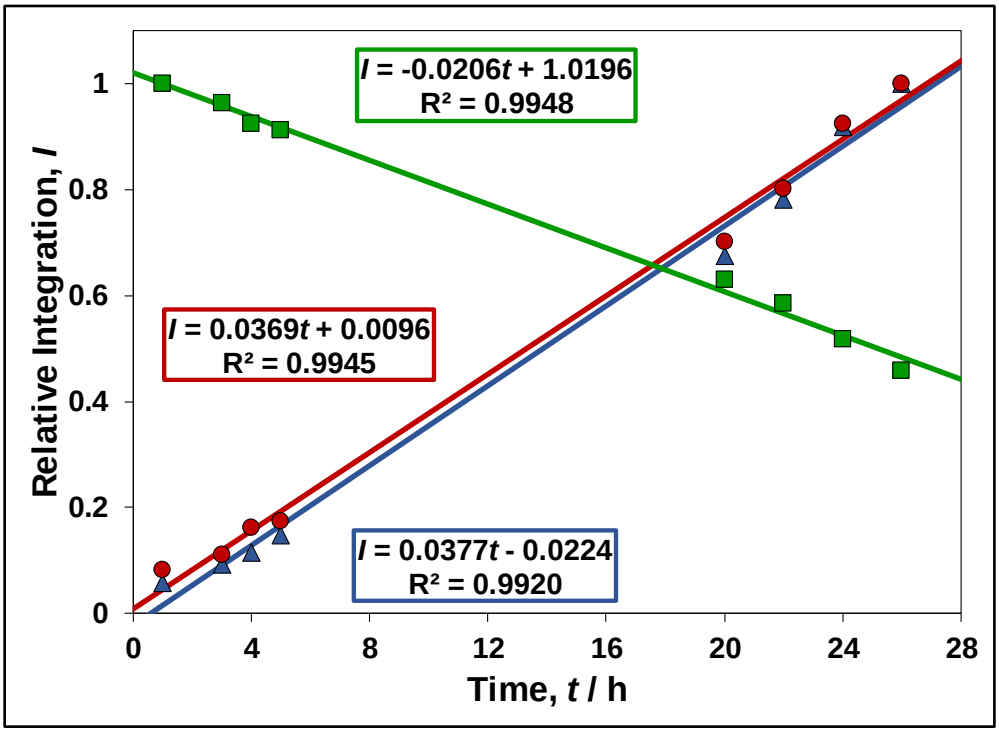

Figure S37: Rate of decomposition of [(t-BuN=)$_2$MoCl$_2$]$_2$ **2** (green squares) in C_6D_6 at 170 ºC and the rate of formation of isobutylene ($(CH_3)_2C{=}C\boldsymbol{H}_2$: blue triangles, & $(C\boldsymbol{H}_3)_2C{=}CH_2$: red circles). The integration is normalized and is displayed in arbitrary units. The linear trend is indicative of a zero-order decomposition.

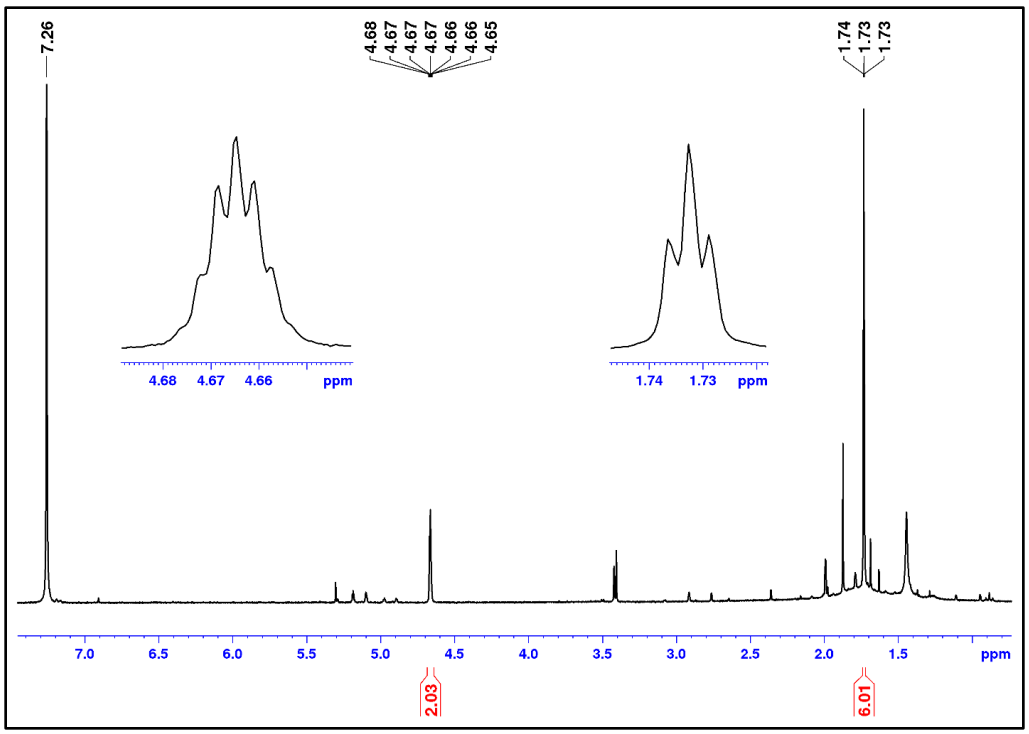

Figure S38: ^{1}H NMR spectrum after the thermolysis of (*t*-BuN=)$_2$MoCl$_2$·dmpe **9** in CDCl$_3$. The flame-sealed NMR tube was stored at 170 ºC for 20 hours. The inset peaks show the formation of isobutylene; the other decomposition product(s) have not been assigned or identified.

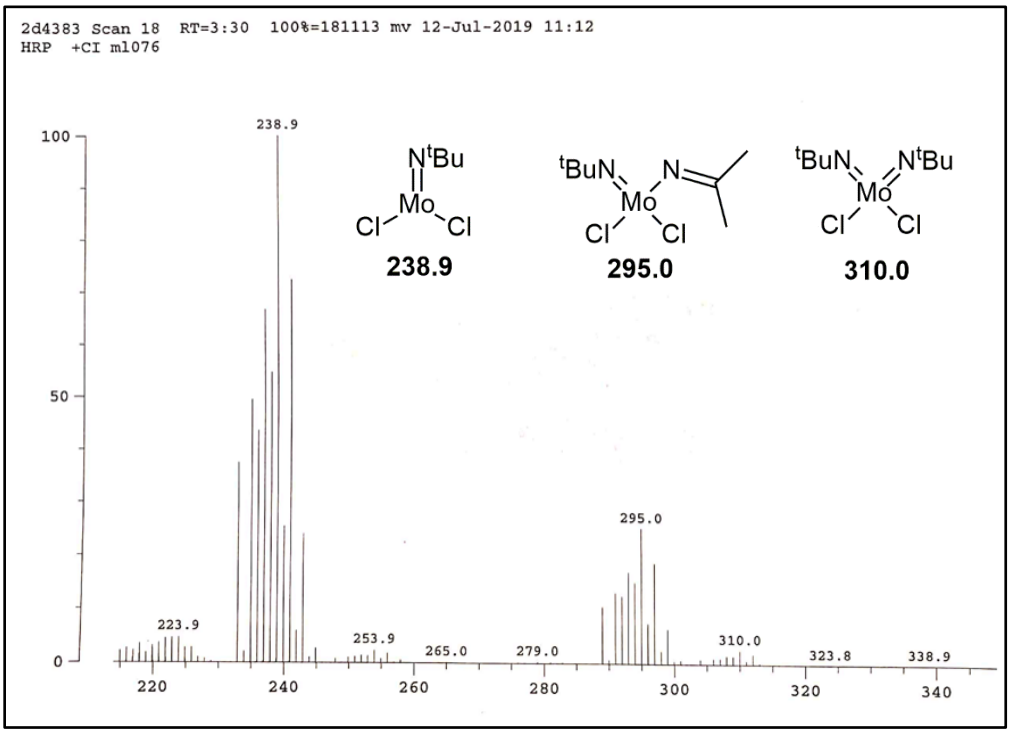

Figure S39: EI-MS (+ve mode) spectrum of [(*t*-BuN=)$_2$MoCl$_2$]$_2$ **2**. The dimer was not detected, as it may not form a stable ion in the gas phase. Insets show the proposed fragmentation products which are supported by their high-resolution accurate masses and isotopic ratios.

Energy Dispersive X-Ray Spectroscopy (EDS) of Decomposition Products

The materials used for EDS were the residual solids that remained in the pans after TGA. The decomposition products were mounted on conductive carbon tape. Scanning electron microscopy (SEM) and EDS was performed at the Carleton University Nano Imaging Facility using a Tescan Vega-II XMU SEM and Oxford Inca Energy 250X EDS.

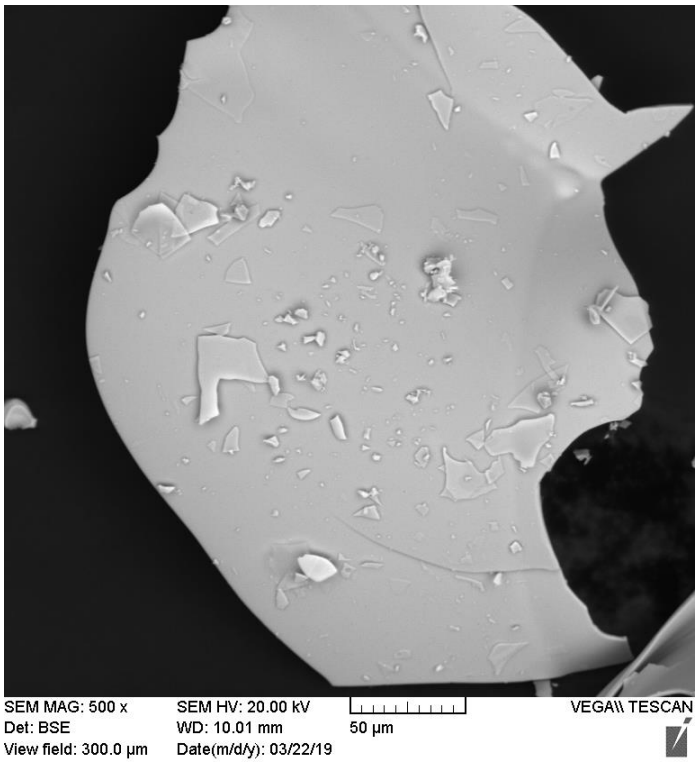

Figure S40: SEM image of the non-volatile decomposition product from the thermolysis of (*t*BuN=)$_2$MoCl$_2$·dme **1** at 500 ºC.

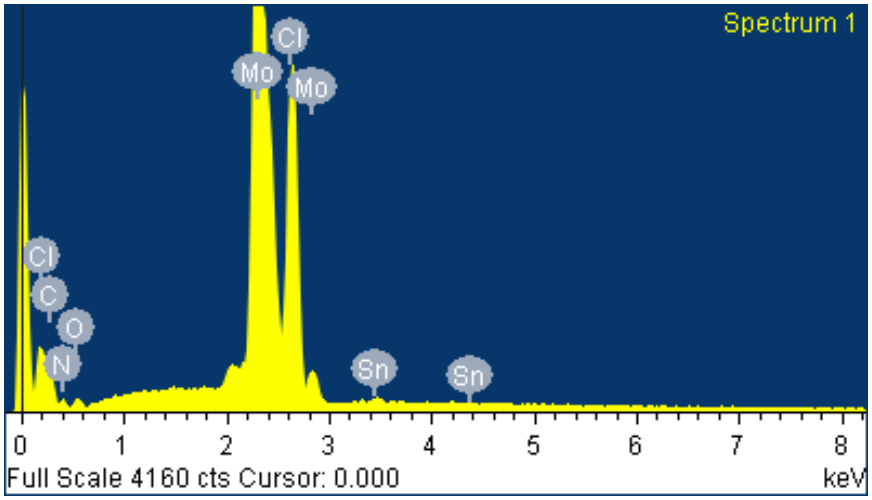

Figure S41: EDS spectrum of the residue shown in Figure S41. The tin is likely a trace impurity from the TGA pan.

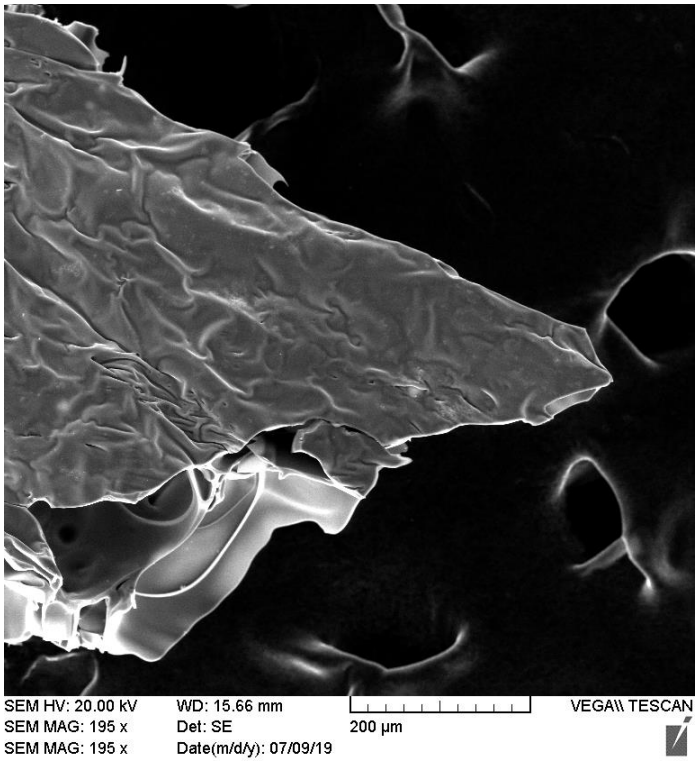

Figure S42: SEM image of the non-volatile decomposition product from the thermolysis of (tBuN=)$_2$MoCl$_2$·dmpe **9** at 500 ºC.

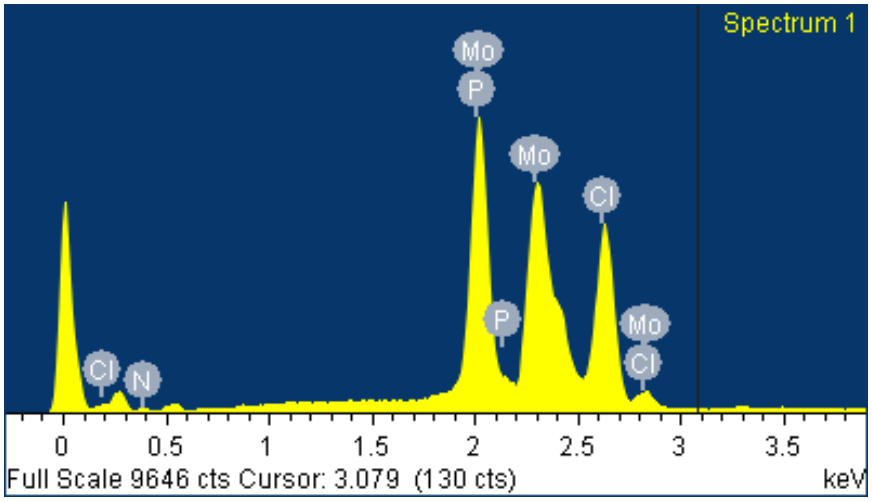

Figure S43: EDS spectrum of the residue shown in Figure S42.

Additional Crystallographic Details and Images

Table S2: Crystal data and structure refinement details.

Identification code	**1**	**2**	**4**	**6**	**7**	**8**	**9**	**10**	**13**
Empirical formula	$C_{12}H_{28}Cl_2MoN_2O_2$	$C_{16}H_{36}Cl_4Mo_2N_4$	$C_{16}H_{34}Cl_2MoN_2O_2$	$C_{14}H_{34}Cl_2MoN_4$	$C_{27}H_{35}Cl_2MoN_4$	$C_{11}H_{27}Cl_2MoN_2P$	$C_{14}H_{34}Cl_2MoN_2P_2$	$C_{19}H_{40}Cl_2MoN_4$	$C_{40}H_{84}Cl_5Mo_2N_9$
Formula weight	399.20	618.17	453.29	425.29	582.43	385.15	459.21	491.39	1061.17
Temperature (K)	125(2)	125(2)	125(2)	125(2)	125(2)	125(2)	125(2)	125(2)	125(2)
Wavelength (Å)	0.71073	0.71073	0.71073	0.71073	0.71073	0.71073	0.71073	0.71073	0.71073
Crystal system	Orthorhombic	Monoclinic	Monoclinic	Orthorhombic	Triclinic	Orthorhombic	Monoclinic	Orthorhombic	Monoclinic
Space group	*Pbca*	$P2_1/n$	$P2_1/c$	*Pbca*	*P*-1	$P2_12_12_1$	$P2_1/c$	*Pnma*	$P2_1/c$
Unit cell dimensions (Å and º)	a = 9.8388(9)	a = 8.8646(10)	a = 12.1959(14)	a = 14.5829(10)	a = 8.9891(9)	a = 8.7819(13)	a = 17.1196(16)	a = 17.511(4)	a = 14.014(2)
	b = 12.4644(12)	b = 16.4145(19)	b = 11.7126(13)	b = 16.5812(12)	b = 11.3454(12)	b = 14.066(2)	b = 9.9078(9)	b = 10.603(2)	b = 14.186(2)
	c = 29.816(3)	c = 9.1243(11)	c = 15.2142(17)	c = 17.0500(12)	c = 14.8627(15)	c = 14.662(2)	c = 13.5612(13)	c = 12.816(3)	c = 27.556(4)
	α = 90	α = 90	α = 90	α = 90	α = 70.9630(10)	α = 90	α = 90	α = 90	α = 90
	β = 90	β = 103.1780(10)	β = 95.7124(11)	β = 90	β = 87.9710(10)	β = 90	β = 106.8553(10)	β = 90	β = 91.855(2)
	γ = 90	γ = 90	γ = 90	γ = 90	γ = 82.0900(10)	γ = 90	γ = 90	γ = 90	γ = 90
Volume (Å^3)	3656.4(6)	1292.7(3)	2162.5(4)	4123.7(5)	1419.2(3)	1811.1(5)	2201.4(4)	2379.5(8)	5475.4(14)
Z	8	2	4	8	2	4	4	4	4
Density (calculated, Mg/m^3)	1.450	1.588	1.392	1.370	1.363	1.413	1.386	1.372	1.287
Absorption coefficient (mm^{-1})	1.010	1.392	0.863	0.896	0.672	1.093	0.981	0.786	0.728
F(000)	1648	624	944	1776	602	792	952	1032	2227
Crystal size (mm^3)	0.380 x 0.220 x 0.090	0.525 x 0.310 x 0.250	0.330 x 0.200 x 0.190	0.375 x 0.319 x 0.259	0.325 x 0.300 x 0.300	0.325 x 0.300 x 0.275	0.600 x 0.185 x 0.150	0.312 x 0.175 x 0.112	0.300 x 0.225 x 0.110
Theta range of data (º)	1.366 to 28.850	2.891 to 28.883	1.678 to 28.928	2.210 to 28.935	1.449 to 28.939	2.006 to 28.950	1.243 to 28.880	1.969 to 27.000	1.454 to 27.331
Index ranges	$-12 \le h \le 12$	$-11 \le h \le 11$	$-16 \le h \le 16$	$-19 \le h \le 19$	$-12 \le h \le 12$	$-11 \le h \le 11$	$-22 \le h \le 22$	$-22 \le h \le 22$	$-18 \le h \le 17$
	$-16 \le k \le 16$	$-22 \le k \le 21$	$-15 \le k \le 15$	$-22 \le k \le 21$	$-14 \le k \le 14$	$-19 \le k \le 18$	$-13 \le k \le 13$	$-13 \le k \le 13$	$-18 \le k \le 18$
	$-39 \le l \le 38$	$-12 \le l \le 12$	$-20 \le l \le 19$	$-22 \le l \le 22$	$-19 \le l \le 19$	$-19 \le l \le 19$	$-18 \le l \le 17$	$-16 \le l \le 16$	$-35 \le l \le 35$
Reflections collected	41500	15354	25782	47382	17307	22036	25944	25024	62853
Independent reflections	4626	3229	5415	5265	6843	4542	5469	2747	12322
R(int)	0.0272	0.0130	0.0190	0.0192	0.0137	0.0147	0.0260	0.0754	0.0880
Completeness to 25.242º (%)	99.9	99.9	100.0	100.0	99.8	99.9	100.0	100.0	99.9
Absorption correction	Semi-empirical from equivalents	Semi-empirical from equivalents	Semi-empirical from equivalents	Semi-empirical from equivalents	Semi-empirical from equivalents	Semi-empirical from equivalents	Semi-empirical from equivalents	Semi-empirical from equivalents	Semi-empirical from equivalents
Max. and min. transmission	0.7458 and 0.6611	0.7458 and 0.6452	0.7458 and 0.6844	0.7458 and 0.6890	0.7458 and 0.7052	0.7458 and 0.6967	0.7458 and 0.6745	0.7455 and 0.6618	0.7455 and 0.6766
Refinement method	Full-matrix least-squares on F^2	Full-matrix least-squares on F^2	Full-matrix least-squares on F^2	Full-matrix least-squares on F^2	Full-matrix least-squares on F^2	Full-matrix least-squares on F^2	Full-matrix least-squares on F^2	Full-matrix least-squares on F^2	Full-matrix least-squares on F^2
Data / restrains / parameters	4626 / 0 / 180	3229 / 0 / 124	5415 / 234 / 300	5265 / 122 / 277	6843 / 0 / 313	4542 / 145 / 203	5469 / 0 / 200	2747 / 211 / 215	12322 / 1102 / 733
Goodness-of-fit on F^2	1.050	1.126	1.052	1.080	1.031	1.084	1.026	1.037	1.098
Final R indices [I>2sigma(I)]	R1 = 0.0201	R1 = 0.0143	R1 = 0.0269	R1 = 0.0212	R1 = 0.0192	R1 = 0.0129	R1 = 0.0214	R1 = 0.0305	R1 = 0.1020
	wR2 = 0.0448	wR2 = 0.0367	wR2 = 0.0667	wR2 = 0.0516	wR2 = 0.0509	wR2 = 0.0345	wR2 = 0.0495	wR2 = 0.0642	wR2 = 0.2319
R indices (all data)	R1 = 0.0278	R1 = 0.0148	R1 = 0.0307	R1 = 0.0259	R1 = 0.0210	R1 = 0.0133	R1 = 0.0280	R1 = 0.0492	R1 = 0.1525
	wR2 = 0.0480	wR2 = 0.0370	wR2 = 0.0692	wR2 = 0.0551	wR2 = 0.0521	wR2 = 0.0348	wR2 = 0.0521	wR2 = 0.0708	wR2 = 0.2552
Extinction coefficient	n/a	n/a	n/a	n/a	n/a	n/a	n/a	n/a	n/a
Largest diff. peak and hole (e.Å^{-3})	0.369 and -0.355	0.376 and -0.298	1.830 and -0.707	0.578 and -0.327	0.433 and -0.311	0.226 and -0.374	0.443 and -0.351	0.461 and -0.333	2.553 and -1.346

Specific details of individual refinements:

Compound **1**
In the final refinement one reflection was omitted (1 1 23) because of poor agreement between F^2_{obs} and F^2_{calc}.

Compound **2**
Three reflections with poor agreements between F^2_{obs} and F^2_{calc} were removed from the final refinement (1 1 0; 0 1 1; 0 2 0).

Compound **4**
There was some minor disorder in the structure, involving one of the THF rings and the *tert*-butyl group coordinated *trans* to it across the Mo center. Each was split over two positions with the occupancies of each part refined. The CO and CC bond lengths in the disordered THF ring were restrained to be similar using individual SADI commands. All of the disordered ring carbon atoms were restrained to have similar atomic displacement parameters. The THF disorder refined to a ratio of 53.9(16)/46.1 % for parts 1 and 2, respectively. The same types of restraints were used on the disordered *tert*-butyl group, where the CC bonds lengths and the thermal parameters of the carbon atoms were restrained to be similar. The *tert*-butyl disorder refined to a ratio of 82.2(7)/17.8 % for parts 1 and 2, respectively.

Compound **6**
20 second frames were used in this data collection. There was some disorder in the structure, involving the N_2C_6 ring (TMEDA ligand). The ring atoms were split over two positions with the occupancies of each part refined. A SAME instruction was used to add restraints to keep the two parts similar. Around the ring, each type of bond, MoN, NC and CC, was restrained to be of similar length. The carbon atoms of the ring were restrained to have similar thermal parameters, as were the nitrogen atoms. The occupancies of the disordered ring refined to 62.2(5)/37.8% for part 1 and part 2, respectively.

Compound **8**
There was some minor disorder in the structure, involving one of the *tert*-butyl groups. It was split over two positions with the occupancies of each part refined (88.21% and 11.79% with a standard uncertainty of 0.46%). A SAME instruction was used to add restraints to keep the geometries of the two parts similar. SIMU restraints were used to keep the CN and CC bonds of the disordered group of reasonable lengths. Finally, all of the disordered *tert*-butyl methyl carbon atoms were restrained to have similar atomic displacement parameters and the atoms in the minor component were also restrained to be more isotropic.

Compound **10**
60 second frames were used in this data collection as the crystals were very small and did not diffract well. This data collection had to be stopped about one hour before completion because of a planned power outage. Only 300 of the usual 366 frames in the fourth frame set were collected.

There was considerable disorder in the structure, involving one of the *tert*-butyl groups on the ring and one of the *tert*-butyl group coordinated through nitrogen to the metal. In the latter group, the

two part disorder was modelled by setting the occupancy of each atom to 0.25 because of symmetry. The CN and CC bond lengths in the disordered group were restrained to be similar using individual SADI commands. The 1,3 C…C distances were also restrained using a looser SADI command. All of the disordered carbon atoms were restrained to have similar atomic displacement parameters. The same types of restraints were used on the second disordered ring *tert*-butyl group, where the CC bonds lengths and the thermal parameters of the carbon atoms were restrained to be similar. The occupancies of the atoms in the two parts were refined using a free variable, giving final values of 90.7(5) / 9.3 % for parts 1 and 2, respectively.

Compound **13**

This data set was collected with a 45 second frame time. The resulting structure was very disordered, involving all of the cations and anions in the asymmetric unit. Most of this was just rotating *tert*-butyl groups on the cations and anions. However, in addition one of the Mo anions was occupationally disordered, with one site partially occupied by a chloride group 82.2(12) % of the time and by an acetonitrile-derived cyanomethyl ligand 17.8 % of the time. Multiple restraints were placed on the bond lengths and the thermal parameters to model the disorder present. Even after all of this, several level B alerts remained in the final checkcif file. The first two of these could have been eliminated but were left in place for the following reasons:

(1) Short C(sp^3)−C(sp) Bond C18 − C19 . 1.25 Å. This warning could have been removed if a restraint had been placed on the geometry of the coordinated cyanomethyl groups. This was not done. The structure was left as it refined to be sure that the results were not incorrectly biased.

(2) Long H...A H-Bond Reported H31...Cl5 . 3.30 Å. This warning would also have been eliminated if this hydrogen bond had simply been removed from the parameters calculated. However, it is the second, longer component of a bifurcated hydrogen bonding interaction. It makes quite a linear angle with the C-H group of the imidazolium cation and likely contributes to the hydrogen bonding at that center.

The final warning could not be eliminated.

(3) Check Calcd Resid. Dens. 0.98A From Mo1 2.59 eÅ^{-3}. The value of μ·r was varied when scaling the data, however this did not help to decrease the residual density in the final model. This problem, together with the rather high final residuals of the refinement (level C warnings for R1 and wR2), suggest that the crystal was not of the finest quality and that the overall data collection suffered as a result. This, in turn, was likely the result of having a large, floppy structure that did not pack efficiently.

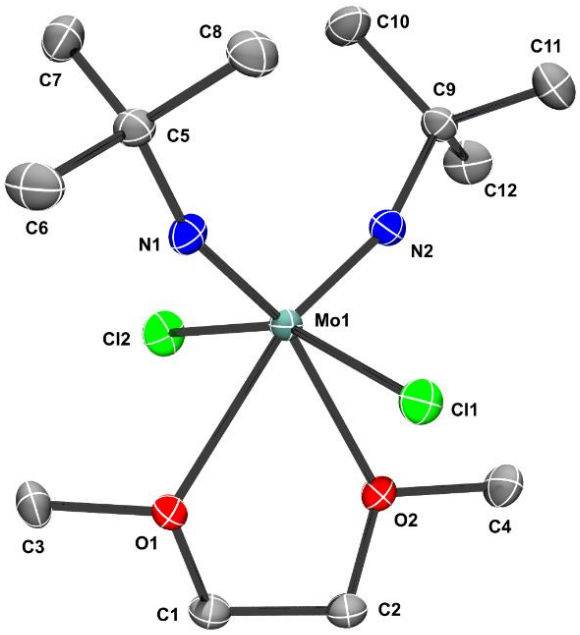

Figure S44: Solid-state structure of (*t*-BuN=)$_2$MoCl$_2$·dme **1** with all heavy atoms labelled. Hydrogen atoms have been omitted for visual clarity. Thermal ellipsoids are drawn at the 50% probability level.

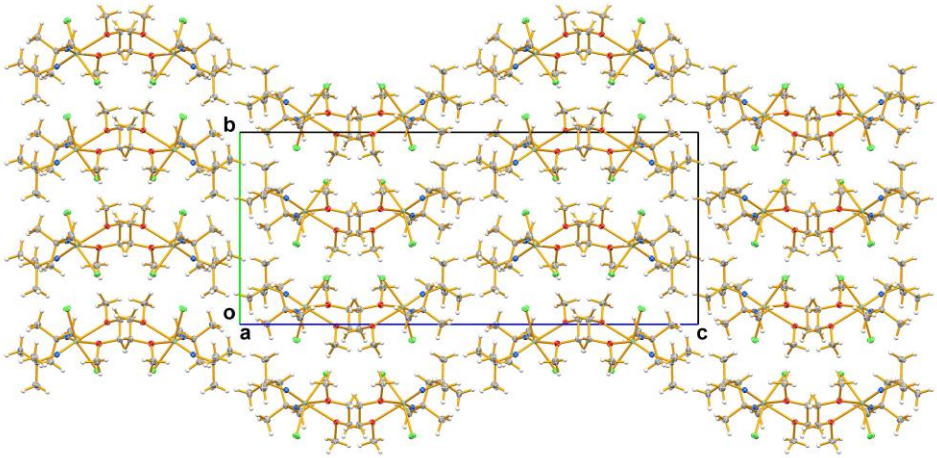

Figure S45: Solid-state packing diagram of (*t*-BuN=)$_2$MoCl$_2$·dme **1**, viewed down the *X*-axis.

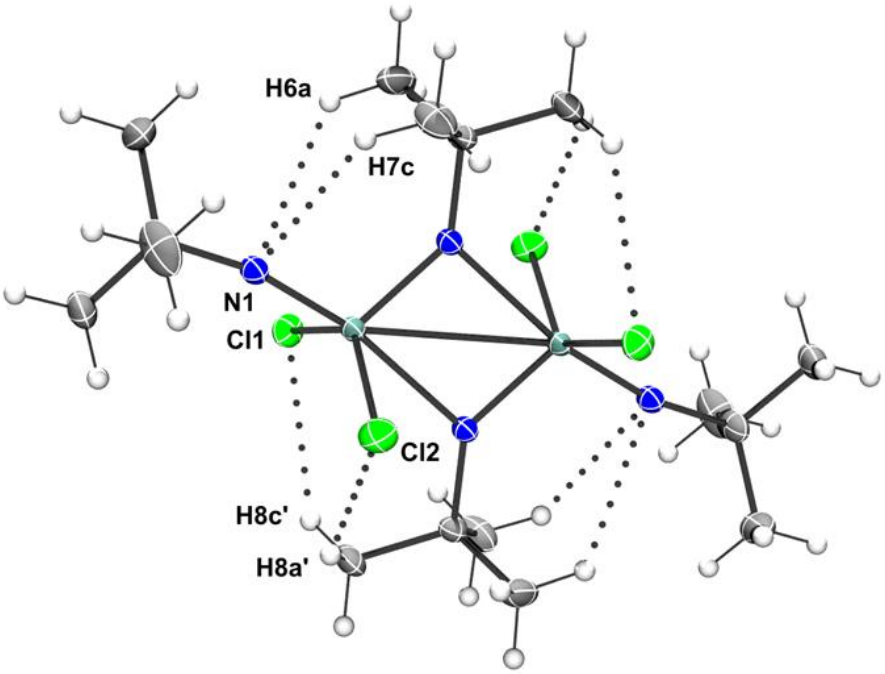

Figure S46: Short intramolecular interactions (below the sum of the Van der Waals radii) that hold the dimer together in the solid-state structure of $[(t\text{-BuN=})_2MoCl_2]_2$ **2**. A fully labelled image can be found in the main text. H6a…N1 = 2.84 Å [C6−H6a…N1 = 129º], H7c…N1 = 2.60 Å [C7−H7c…N1 = 133º], H8c'…Cl1 = 2.76 Å [C8'−H8c'…Cl1 = 133º], H8a'…Cl2 = 2.81 Å [C8'−H8a'…Cl2 = 138º].

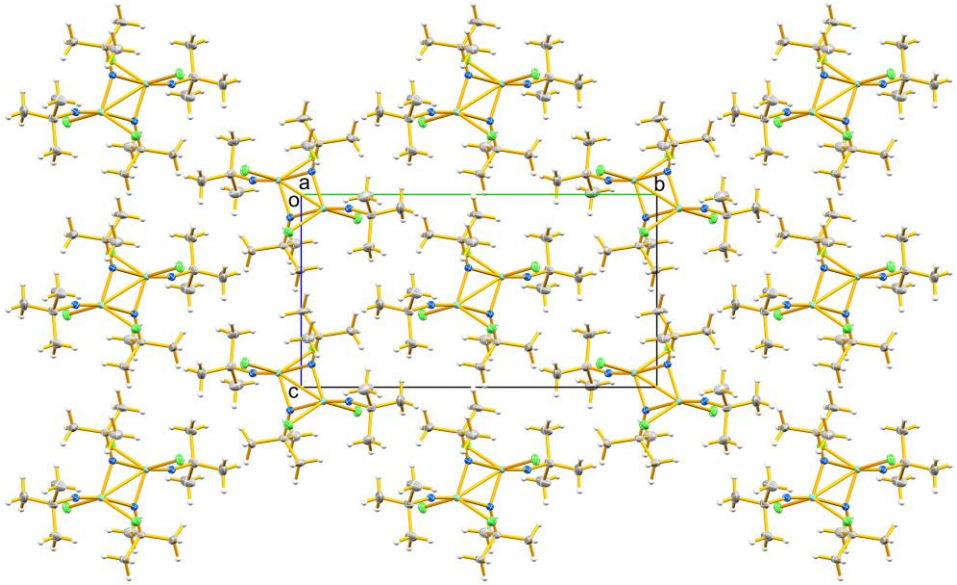

Figure S47: Solid-state packing diagram of $[(t\text{-BuN=})_2MoCl_2]_2$ **2**, viewed down the *X*-axis.

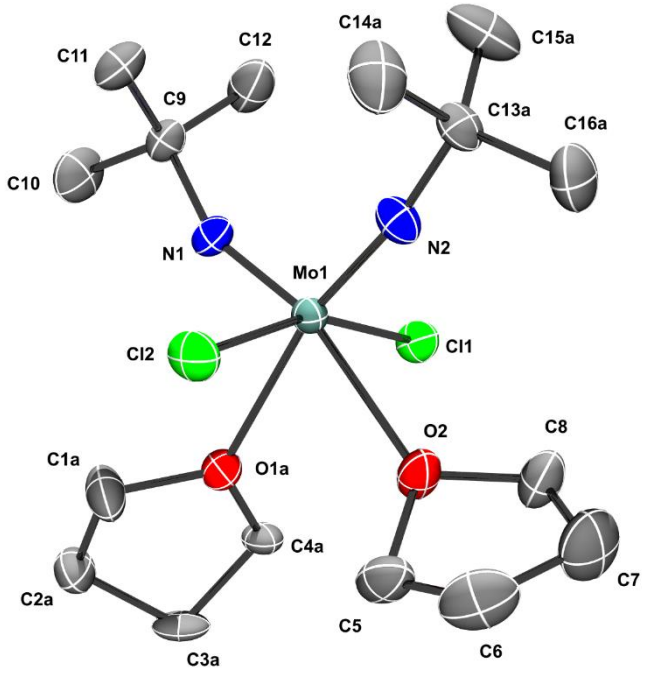

Figure S48: Solid-state structure of (t-BuN=)$_2$MoCl$_2$·(THF)$_2$ **4** with all heavy atoms labelled. Hydrogen atoms have been omitted for visual clarity. Thermal ellipsoids are drawn at the 50% probability level. The *tert*-butyl group attached to N2, and the entire THF ligand containing O1, are disordered over two positions, however, only part A of the disorder is shown for visual clarity.

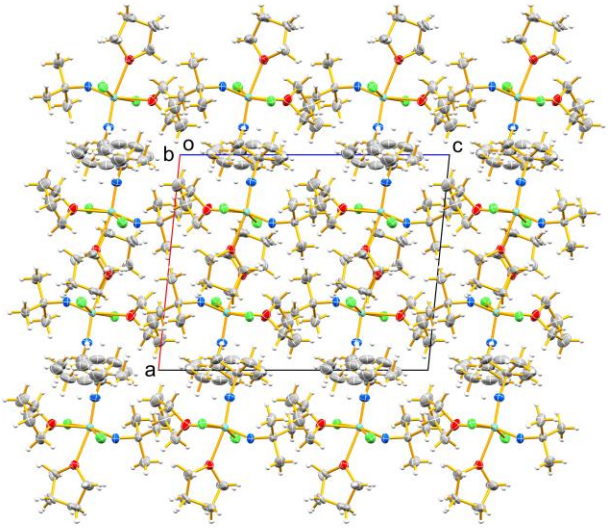

Figure S49: Solid-state packing diagram of [(t-BuN=)$_2$MoCl$_2$]$_2$ **4**, viewed down the *Y*-axis.

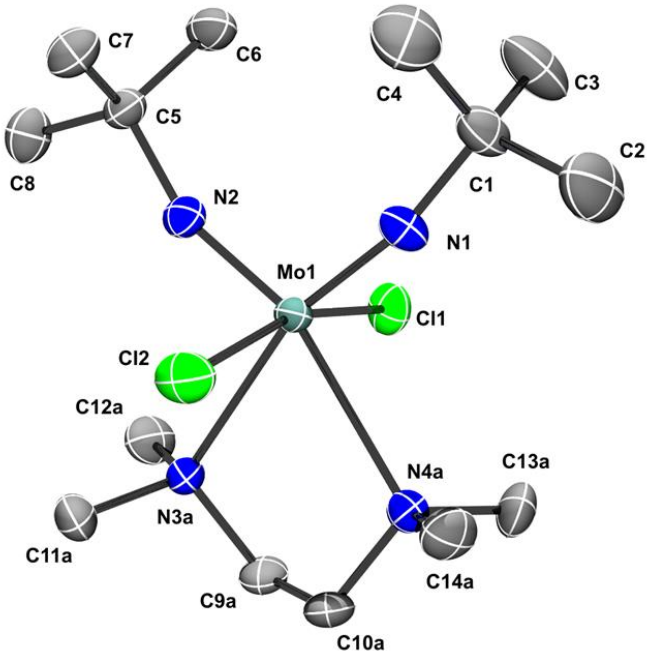

Figure S50: Solid-state structure of (*t*-BuN=)$_2$MoCl$_2$·TMEDA **6** with all heavy atoms labelled. Hydrogen atoms have been omitted for visual clarity. Thermal ellipsoids are drawn at the 50% probability level. The entire TMEDA ligand is disordered over two positions, however, only part A of the disorder is shown for visual clarity.

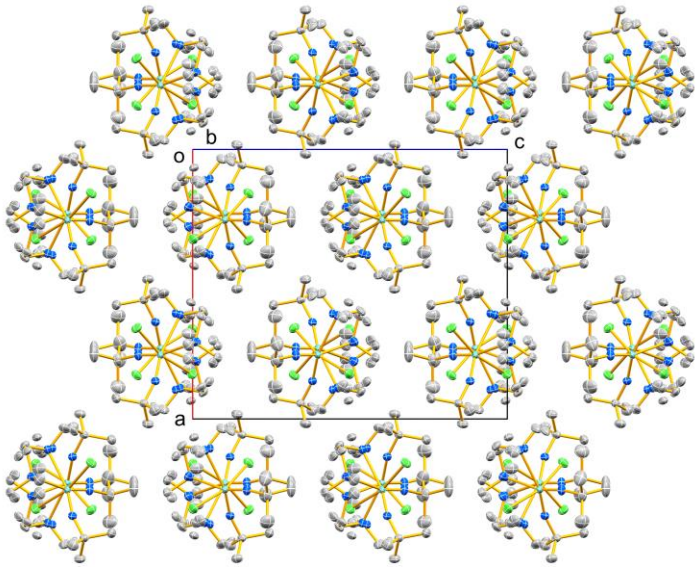

Figure S51: Solid-state packing diagram of (*t*-BuN=)$_2$MoCl$_2$·TMEDA **6**, viewed down the *Y*-axis.

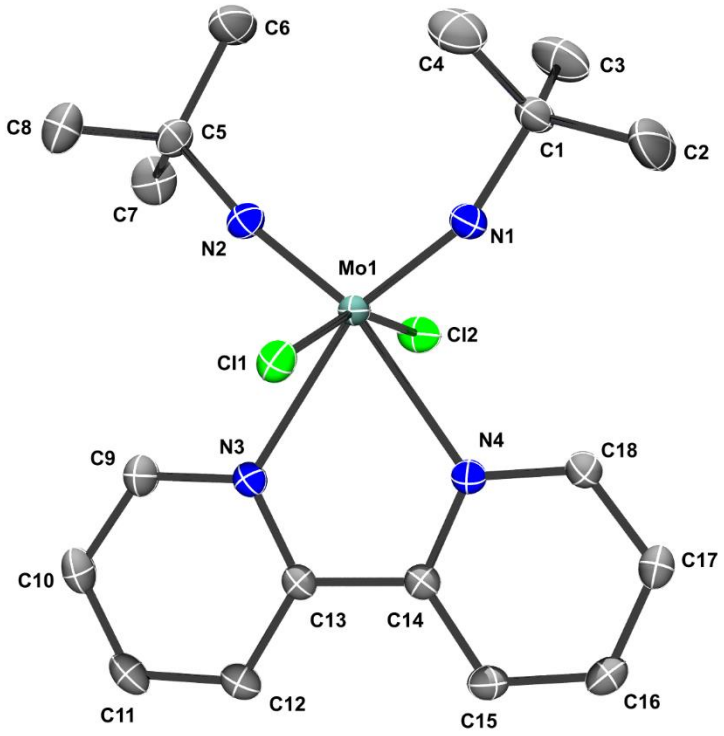

Figure S52: Solid-state structure of (t-BuN=)$_2$MoCl$_2$·bpy **7**·(C$_6$H$_6$)$_{1.5}$ with all heavy atoms labelled. Hydrogen atoms have been omitted for visual clarity. Thermal ellipsoids are drawn at the 50% probability level. The structure also contains 1.5 C$_6$H$_6$ solvent molecules, however, they have also been omitted for visual clarity.

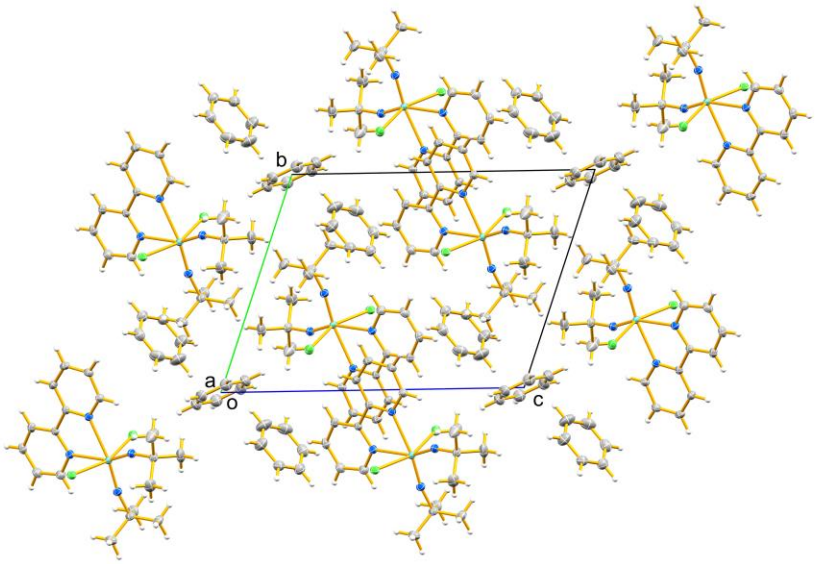

Figure S53: Solid-state packing diagram of (t-BuN=)$_2$MoCl$_2$·bpy, **7**·(C$_6$H$_6$)$_{1.5}$, viewed down the X-axis. Note the π-stacking interactions that can also be seen in this structure.

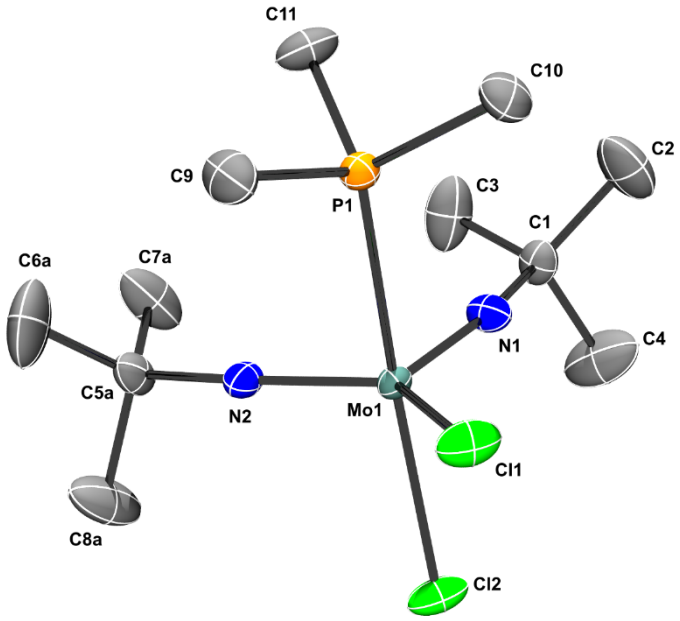

Figure S54: Solid-state structure of (*t*-BuN=)$_2$MoCl$_2$·PMe$_3$ **8** with all heavy atoms labelled. Hydrogen atoms have been omitted for visual clarity. Thermal ellipsoids are drawn at the 50% probability level. The *tert*-butyl group attached to N2 is disordered over two positions, however, only part A of the disorder is shown for visual clarity.

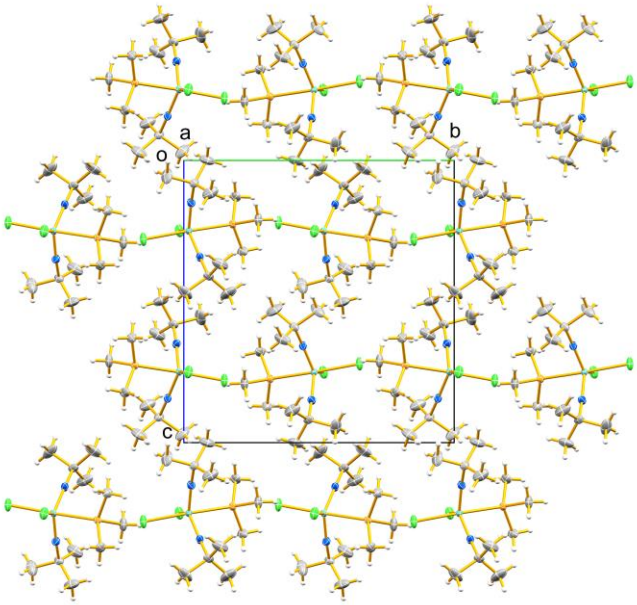

Figure S55: Solid-state packing diagram of (*t*-BuN=)$_2$MoCl$_2$·PMe$_3$ **8**, viewed down the *X*-axis.

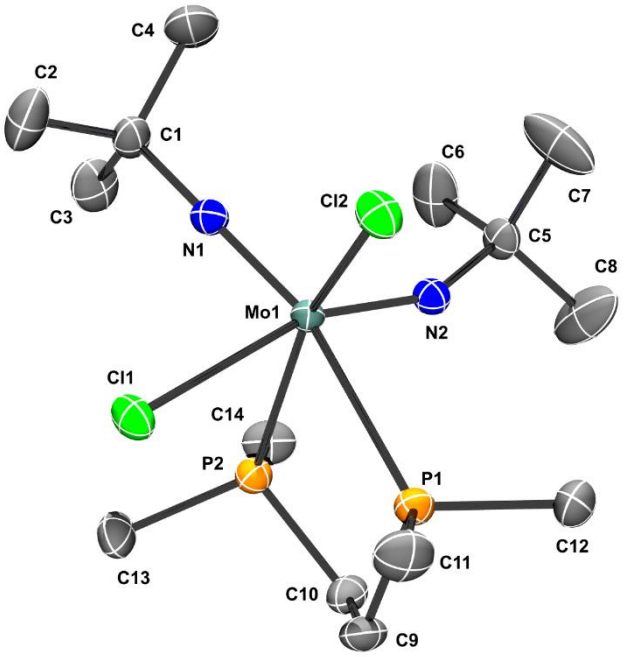

Figure S56: Solid-state structure of (*t*-BuN=)$_2$MoCl$_2$·dmpe **9** with all heavy atoms labelled. Hydrogen atoms have been omitted for visual clarity. Thermal ellipsoids are drawn at the 50% probability level.

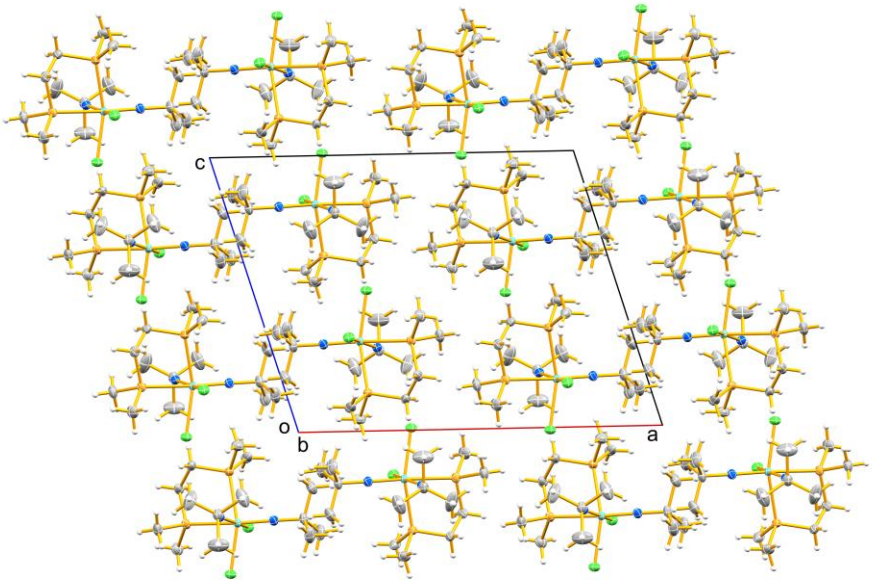

Figure S57: Solid-state packing diagram of (*t*-BuN=)$_2$MoCl$_2$·dmpe **9**, viewed down the *Y*-axis.

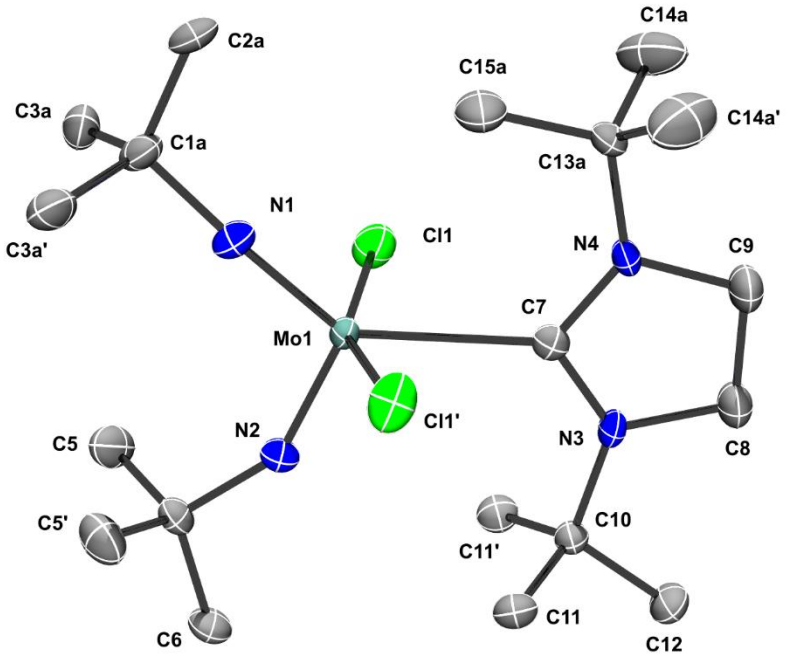

Figure S58: Solid-state structure of (*t*-BuN=)$_2$MoCl$_2$·(SI*t*-Bu) **10** with all heavy atoms labelled. Hydrogen atoms have been omitted for visual clarity. Thermal ellipsoids are drawn at the 50% probability level. The *tert*-butyl groups attached to N1 and N4 are disordered over two positions, however, only part A of the disorder is shown for visual clarity. Some of the atoms were generated by symmetry and they are denoted with a prime symbol.

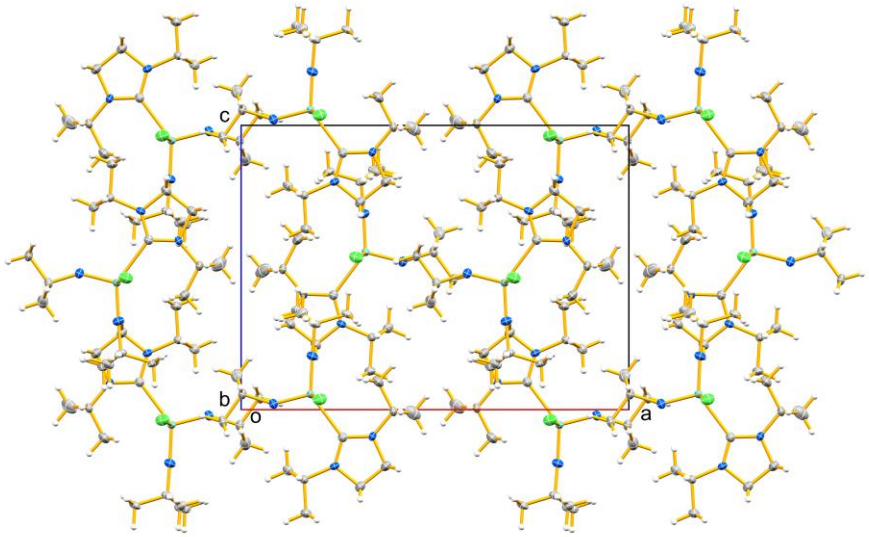

Figure S59: Solid-state packing diagram of (*t*-BuN=)$_2$MoCl$_2$·(SI*t*-Bu) **10**, viewed down the *Y*-axis.

Solid-State Structure of [SIt-BuH]$_2$[(t-BuN=)$_2$MoCl$_2$(CH$_2$CN)][(t-BuN=)$_2$MoCl$_3$] **13**. In an early attempt to recrystallize (*t*-BuN=)$_2$MoCl$_2$·(SI*t*-Bu) **10**, it was dissolved in acetonitrile. The solvent was removed by slow evaporation in a sealed, nitrogen-filled 250-mL glass jar, over two days, resulting in the formation of yellow plate-like crystals, coated in a beige oil. The crystals were studied using X-ray crystallography; however, the material could not be purified and there is no additional spectroscopic data to support the formulation of this compound. Therefore, we do not report the synthesis of this compound, but are rather only reporting the results of a single-crystal structural analysis. Additionally, the composition of the non-crystalline material was also not investigated. The structure was determined to be an ionic salt, containing two protonated imidazolium cations ([SI*t*-Bu]H$^+$). One of the counterions was comprised of the (*t*-BuN=)$_2$MoCl$_2$ moiety, complexed by a cyanomethyl anion ($^-$CH$_2$CN). The second anion was a chloride complex of the (*t*-BuN=)$_2$MoCl$_2$ moiety, which likely scavenged a transient chloride anion. As described in the main text, **10** has a long Mo−C bond length, and appears to be labile in solution, readily undergoing the acid-base chemistry observed here. This structure was also deposited at the CCDC: 1944220.

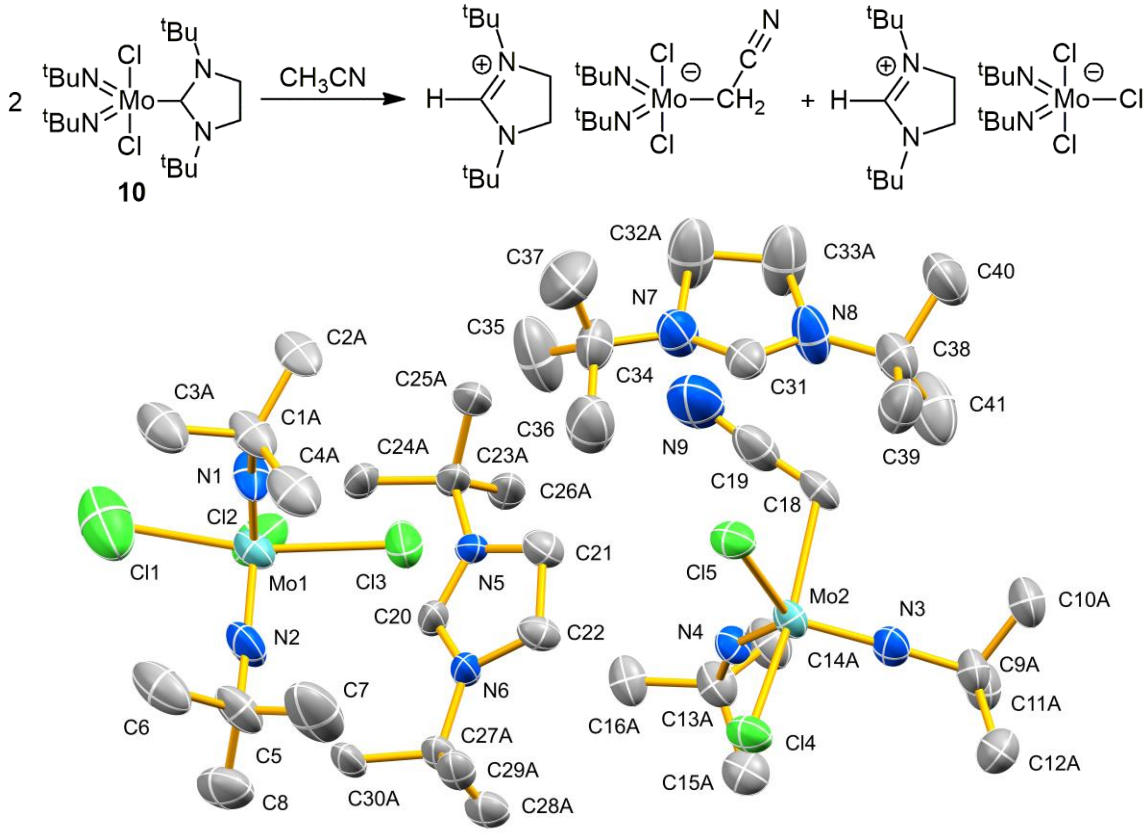

Figure S60: Solid-state structure of the imidazolium co-crystal **13**. Hydrogen atoms have been omitted for visual clarity. Thermal ellipsoids are drawn at the 50% probability level. One of the chlorine atoms (Cl3) is disordered with an 82.2(12)% occupancy; the other 17.8(12)% of the occupancy is a cyanomethyl group (omitted for visual clarity). The *tert*-butyl groups attached to N1, N3, N4, N5, and N6 are disordered over two positions, however, only part A of the disorder is shown for visual clarity.

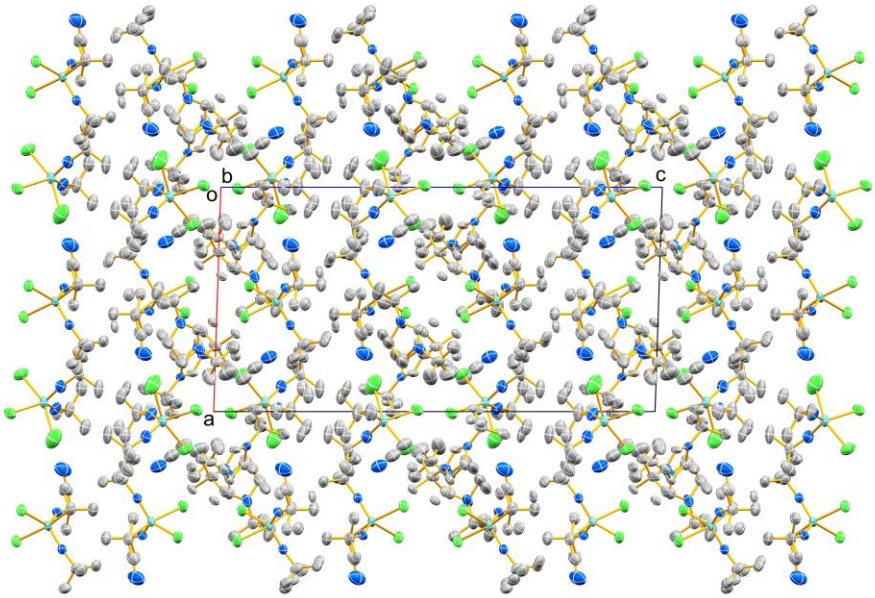

Figure S61: Solid-state packing diagram of the imidazolium co-crystal **13**, viewed down the *Y*-axis.

NMR Spectroscopy of Compounds

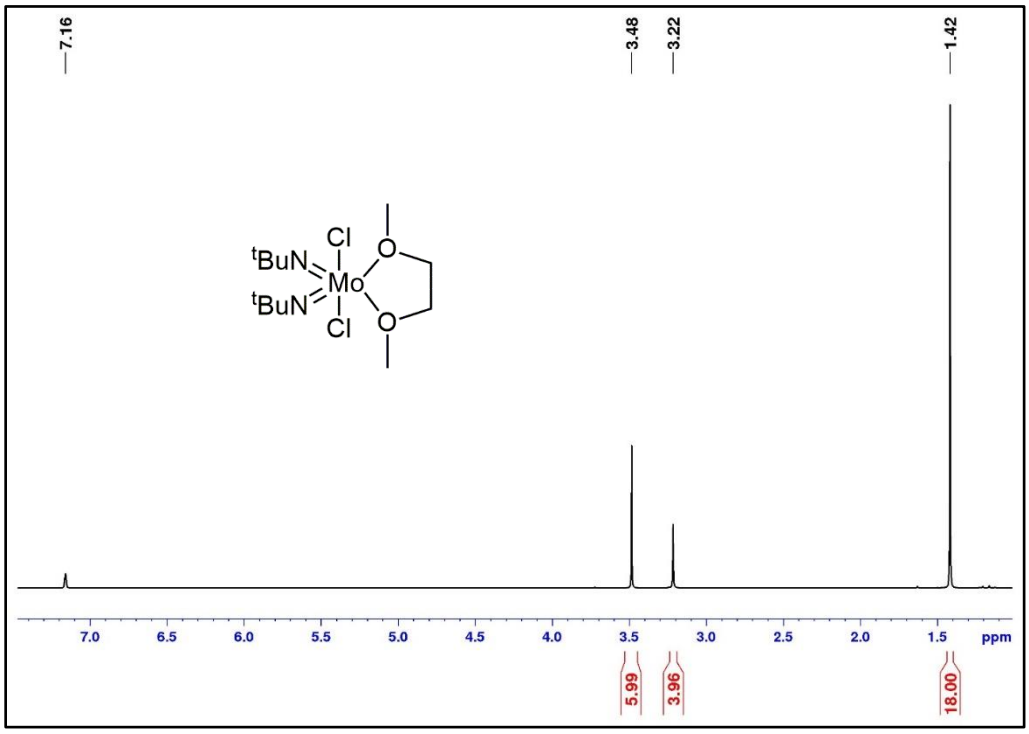

Figure S62: ^{1}H NMR spectrum of (*t*-BuN=)$_2$MoCl$_2$·dme **1** in C_6D_6.

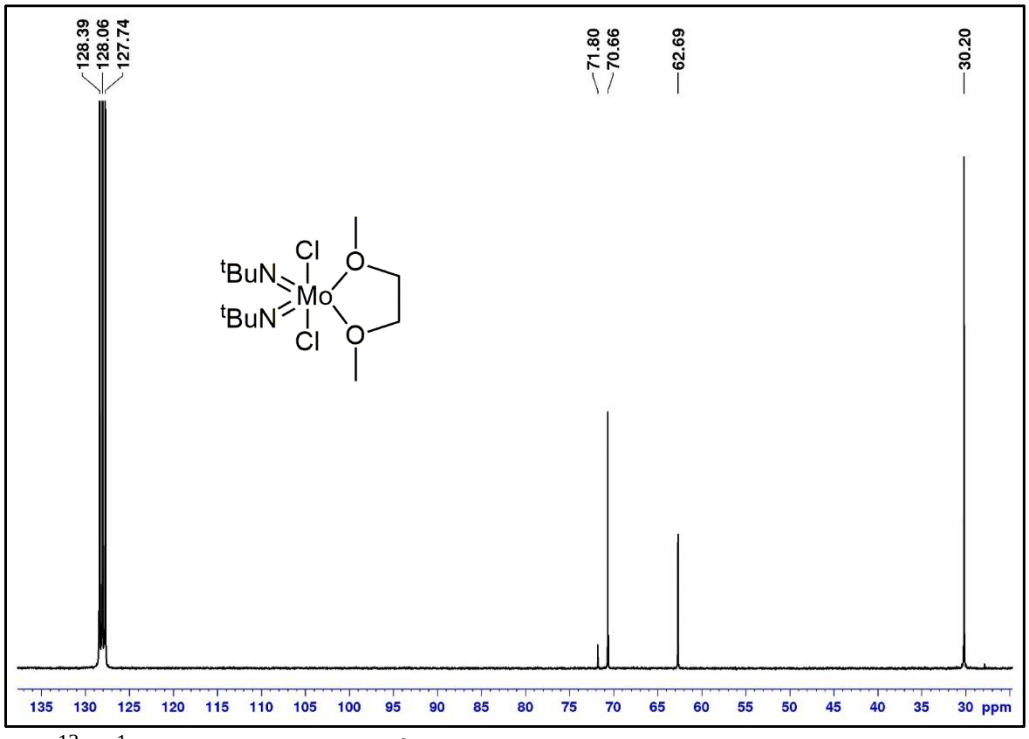

Figure S63: ^{13}C{^{1}H} NMR spectrum of (*t*-BuN=)$_2$MoCl$_2$·dme **1** in C_6D_6.

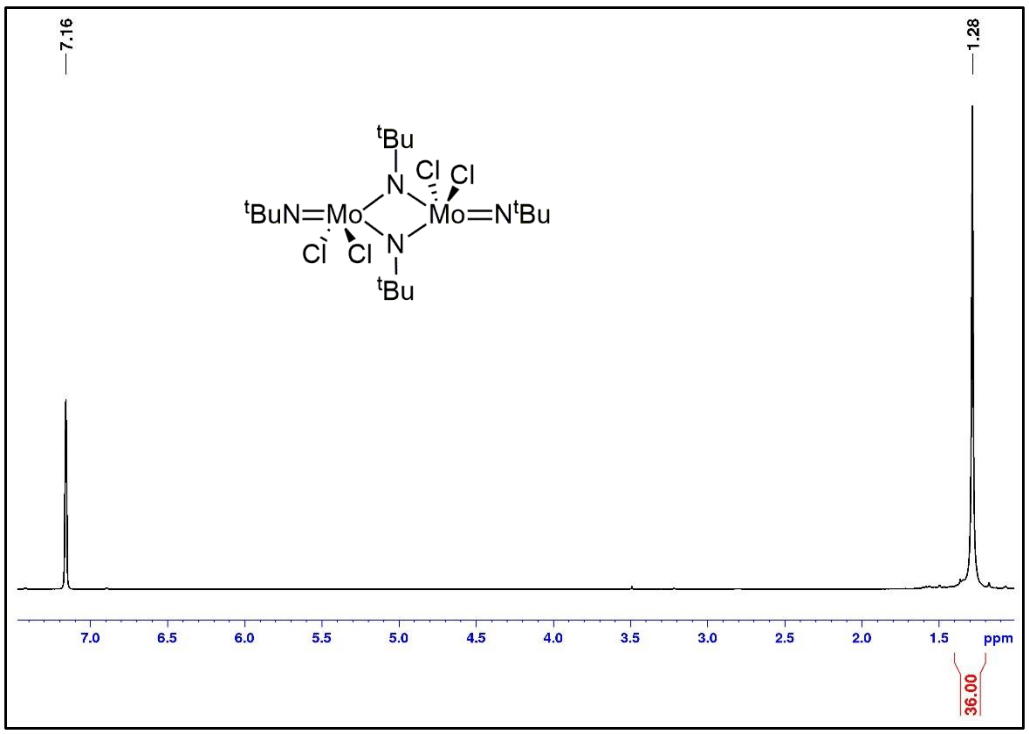

Figure S64: ^{1}H NMR spectrum of [(*t*-BuN=)$_2$MoCl$_2$]$_2$ **2** in C_6D_6.

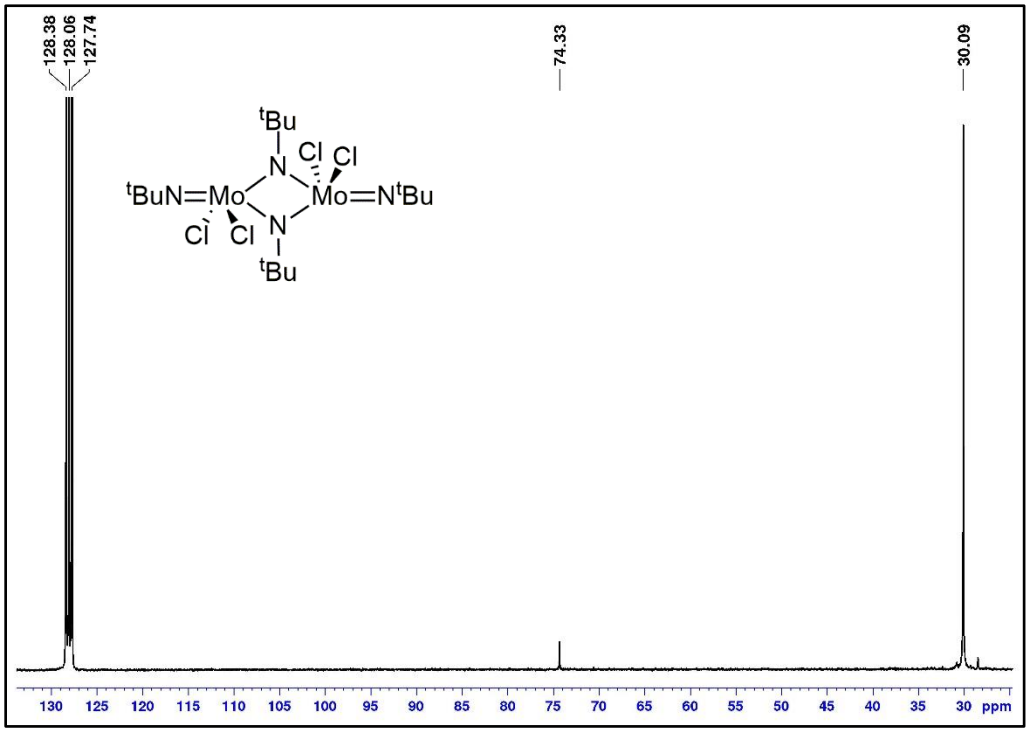

Figure S65: ^{13}C{^{1}H} NMR spectrum of [(*t*-BuN=)$_2$MoCl$_2$]$_2$ **2** in C_6D_6.

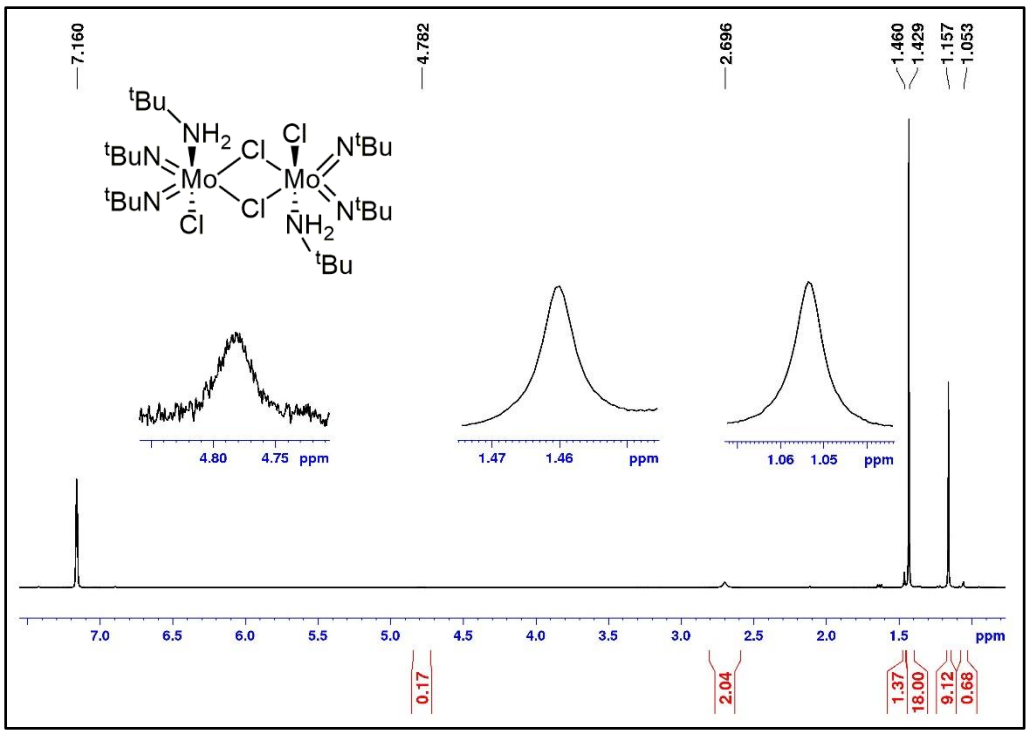

Figure S66: ^{1}H NMR spectrum of [(*t*-BuN=)$_2$MoCl$_2$·(*t*-BuNH$_2$)]$_2$ **3** in C_6D_6. A second isomer (or the monomer) is present in a ratio of 13:1 (as shown by the inset peaks).

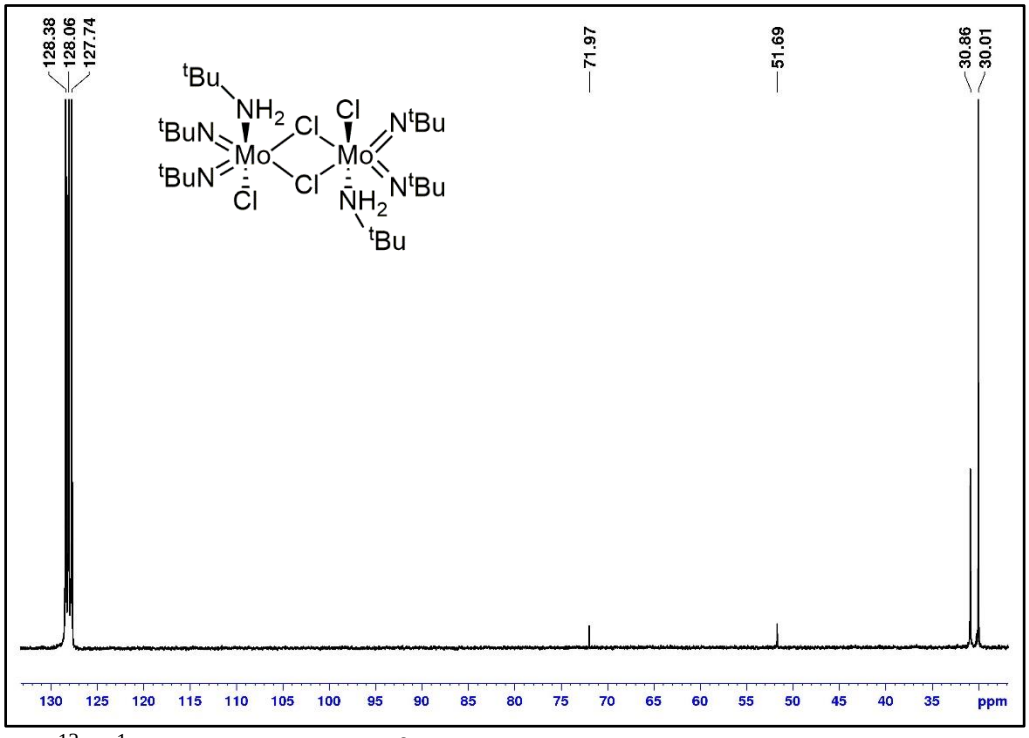

Figure S67: ^{13}C{^{1}H} NMR spectrum of [(*t*-BuN=)$_2$MoCl$_2$·(*t*-BuNH$_2$)]$_2$ **3** in C_6D_6.

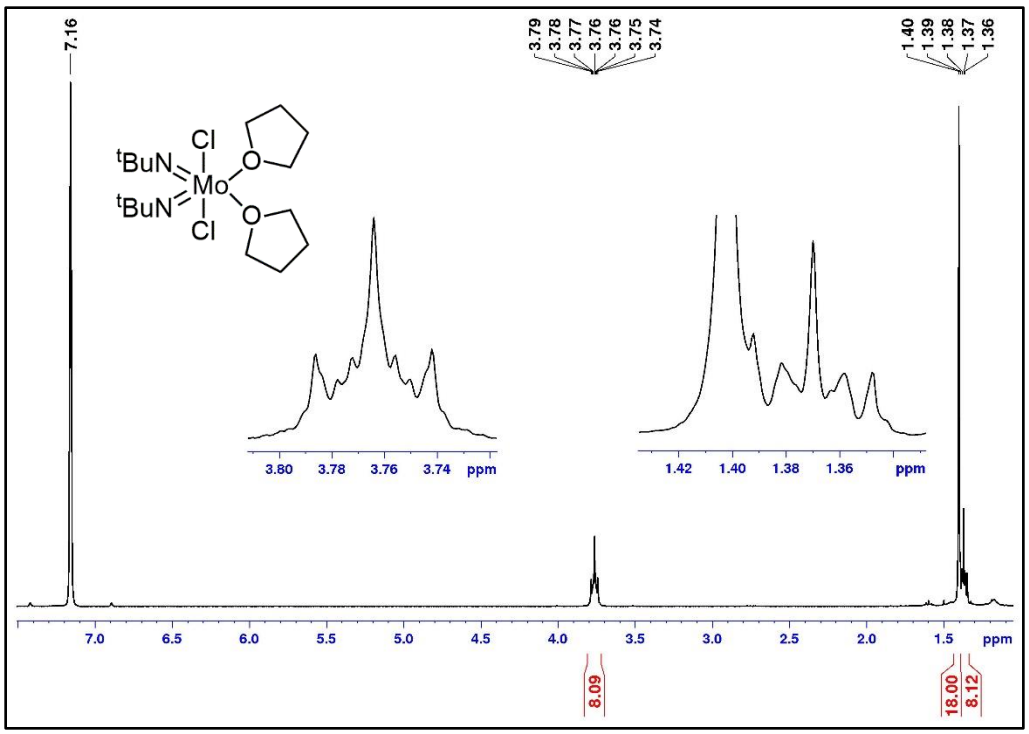

Figure S68: ^{1}H NMR spectrum of (*t*-BuN=)$_2$MoCl$_2$·(THF)$_2$ **4** in C_6D_6.

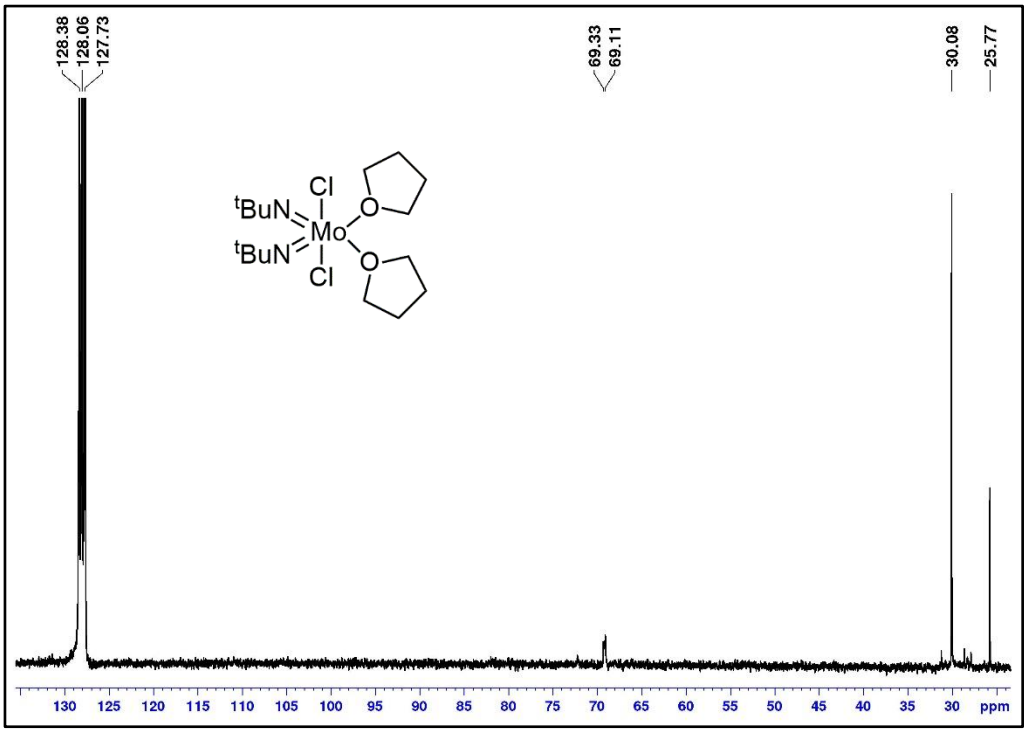

Figure S69: ^{13}C{^{1}H} NMR spectrum of (*t*-BuN=)$_2$MoCl$_2$·(THF)$_2$ **4** in C_6D_6.

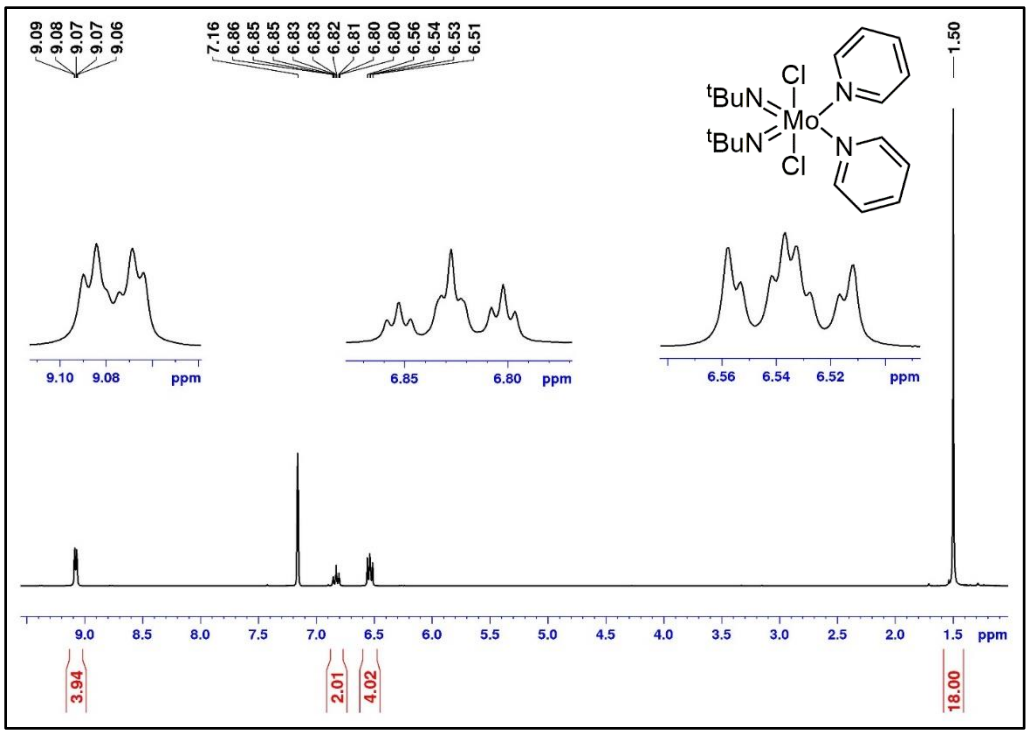

Figure S70: ^{1}H NMR spectrum of (*t*-BuN=)$_2$MoCl$_2$·(py)$_2$ **5** in C_6D_6.

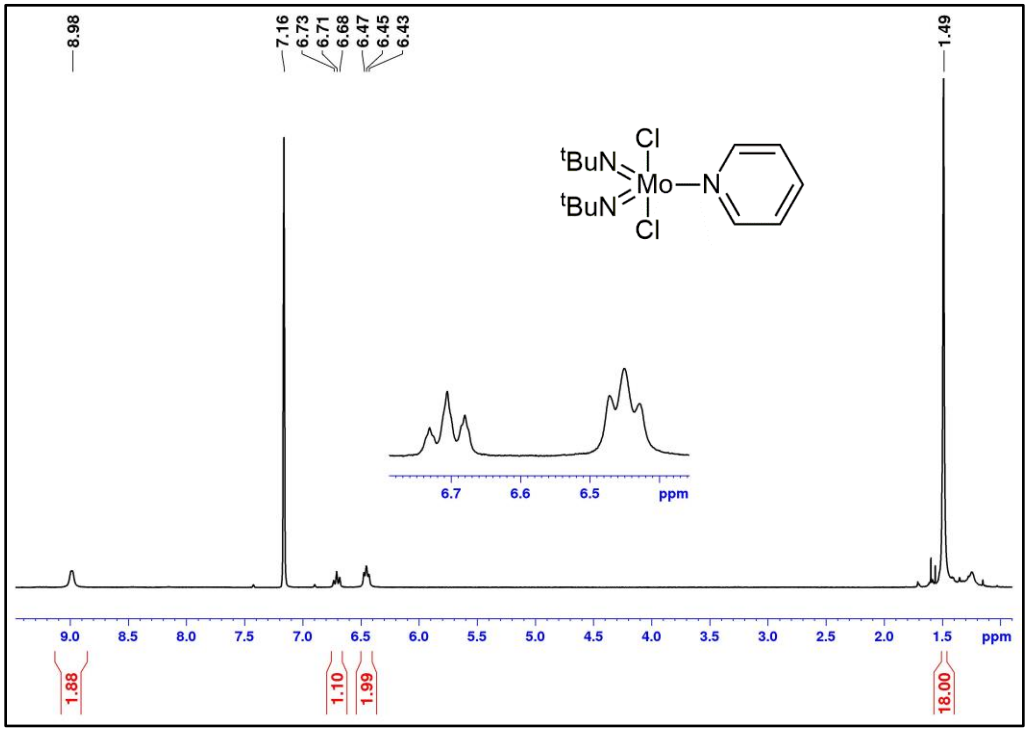

Figure S71: ^{1}H NMR spectrum of the material isolated after subliming (*t*-BuN=)$_2$MoCl$_2$·(py)$_2$ **5** at 100 ºC (10 mTorr), in C_6D_6. The relative integration suggest one pyridine ligand was removed which is consistent with TGA data (Figure S9).

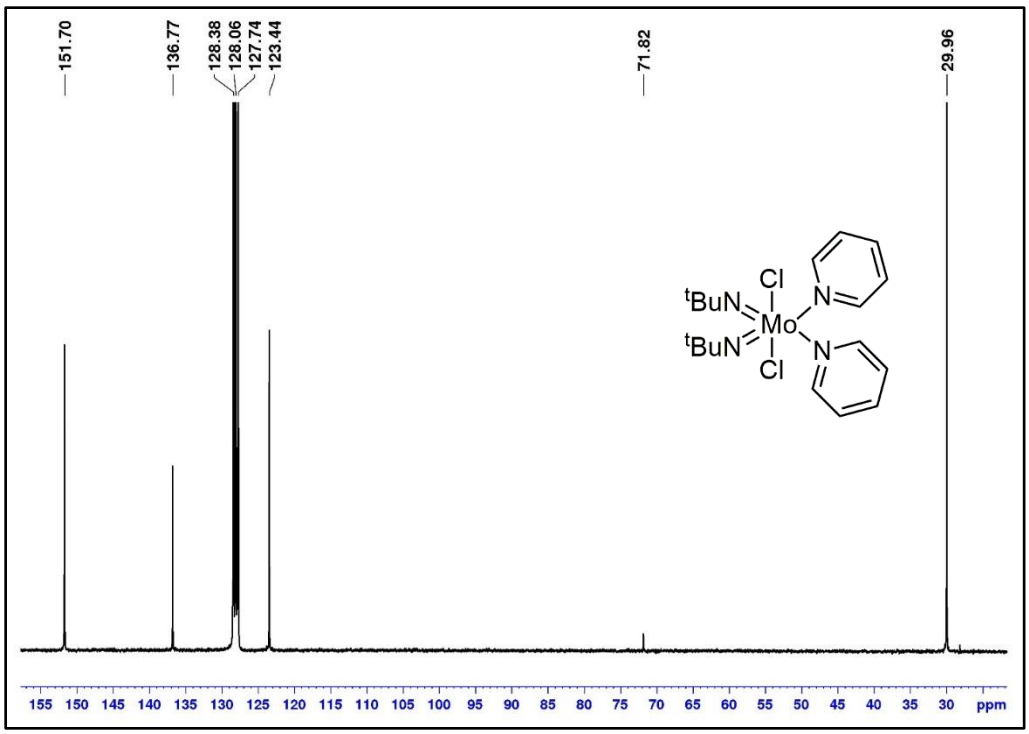

Figure S72: $^{13}C\{^{1}H\}$ NMR spectrum of (*t*-BuN=)$_2$MoCl$_2$·(py)$_2$ **5** in C_6D_6

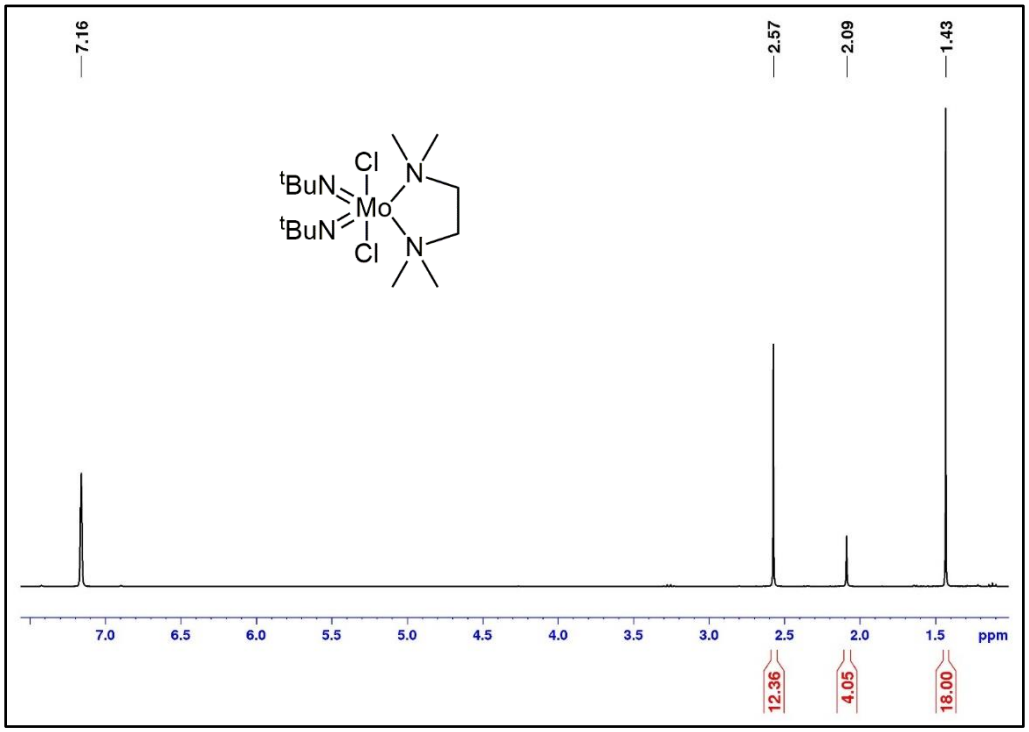

Figure S73: ^{1}H NMR spectrum of (*t*-BuN=)$_2$MoCl$_2$·TMEDA **6** in C_6D_6.

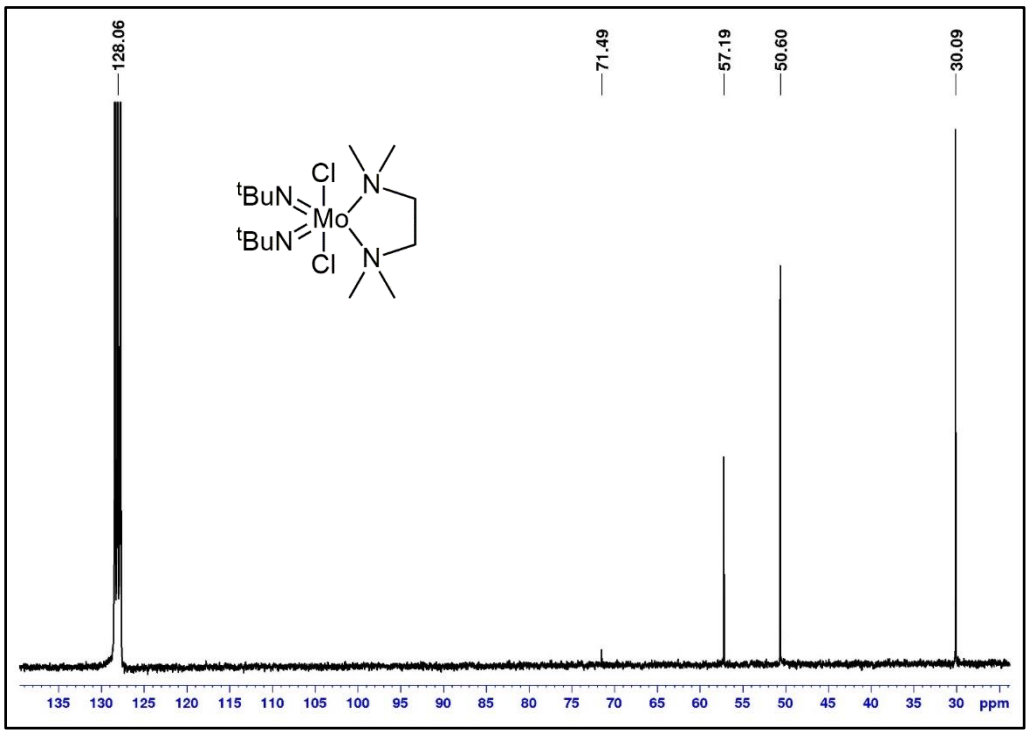

Figure S74: $^{13}C\{^{1}H\}$ NMR spectrum of (*t*-BuN=)$_2$MoCl$_2$·TMEDA **6** in C_6D_6.

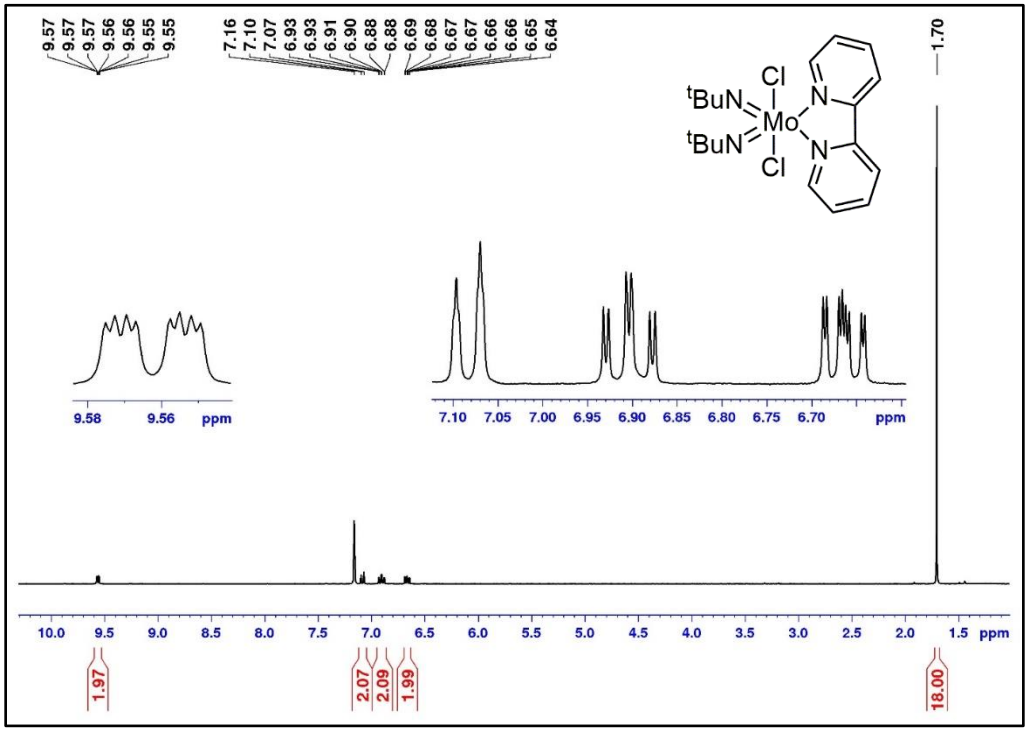

Figure S75: ^{1}H NMR spectrum of (*t*-BuN=)$_2$MoCl$_2$·bpy **7** in C_6D_6.

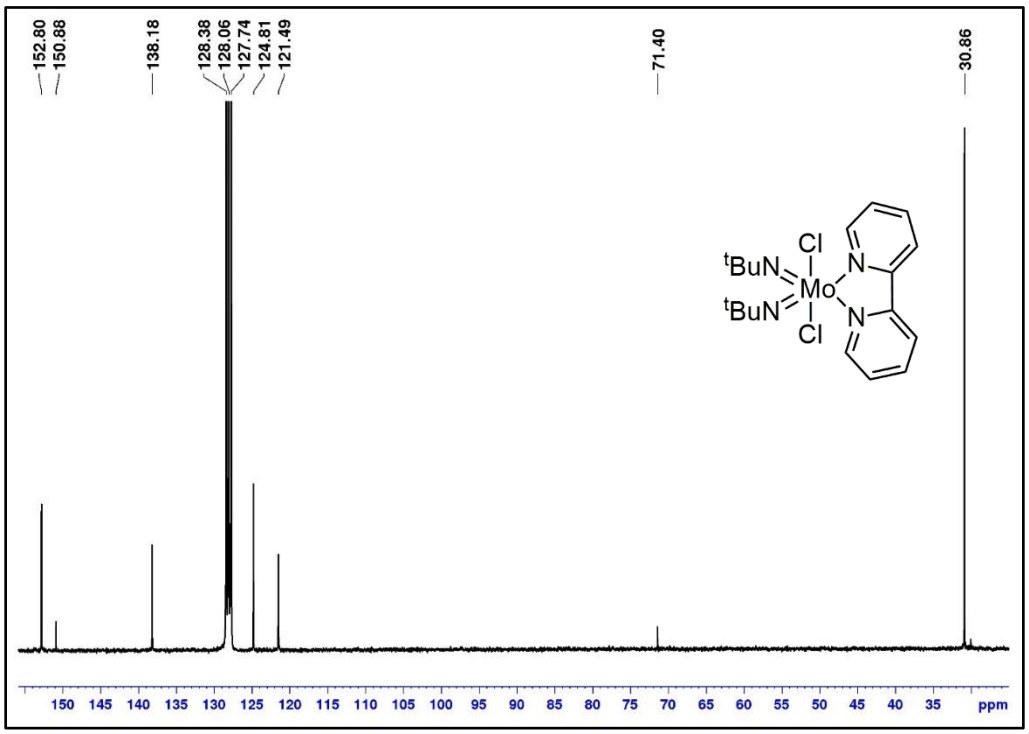

Figure S76: $^{13}C\{^{1}H\}$ NMR spectrum of (*t*-BuN=)$_2$MoCl$_2$·bpy **7** in C_6D_6.

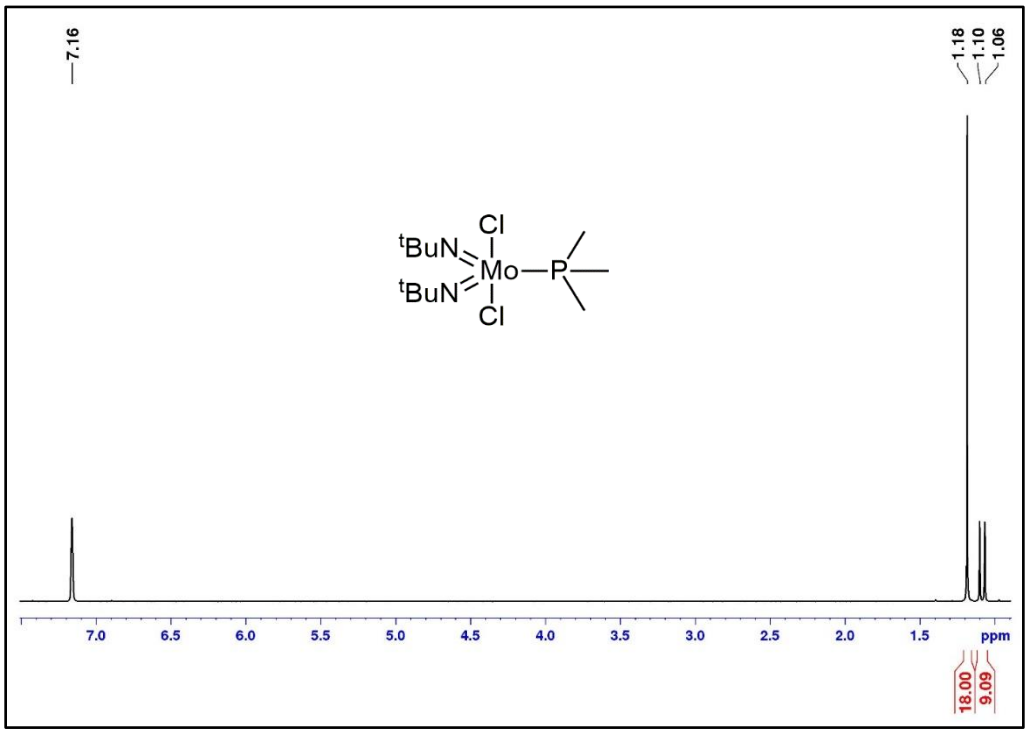

Figure S77: ^{1}H NMR spectrum of (*t*-BuN=)$_2$MoCl$_2$·PMe$_3$ **8** in C_6D_6.

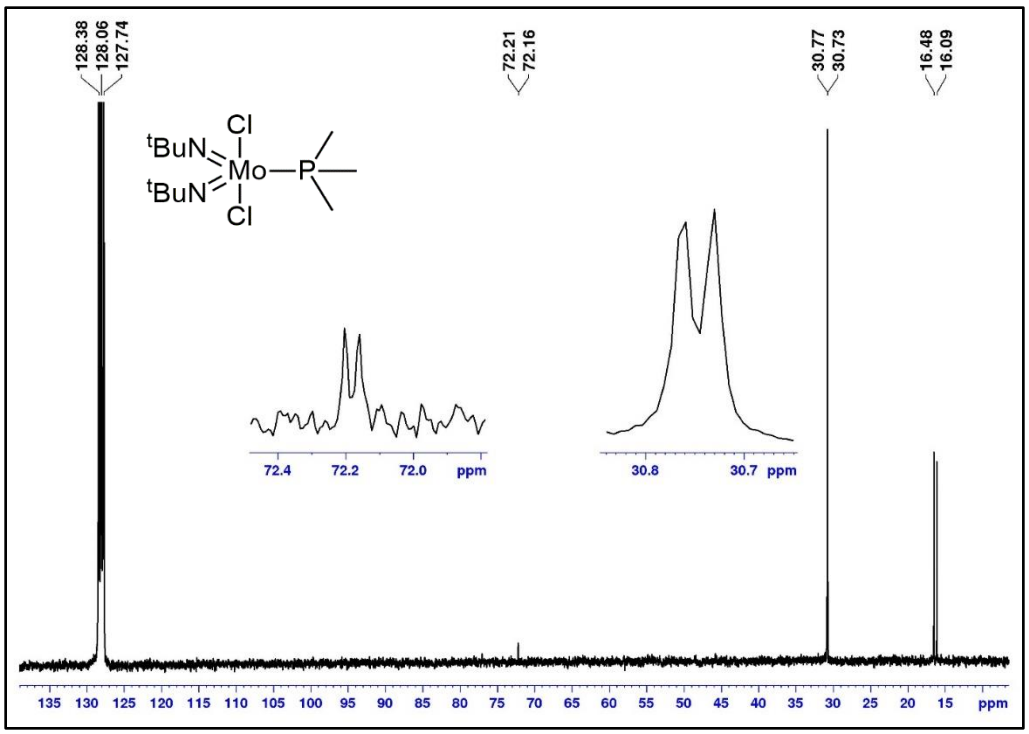

Figure S78: $^{13}C\{^{1}H\}$ NMR spectrum of (*t*-BuN=)$_2$MoCl$_2$·PMe$_3$ **8** in C_6D_6.

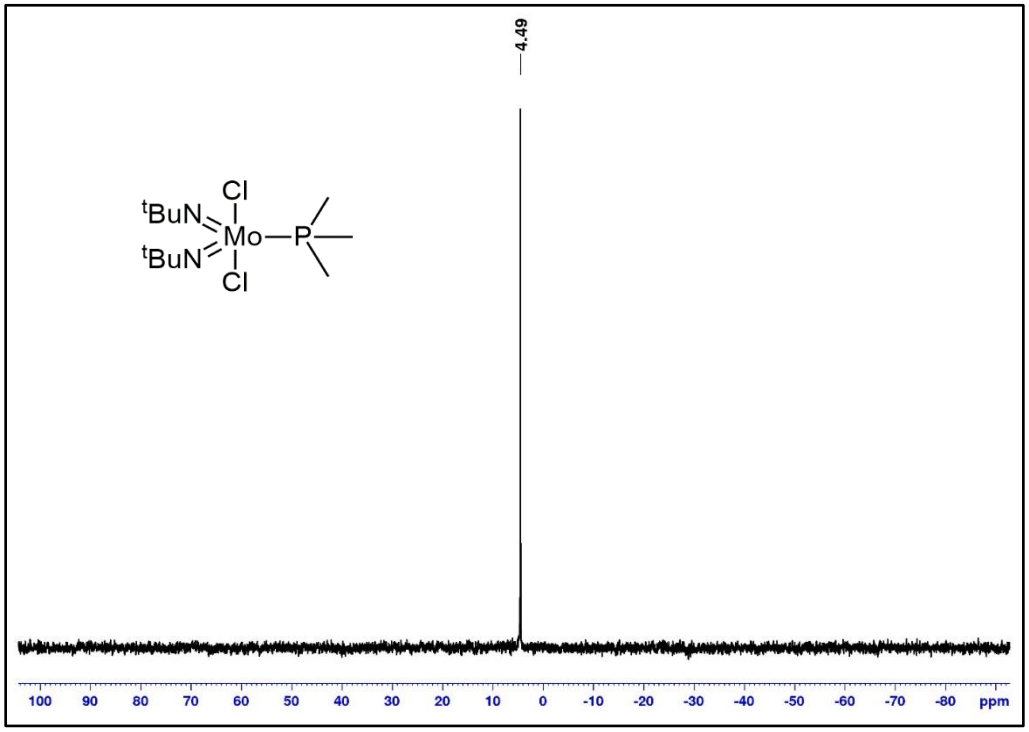

Figure S79: $^{31}P\{^{1}H\}$ NMR spectrum of (*t*-BuN=)$_2$MoCl$_2$·PMe$_3$ **8** in C_6D_6.

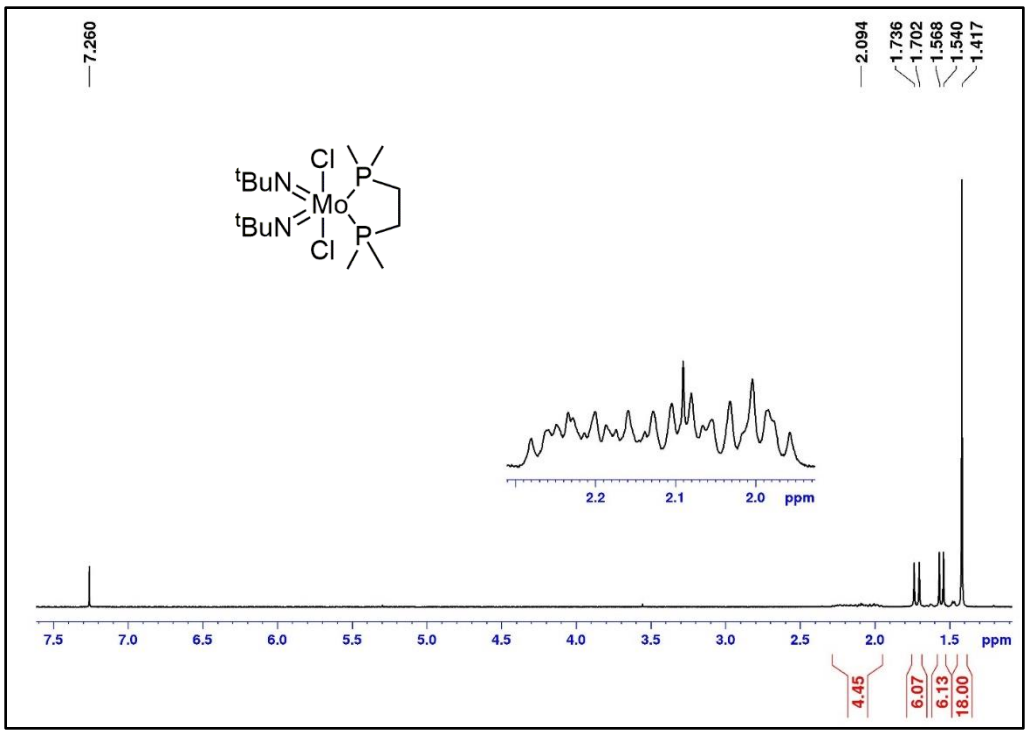

Figure S80: ^{1}H NMR spectrum of (*t*-BuN=)$_2$MoCl$_2$·dmpe **9** in CDCl$_3$.

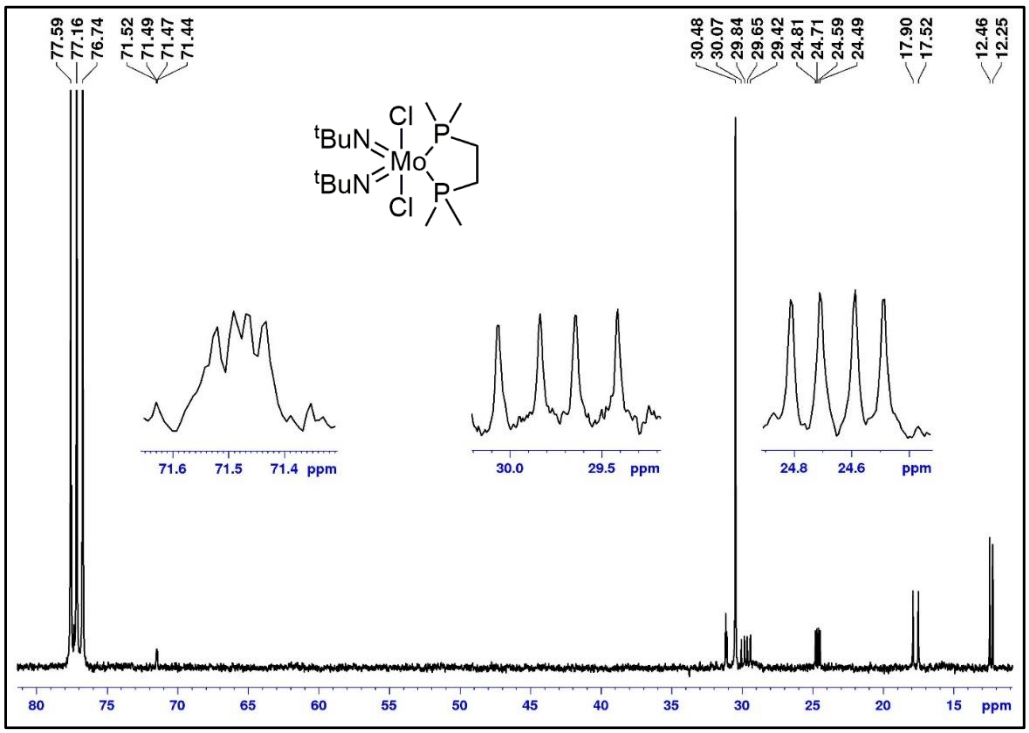

Figure S81: ^{13}C{^{1}H} NMR spectrum of (*t*-BuN=)$_2$MoCl$_2$·dmpe **9** in CDCl$_3$. The signal at 31.17 ppm has not been assigned.

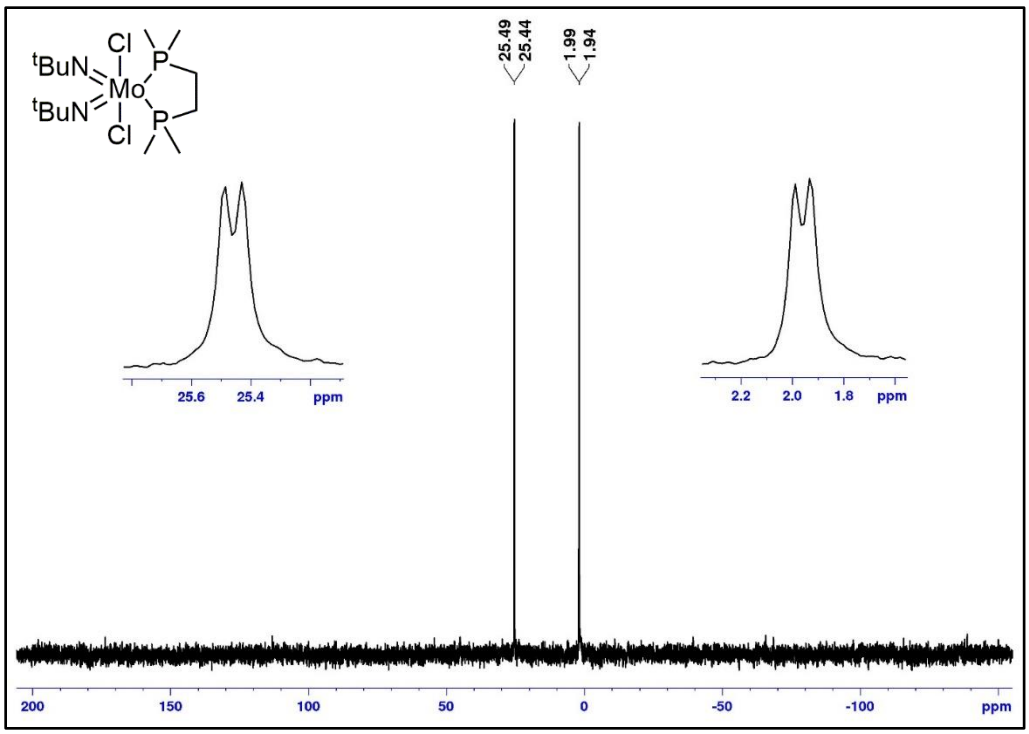

Figure S82: $^{31}P\{^{1}H\}$ NMR spectrum of (t-BuN=)$_2$MoCl$_2$·dmpe **9** in $CDCl_3$.

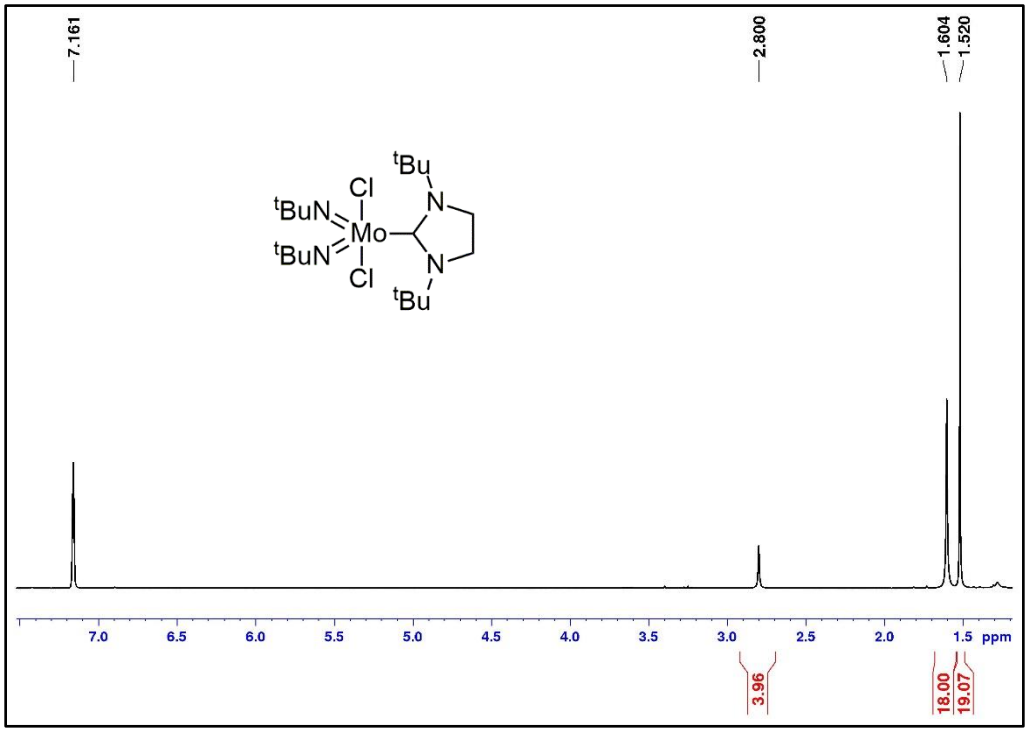

Figure S83: ^{1}H NMR spectrum of (t-BuN=)$_2$MoCl$_2$·(Sit-Bu) **10** in C_6D_6.

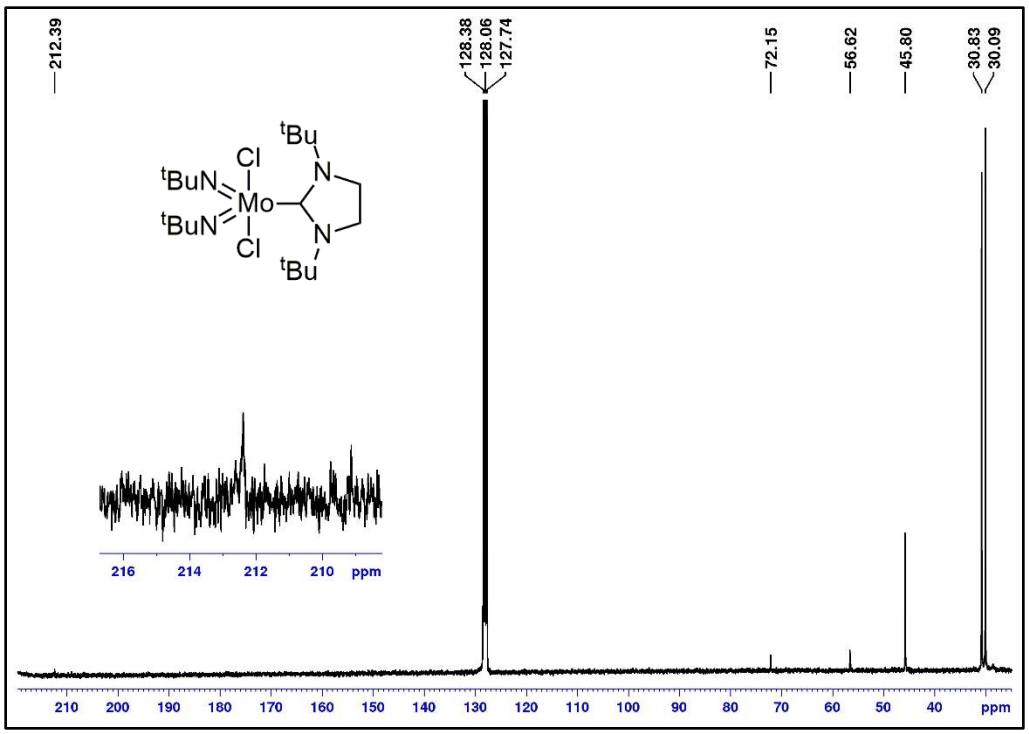

Figure S84: $^{13}C\{^{1}H\}$ NMR spectrum of (*t*-BuN=)$_2$MoCl$_2$·(SI*t*-Bu) **10** in C_6D_6.

IR Spectroscopy of Compounds

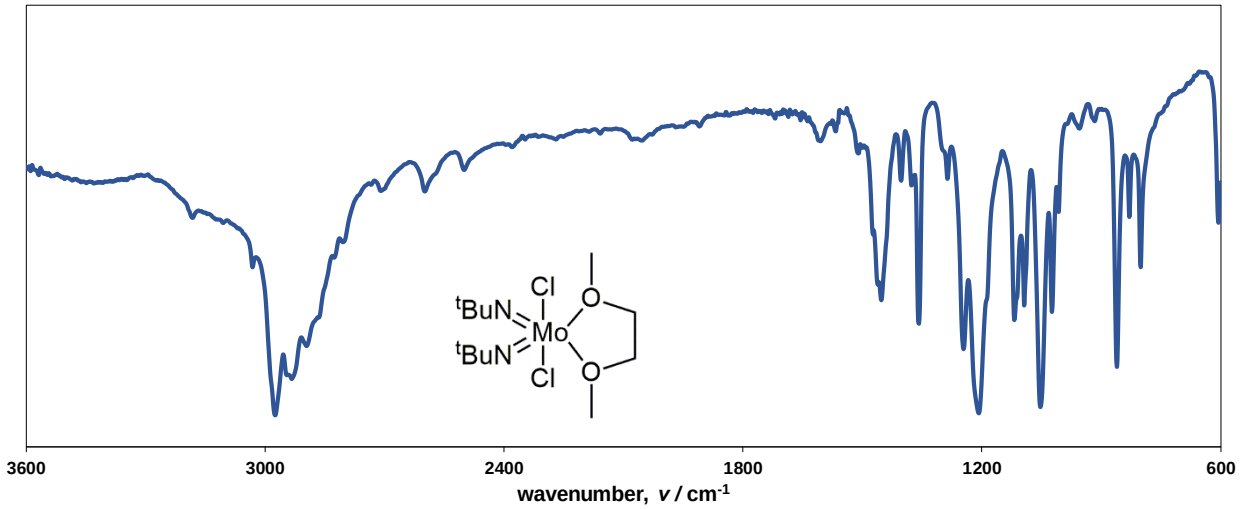

Figure S85: IR spectrum of (*t*-BuN=)$_2$MoCl$_2$·dme **1**, obtained as a KBr pellet.

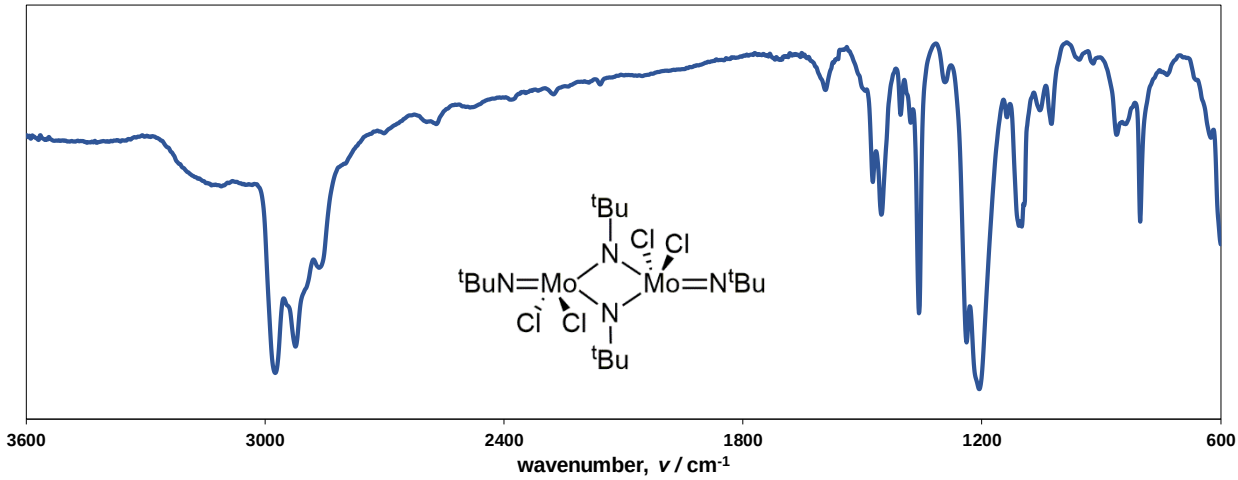

Figure S86: IR spectrum of $[(t\text{-BuN=})_2MoCl_2]_2$ **2**, obtained as a KBr pellet.

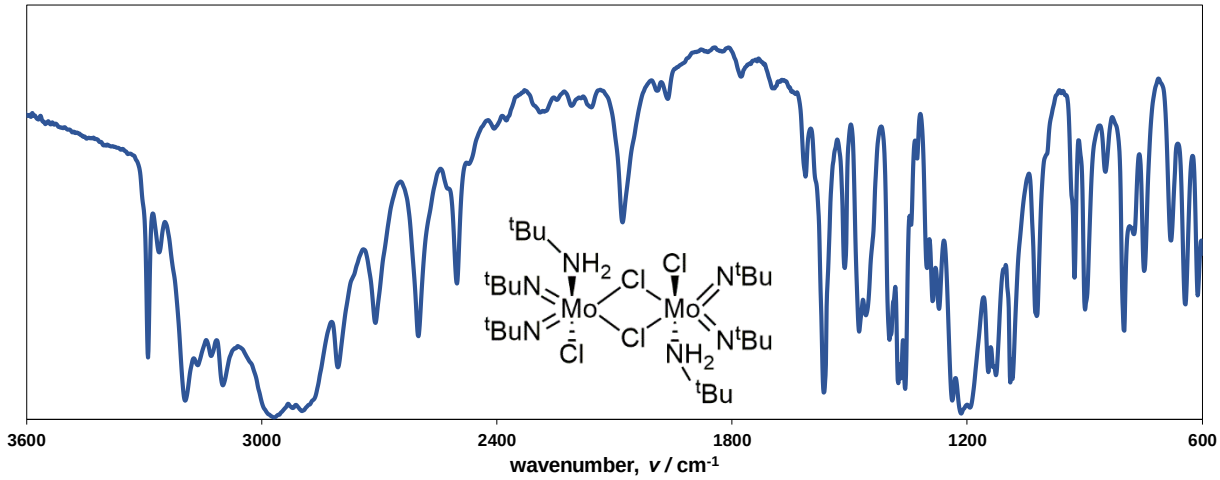

Figure S87: IR spectrum of $[(t\text{-BuN=})_2MoCl_2\cdot(t\text{-BuNH}_2)]_2$ **3**, obtained as a KBr pellet.

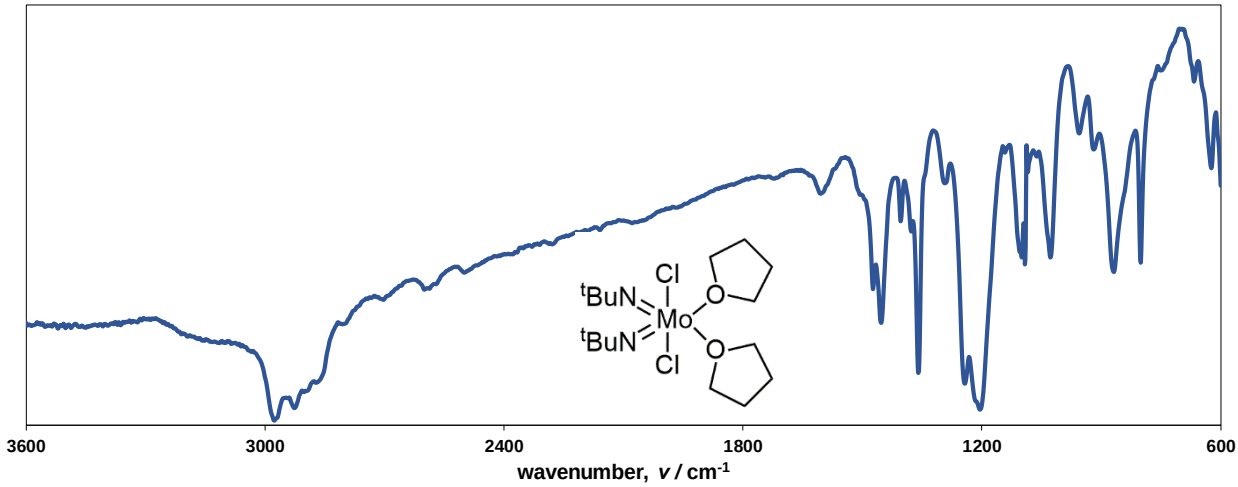

Figure S88: IR spectrum of $(t\text{-BuN=})_2MoCl_2\cdot(THF)_2$ **4**, obtained as a KBr pellet.

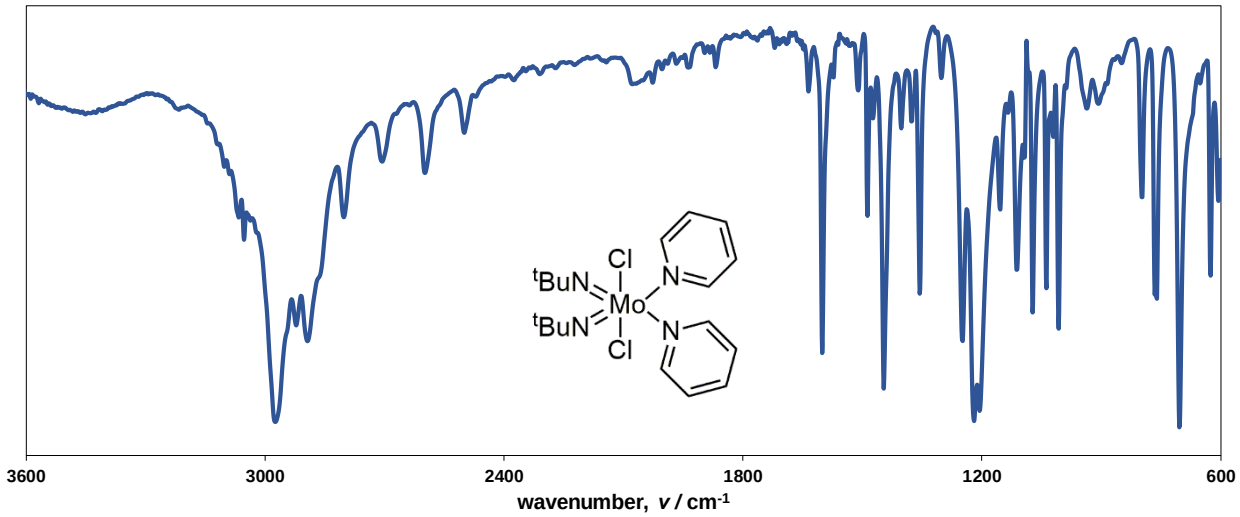

Figure S89: IR spectrum of (t-BuN=)$_2$MoCl$_2$·(py)$_2$ **5**, obtained as a KBr pellet.

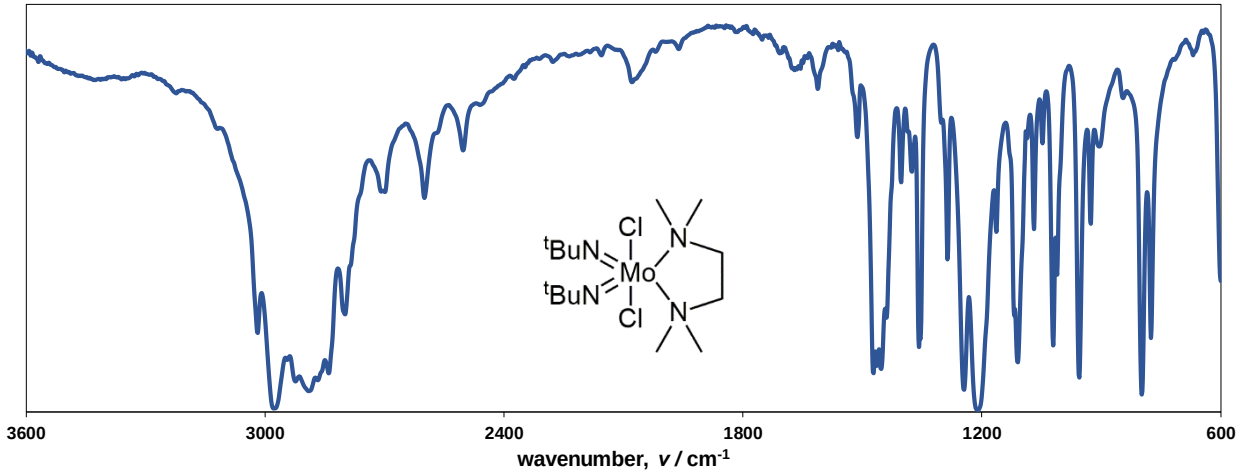

Figure S90: IR spectrum of (t-BuN=)$_2$MoCl$_2$·TMEDA **6**, obtained as a KBr pellet.

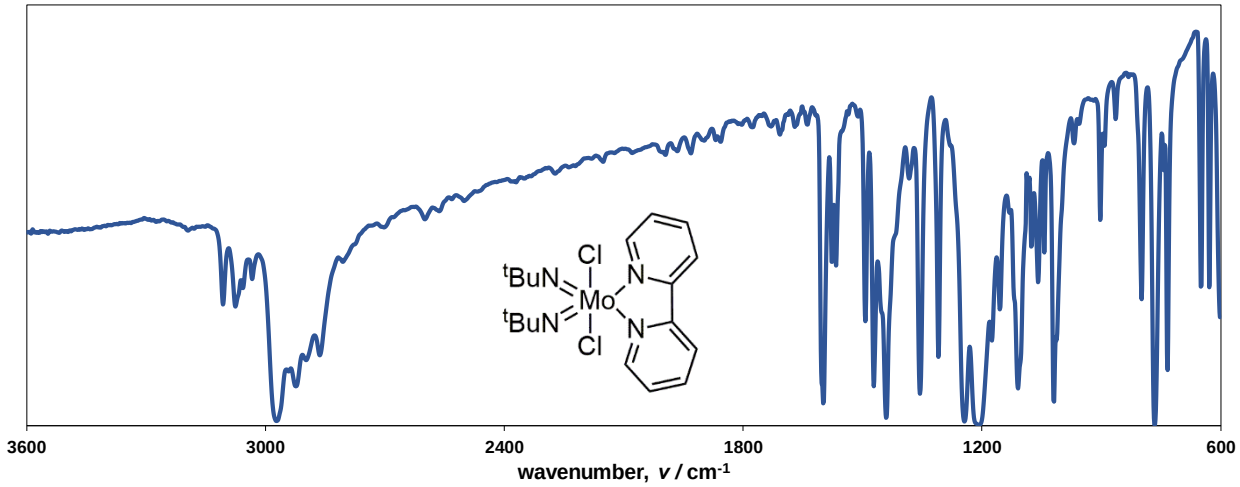

Figure S91: IR spectrum of (t-BuN=)$_2$MoCl$_2$·bpy **7**, obtained as a KBr pellet.

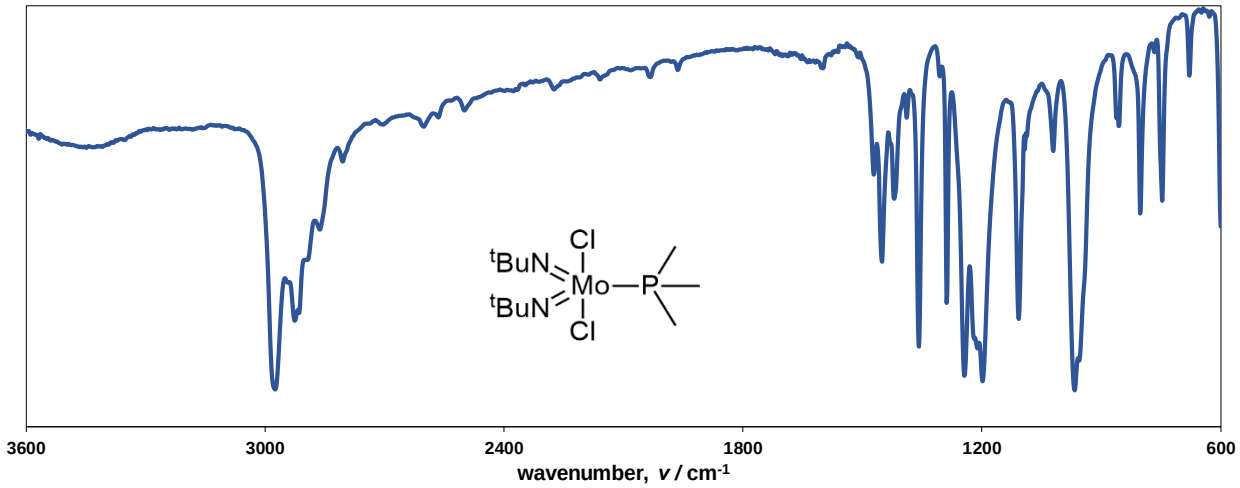

Figure S92: IR spectrum of (*t*-BuN=)$_2$MoCl$_2$·PMe$_3$ **8**, obtained as a KBr pellet.

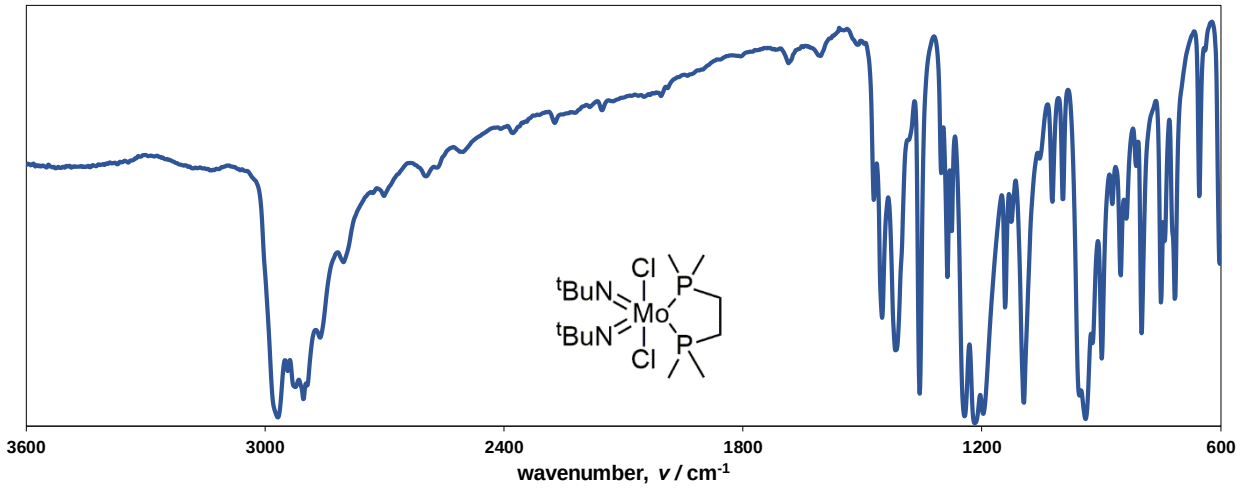

Figure S93: IR spectrum of (*t*-BuN=)$_2$MoCl$_2$·dmpe **9**, obtained as a KBr pellet.

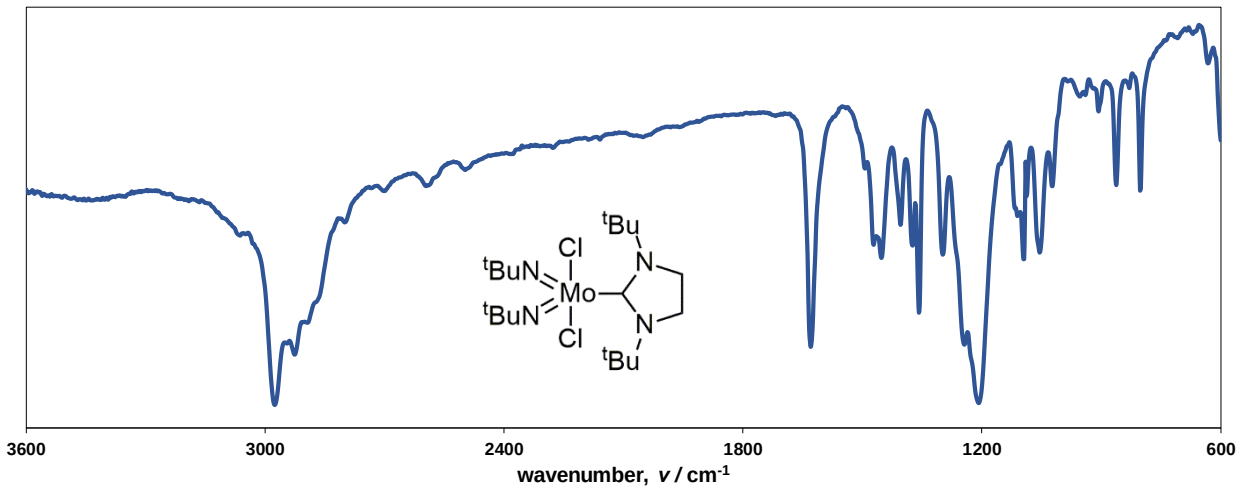

Figure S94: IR spectrum of (*t*-BuN=)$_2$MoCl$_2$·(SI*t*-Bu) **10**, obtained as a KBr pellet.